University of Alberta

Interfacial Tension, Blending and Morphology of Linear Low Density Polyethylenes with Polypropylene

by

Nikhil Rao ©

A thesis submitted to the Faculty of Graduate Studies and Research
in partial fulfillment of the requirements for the degree of
Master of Science
in
Chemical Engineering

Department of Chemical and Materials Engineering

Edmonton, Alberta
Spring, 1999

National Library of Canada
Acquisitions and Bibliographic Services
395 Wellington Street
Ottawa ON K1A 0N4
Canada

Bibliothèque nationale du Canada
Acquisitions et services bibliographiques
395, rue Wellington
Ottawa ON K1A 0N4
Canada

Your file Votre référence

Our file Notre référence

The author has granted a non-exclusive licence allowing the National Library of Canada to reproduce, loan, distribute or sell copies of this thesis in microform, paper or electronic formats.

L'auteur a accordé une licence non exclusive permettant à la Bibliothèque nationale du Canada de reproduire, prêter, distribuer ou vendre des copies de cette thèse sous la forme de microfiche/film, de reproduction sur papier ou sur format électronique.

The author retains ownership of the copyright in this thesis. Neither the thesis nor substantial extracts from it may be printed or otherwise reproduced without the author's permission.

L'auteur conserve la propriété du droit d'auteur qui protège cette thèse. Ni la thèse ni des extraits substantiels de celle-ci ne doivent être imprimés ou autrement reproduits sans son autorisation.

0-612-40097-2

Canada

University of Alberta

Library Release Form

Name of Author: Nikhil Rao

Title of Thesis: Interfacial Tension, Blending and Morphology of Linear Low Density Polyethylenes with Polypropylene.

Degree: Master of Science

Year this Degree Granted: 1999

Permission is hereby granted to the University of Alberta Library to reproduce single copies of this thesis and to lend or sell such copies for private, scholarly, or scientific research purposes only.

The author reserves all other publication and other rights in association with the copyright in the thesis, and except as hereinbefore provided, neither the thesis nor any substantial portion thereof may be printed or otherwise reproduced in any material form whatever without the author's prior written permission.

Nikhil Rao

Nikhil Rao

11025 Saskatchewan Drive
Edmonton, Alberta T6G 2B4

Date: 29 January, 1999

University of Alberta

Faculty of Graduate Studies and Research

The undersigned certify that they have read, and recommend to the Faculty of Graduate Studies and Research for acceptance, a thesis entitled **Interfacial Tension, Blending and Morphology of Linear Low Density Polyethylenes with Polypropylene** submitted by **Nikhil Rao** in partial fulfillment of the requirements for the degree of Master of Science in Chemical Engineering.

Sieghard E. Wanke (Supervisor)

Michael C. Williams

Celine T. Bellehumeur

Dongqing Li

Dated : 25 January, 1999

Dedicated to my dear Parents

"To me it suffices to wonder at these secrets and to attempt humbly to grasp with my mind a mere image of the lofty structure of all there is."

- Albert Einstein

Abstract

The research presented in this study deals with the relationships between interfacial properties, morphology and notched Izod impact strength of linear low density polyethylenes (LLDPE) and polypropylene (PP) blends with an aim to determine the effect of branch type, branch content, and branch distribution of LLDPEs on the blend properties. Eight commercial LLDPEs (of varying comonomer types 1-propene, 1-butene, 1-hexene and 1-octene), four prepared with metallocene catalysts and four prepared with Ziegler-Natta catalysts were used to prepare blends with a low molar mass PP. The branching distribution of LLDPEs was measured by analytical temperature rising elution fractionation (TREF) and the interfacial tensions (σ) at 200°C, 220°C and 260°C were measured using the breaking thread method. The interfacial tensions were in the range of $0.6 < \sigma < 2.6$ mN/m. Predictions of the interfacial tension using the group contribution approach assuming a uniform distribution of branches did not agree well with the experimental values. The scatter in the measured interfacial tension values indicated that interfacial tensions are not solely dependent on the branch type and branch content.

Izod impact strength was measured for blends containing 5, 10 and 20 wt% LLDPE. The fracture surfaces of the Izod specimen were analyzed for dispersed dropsizes using scanning electron microscopy (SEM). Some of the other features observed by SEM included fibers, web-like structures extending from droplets to the matrix cavity, and sheet-like co-continuous morphology. Some of these were attributed to plastic deformation and shrinkage of the LLDPE phase upon cooling.

The results of this study favour the 1-butene LLDPEs for impact modification of PP because the 1-butene LLDPEs showed the lowest interfacial tensions. The metallocene LLDPEs showed an advantage over the Ziegler-Natta polyethylenes at higher concentrations and a dramatic increase in the impact strength was observed for the 20% LLDPE/PP blends with the higher viscosity (η_{LLDPE}/η_{PP}) ratios. It was evident that the characterization of the LLDPEs was insufficient for a detailed interpretation of the observed phenomena and future studies should include a detailed characterization of both intermolecular and intramolecular heterogeneity in addition to short chain branching distributions.

Acknowledgments

I am indebted to Dr. Sieghard Wanke, my supervisor, for his guidance and support throughout the course of my Masters program. His accessibility for discussions, even while handling the demanding position of Department Chair is truly appreciated. I am also thankful to Dr. U. Sundararaj for providing direction during the initial phase of my work and continued interest in my research even after having joined GE Plastics. I thank my examining committee especially Dr. Celine Bellehumeur and Dr. Michael Williams for spending time to read my thesis thoroughly. Acknowledgments are also due to Dr. Thomas Yu of Exxon Chemicals, for providing metallocene LLDPE samples and polypropylenes as well as Dr. Peter Hoang and Dr. Shiv Goyal of Nova Chemicals for the Ziegler Natta LLDPE samples used in this study. I am also thankful to Imperial Oil for funding a part of this research.

I am also in gratitude for the support that the departmental staff has shown me. Many thanks are due to Mrs. Christina Barker for her ever accommodating help with SEM, Mrs. Naiyu Bu for carrying out GPC, Walter and Richard Boddez for spontaneously lending a hand with setting up equipment and the workshop staff including Bob Scott and Keith Faulder for carefully fabricating the visualization stand, TREF sample holder, Izod specimen and other items.

This research would also not have been possible without the help and support of many of my colleagues. These include, Mr. Long Wu for showing me the use of polymerization equipment and his insightful discussions on polyethylene behaviour, Mr. Parag Ghodgaonkar for sharing his expertise in blending, Mr. Ibnelwaleed Hussein and Mr. Weiyan Wang for providing me rheological measurements, Mr. Mingqian Zhang for sharing some of his TREF results and Mr. Mark Mulder for sharing his crystallinity data on the polymers used in this study. I am also thankful to Mr. Larry Unsworth for conducting experiments which later set the stage for my research.

Last but not the least, I thank my family for always giving me mental strength and my friends Manav and Deepika Lahoti, Rohit Patwardhan, the many wonderful denizens of 11025 Saskatchewan Drive including Apoorva Sharma, Andrew McCracken, Steve Sutankayo, Alan Wharmby, Ryan Harty, Ashish Malhotra, Sachin Kansal and Misha Monder and many others for providing a truly worthwhile stay at the University which I will cherish lifelong.

Table of Contents

Chapter 1: Introduction

1.1 Motivation 1

1.2 Overview of chapters 3

Chapter 2: Material Selection and Characterization

2.1 Introduction 5

2.1 Experimental methods and description 5

2.2.1 Melt Index 5

2.2.2 Molar Mass and MWD using GPC 4

2.2.3 Rheological properties of melts 6

2.2.4 Temperature rising elution fractionation 8

2.2.4.1 TREF-Experimental procedure 10

2.2.4.2 Interpretation of TREF profiles 13

2.3 Results and discussion 15

2.4 Recommendations and concerns 27

Chapter 3: Interfacial Tension and the Breaking Thread Method

3.1 Introduction 29

3.2 Polymer Interfacial Tension 30

3.2.1 Experimental methods of measuring polymer interfacial tension 30

3.2.2 Theoretical methods for predicting polymer interfacial tension 34

3.3 Breaking thread method 34

3.3.1 Theory 34

3.3.2 Equipment and Procedure 36

3.3.3 Calculations 40
3.4 Results 42
3.5 Discussion 46
3.6 Predictions of interfacial tension 59
3.7 Conclusions 64

Chapter 4: Morphology and Impact Strength of Blends

4.1 Introduction 67
4.1.1 Factors affecting the morphology of the dispersed phase 68
4.1.1.1 Process conditions affecting morphology 68
4.1.1.2 Material properties affecting morphology 70
4.1.2 Development of blend morphology 74
4.1.3 Fracture surface development 75
4.2 Experimental 76
4.2.1 Blending procedure 76
4.2.2 Izod impact test specimen preparation procedure 78
4.2.3 Scanning electron microscopy of blend samples 79
4.3 Results 83
4.3.1 Torque profiles in the Haake mixer 83
4.3.2 Results of impact strength testing using ASTM D256 83
4.3.3 Results from SEM 89
4.3.3.1 Morphological observations 89
4.3.3.2 Dropsize analysis 100
4.4 Discussion 106
4.4.1 Discussion of torque profiles 106
4.4.2 Fracture surface development 110
4.4.3 Factors affecting morphology 115
4.4.4 Morphological features and their origin 117
4.4.5 Effect of various factors on impact strength 120
4.4.6 Dropsizes 123

4.5 Summary and conclusions 125

Chapter 5: Summary, Conclusions and Future Work 128

References 133

APPENDICES

A TREF Details. 142

B LLDPE synthesis using slurry phase polymerization. 152

C Details of interfacial tension measurements. 165

D Izod impact testing of PP blends. 173

E Dropsize measurement using SEM. 175

List of Tables

2.1	Polymer porperties.	17
2.2	Copolymer content and methyl group concentration in LLDPEs.	23
3.1	Effect of thread phase additives on the interfacial tension between PS and PP1 at 200°C.	43
3.2	PP1/LLDPE interfacial tension results.	44
3.3	Molar volume and attraction constants for equation 3-7.	61
3.4	Prediction of interfacial tension from group contribution method.	63
4.1	Izod impact strength of PP blends at 23°C using ASTM D256-93.	86
4.2	Dropsize information obtained from SEM micrographs of fractured surfaces of LLDPE/PP blends.	101
4.3	Van Oene's criterion for drop-matrix morphology.	105
B.1	Conditions for slurry phase Ziegler-Natta polymerization of 1-butene copolymers in a 1 L reactor at 70°C.	157
C-II	Breaking thread method parameters and interfacial tensions of	
	(a) PP/PS systems at 200°C	167
	(b) PP1/PS systems with different contrast enhancing additives at 200°C	168
C-III	Breaking thread method parameters and interfacial tensions of	
	(a) PP1/LLDPE systems at 200°C	169
	(b) PP1/LLDPE systems at 220°C	170
	(c) PP1/LLDPE systems at 260°C	172
D.1	Izod impact testing of PP blends at 23°C using ASTM D256-93a	174

List of Figures

2.1	Typical molar mass distribution curve (GPC Profile).	7
2.2	Dynamics of crystallization and elution of polymer molecules.	9
2.3	TREF column and schematic of elution apparatus.	11
2.4	Typical TREF profile.	14
2.5	Complex viscosity of the polymers.	18
2.6	Complex elasticity of the polymers.	19
2.7	TREF profiles for LLDPE 1-4.	21
2.8	TREF profiles for LLDPE 5-8.	22
2.9	TREF profile at different elution rates and sample preparation temperatures.	26
3.1	Different methods for interfacial tension measurement	31
3.2	(a) Slotted plate and sample preparation	39
	(b) Observation set-up for breakup of the thread	39
3.3	Dimensionless distortion amplitude as a function of time.	41
3.4	Logarithm of dimensionless distortion amplitude as a function of time for various LLDPEs used in the breaking thread method with a PP1 thread.	41
3.5	Symmetric breakup observed for the PP1-LLDPE2o system at 220°C.	45
3.6	Effect of molar mass on interfacial tension of LLDPE/PP systems.	52
3.7	Effect of temperature on interfacial tension of LLDPE/PP systems.	52
3.8	Crystallization observed at interface during cooling of PP1-LLDPE5o system after breakup.	53
3.9	Asymmetric breakup of a PP1 thread inside an LLDPE1b matrix at 200°C shown along with the growth of dimensionless distortion amplitude with time.	56
3.10	Comparison of interfacial tension measurements (breaking thread method) with values reported by Carriere et al. (1997) and predictions obtained by the Helfland and Tagami method (1972).	62
3.11	Comparison of trends predicted by Flory Huggins Theory with Experimental results from the breaking thread method.	62

4.1	Morphology development in a polymer blend via dispersion.	74
4.2	Morphological zones in a rubber modified blend.	75
4.3	Haake mixing chamber.	77
4.4	Schematic of fracture surfaces originating from different procedures.	80
4.5	Effect of dispersed phase concentration on the mixer torque for LLDPE1b/PP1 blends prepared at 220°C.	84
4.6	Effect of dispersed phase concentration on the mixer torque for LLDPE2o/PP1 blends prepared at 220°C.	85
4.7	Izod impact strengths as a function of the dynamic viscosity ratio for LLDPE/PP blends.	87
4.8	Impact strength as a function of dispersed phase concentration.	87
4.9	Fracture surfaces of PI-Izod specimen showing increase in strength with amount of crazing for a 10% LLDPE2o/PP1 blend.	88
4.10	Changing morphology along the surface of a fractured Izod specimen of a 5% LLDPE1b/PP blend fractured at room temperature.	90
4.11	Morphological zones in thickness-wise fractured QFPI-Izod specimen of a 20% LLDPE8b/PP1 blend observed by SEM.	92
4.12	Morphology of fracture surfaces of metallocene LLDPE/PP blends prepared at 220°C.	94
4.13	Morphology of fracture surfaces of Ziegler-Natta LLDPE/PP blends prepared at 220°C.	95
4.14	Fibre formation in blends due to crazing or morphology development.	97
4.15	Shrinkage of the minor phase LLDPE causes cavitation in systems with low adhesion and formation of web-like structures in systems with strong adhesion at the interface.	97
4.16	Sheet-like morphology typical of co-continuous phases observed in A.) 10% LLDPE4p/PP1 and B.) 10% LLDPE6b/PP1.	99
4.17	Unusual features observed in some of the blends.	99
4.18	Effect of viscosity ratio (p) on dispersed drop diameter versus concentration for LLDPE1b/PP1 blends.	102
4.19	Concentration dependence of dispersed phase drop sizes for different LLDPE/PP1 blends at 220°C.	102
4.20	Unit cell chosen to estimate interparticle distance.	103

4.21 (a) Interparticle distance as a function of dispersed phase concentration. 104

(b) Interparticle distance as a function of viscosity ratio. 104

4.22 Breakup of a thread of LLDPE1b into droplets observed captured in a 20% LLDPE1b/PP1 blend after blending for 5 minutes at 220°C. 108

4.23 SEM pictograph of a QFAB 10% PP5/PS blend (p=1.2) sample showing coalescence of dispersed phase droplets. 108

4.24 Comparison of metallocene and Ziegler-Natta LLDPEs for impact modification of PP. 122

4.25 Capillary number as a function of viscosity ratio - Comparison of experimental observation with Newtonian limit predicted by Taylor and correlation given by Wu for blends processed in a twin screw extruder. 122

A-I (a) Temperature set points used for the programmable temperature controlled bath for crystallization. 143

(b) Temperature set points used in the programmable oven for TREF elution. 143

B.1 Schematic of the polymerization equipment. 154

B.2 (a) Process conditions for run NR5 in the steel reactor.(homopolymer) 160

(b) Process conditions for run NR3 in the steel reactor.(10ml 1-butene) 160

(c) Process conditions for run NR4 in the steel reactor. (20ml 1-butene) 161

(d) Process conditions for run NR6 in the steel reactor. (30ml 1-butene) 161

(e) Process conditions for run NR7 in the steel reactor. (40ml 1-butene) 162

(f) Initial process conditions while charging reactants for run NR6. (30ml 1-butene) 162

(g) Initial process conditions while charging reactants for run NR7. (40ml 1-butene) 163

B.3 (a) Complex viscosity of laboratory synthesized butene copolymers at 200°C and 10% strain. 164

(b) The effect of comonomer addition on the zero shear viscosity of butene copolymers. 164

C-I Tomotika's distortion function plotted against viscosity ratio 166

D.1 (a) Mold for Izod specimen and (b) Dimensions of Izod specimen. 173

E.1 Reducing an SEM pictograph to a bitmap file for dropsize analysis. 175

List of Abbreviations

ATREF	:	Analytical TREF
BTM	:	Breaking thread method
Coho	:	Copolymer - homopolymer (ratio)
eEPDM	:	Epoxidized EPDM
EPDM	:	Ethylene propylene diene methylene (elastomer)
FTIR	:	Fourier transform infra red (spectroscopy)
GPC	:	Gel permeation chromatography
H&T	:	Helfland and Tagami
HDPE	:	High density polyethylene
HPLC	:	High pressure liquid chromatography
i-PP	:	Isotactic polypropylene
ID	:	Interparticle distance
IR	:	Infra red
LLDPE	:	Linear low density polyethylene
MI	:	Melt Index
MSL	:	Methylene sequence length
NMR	:	Nuclear magnetic resonance
o-DCB	:	Ortho - dichloro benzene
PE	:	Polyethylene
PI	:	Post impact (Izod specimen)
PP	:	Polypropylene
PS	:	Polystyrene
PTREF	:	Preparative TREF
QFAB	:	Quench fractured as-blended (Izod specimen)
QFPI	:	Quench fractured post impact (Izod specimen)
SEC	:	Size exclusion chromatography
TREF	:	Temperature rising elution fractionation
ZN	:	Ziegler-Natta

List of Symbols

a	:	Diameter at trough of sinusoidal distortion on thread
A	:	Amplitude of distortion
A_{disp}	:	Fractional area of dispersed phase present on fracture surface
b	:	Diameter at crest of sinusoidal distortion on thread
B	:	Effective length of monomer unit
Ca	:	Capillary number
D	:	Diameter of dispersed phase droplet
D_{avg}	:	Average diameter of thread at any instant during breakup
D_o	:	Initial diameter of thread
F*	:	Molar attraction constants
G"	:	Elastic loss modulus (Coeff. of complex part)
G'	:	Elastic storage modulus (Coefficient of real part)
ID	:	Interparticle distance
k	:	Boltzmann constant
M	:	Molar mass
m	:	Weight of monomer segment
M_n	:	Number averaged molar mass
M_w	:	Weight averaged molar mass
N	:	Number of droplets analysed on a fracture surface by SEM
N_1	:	First normal stress difference
p	:	Viscosity ratio
Pd	:	Polydispersity
q	:	Time constant for exponential growth of distortion
r_o	:	Unperturbed end to end distance
T	:	Temperature
T_{Coho}	:	Copolymer - homopolymer transition temperature
V*	:	Molar volume constants
Vr	:	Reference volume

Greek Symbols

$\dot{\gamma}$	:	Shear rate
$\sigma_{12}^{\infty M}$	:	Interfacial tension between phases 1 and 2, at infinite molar mass
α	:	Dimensionless amplitude of distortion
χ	:	Wavenumber of distortion
χ_{FH}	:	Flory-Huggins chi parameter
χ_m	:	Wavenumber of the dominant perturbation predicted by Tomotika
δ	:	Hildebrand solubility parameter
η	:	Viscosity
η^*	:	Dynamic (complex) viscosity
η_{65}	:	Viscosity at 65 s^{-1}
η_d	:	Dispersed phase viscosity
η_m	:	Matrix viscosity
η_o	:	Zero shear viscosity
φ	:	Volume fraction
λ	:	Wavelength of distortion in thread
ρ_o	:	Number of monomer units per cm^3
σ	:	Interfacial tension
σ_{12}	:	Interfacial tension between phases 1 and 2
σ_{mp}	:	Most probable interfacial tension
ω	:	Frequency
Ω	:	Tomotika's distortion function
Ω_m	:	Tomotika's distortion function corresponding to the dominant perturbation
ψ	:	Phase lag between signal and response while testing a viscoelastic material

Introduction

Chapter 1

1.1 Motivation

In the past decade there has been increasing interest in studying the behavior of linear low density polyethylenes (LLDPE). This has been fueled by technological advances in polymerization catalysis as well as high-tech applications requiring superior performance and high reliability and robustness of the materials used. The local industry in Alberta has seen continuous expansions in petrochemicals and polymers. This trend is continuing with the upcoming expansions in ethylene and polyethylene related activities in the Joffre (NOVA Chemicals, Amoco and Union Carbide) and Fort Saskatchewan (Dow Chemicals) regions. A majority of these expansions will be directed towards production of LLDPE using technology such as the Advanced Sclairtech process of Nova Chemicals, the Insite technology of Dow, and the Unipol II process at Union Carbide. The global increase in annual LLDPE consumption is around 5% and the last ten years have always seen demand surpass supply. Therefore, the study of LLDPE properties and applications is of great industrial importance.

One area of application for polyethylenes is in blends with polypropylene (PP). PPs are used in a variety of applications including automotive bumper facia, stretch bags, and injection molded parts. PP possesses useful properties such as solvent resistance, transparency, UV resistance and hardness. The addition of polyethylene adds strength and toughness to the blend. Conventional impact modification of PP is carried out by adding EPDM (ethylene-propylene-diene-methylene copolymer) or EPR (ethylene-propylene rubber) (Utracki, 1995); both EPDM and EPR are rubbery copolymers with fairly high

molecular weight. The development of low molar mass PP for achieving higher throughput causes a mismatch in the viscosity resulting in poor dispersion of one phase in the other (Yu, 1995). Recent developments in polyethylene synthesis allow for narrow molar mass distribution of LLDPEs and superior control over the branching distribution. This allows for a highly branched yet free-flowing polymer which can be processed using existing plastics processing equipment (Dharmarajan and Yu, 1996). The current research was carried out to determine which properties influence the strength of LLDPE/PP blends the most and whether the use of commercial LLDPEs is viable for blending with PP for strength and toughness enhancement.

There have been several attempts at studying the phase miscibility and blend properties of PE/PP blends in the past and the greatest cause for concern has been the incompatibility of the two materials. Various methods have been used to remedy this problem, which include, using compatibilizers (Cser et al., 1997) and graft copolymers (Datta and Lohse, 1993), peroxide aided crosslinking (Chiu and Fang, 1985, Kim, 1996) and ternary blends (Kesari and Salovey, 1984). However, early attempts at characterizing LLDPE/PP blends indicated a partial compatibility even without the addition of a block copolymer (Kryszewski et al., 1973, Dumoulin et al., 1984). Bains et al. (1994) have observed that matching the viscosity of the blend components resulted in higher performing LLDPE/PP blends. It is desirable to know what attributes of LLDPE lead to greater strength and compatibility of these blends.

LLDPEs are synthesized by copolymerizing ethylene with α-alkenes such as 1-butene, 1-hexene and 1-octene. Two broad classes of catalysts namely, Ziegler-Natta catalysts and metallocene catalysts and a host of processes including gas-phase, slurry-phase and solution-phase polymerization are used to manufacture LLDPEs. Both short chain branching and molar mass distributions have long been known to vary among different processes. More recently however, the short chain branching in LLDPEs has been identified as the more important factor controlling its properties. In this study

LLDPEs of varying comonomer type and distribution, made with both Ziegler-Natta and metallocene catalysts have been used to explore their effect on LLDPE/PP blends.

Most past studies (Elmendorp, 1986, Elemens et al. 1989) strongly support the role of interfacial tension in determining blend morphology in addition to other factors such as viscosity ratio (Favis and Chalifoux, 1987), composition (Favis and Willis, 1990, Favis and Chalifoux, 1988) and processing conditions (Favis, 1990). This study deals qualitatively with the relation of properties such as molar mass, branching density and branch length on bulk properties such as interfacial tension and impact strength of LLDPE/PP blends.

1.2 Overview of Chapters

The first part of this study, presented in Chapter 2, deals with characterization of the polymers used. A special emphasis has been placed on characterizing the branching distribution using temperature rising elution fractionation (TREF). Rheological and molar mass measurements are also included. Initial efforts towards synthesizing Z-N LLDPEs for the study, using a slurry phase process, are summarized in Appendix B.

An overview of different interfacial tension measurement techniques has been presented in Chapter 3 along with interfacial tension measurements for different systems using the breaking thread method (Tomotika, 1935). Theoretical predictions of the interfacial tension were also obtained by applying group contribution methods to branching information obtained from TREF.

Finally, in Chapter 4, results on blend preparation and relation of blend impact strength to various parameters are presented. Scanning electron microscopy (SEM) was used to measure and compare the dispersed phase dropsizes for LLDPE/PP blends in the viscosity ratio (η_{LLDPE}/η_{PP}) range 1-10. Morphological observations of the fracture surfaces have been summarized. The interparticle distance, which has also been found to

affect blend ductile-brittle transition (Wu, 1985), was computed using a simple cubic model. Conclusions and a summary of observations are presented in Chapter 5.

Material Selection and Characterization

Chapter 2

2.1 Introduction

This chapter presents the characterization of all the commercial polymers used in this study. The characterization techniques include molar mass distribution using gel permeation chromatography (GPC), rheological properties such as dynamic viscosity, elasticity and melt index, crystallinity using X-ray diffraction, and finally branching distribution using temperature rising elution fractionation (TREF). A considerable amount of the chapter is focused on TREF as the emphasis of this thesis is to explore the effect of branching of polyolefins on their interfacial behavior.

2.2 Description and Experimental Procedures

2.2.1 Melt Index

Melt index (ASTM D1238) or MI is the measure of the rate (g / 10 min) of polymer extruding through a standard die under a standard load. When chemical structures are similar, MI provides a good indication of the molar mass (M_w) and is used as a quality control tool in industry. Bremner et al. (1990) have reported an inverse relationship between MI and weight averaged molar mass raised to the power of 3.4 - 3.7. Ghosh et al. (1996) and Huang et al. (1997) have confirmed this behavior for various polyethylenes. The choice of polymers for this study was initially made based on their melt indices.

2.2.2 Molar Mass and Molar Mass distribution Using GPC

Gel permeation chromatography is one of the many size exclusion methods used to measure the molar masses and molar mass distribution of polymers based upon their molecular size in a solvent. For GPC analysis the polymer is dissolved in a solvent and the solution is injected in a stream of the solvent flowing through a packed column filled with packing having a range of pore sizes. The polymer concentration of the eluting solution is monitored as a function of time. The large molecules elute first since they cannot diffuse into the smaller pores; the smallest molecules elute last. The molar mass is a function of the elution time and is obtained from calibration curves. The molar mass properties of polymers are usually summarized in terms of number average molar mass (M_n) and mass average molar mass (M_w). The ratio of M_w/M_n is the polydispersity (Pd) which is an indication of the breadth of the molar mass distribution. A typical molar mass distribution curve is shown in Figure 2.1.

In the current study, a Waters 150-C ALC/GPC unit fitted with four Shodex UT-806MS columns, containing crosslinked polystyrene packing, was used to measure the molar mass distribution. Waters Maxima 820 software was used to analyze the GPC data. The eluting solvent was 1,2,4 trichlorobenzene with 2, 6 ditertiary butyl, 4 methyl benzene as an antioxidant and elution was carried out at 140°C. The equipment and conditions used was the same as that used by Jejelowo et al. (1991), but the columns were different. The universal calibration curve was based on standard polystyrene reference samples of known molar masses and standard linear polyethylene samples.

2.2.3 Rheological Properties of Melts

The response of a pure elastic solid to applied stress is expressed by Hooke's law which states that the strain is proportional to the applied stress. Similarly, pure

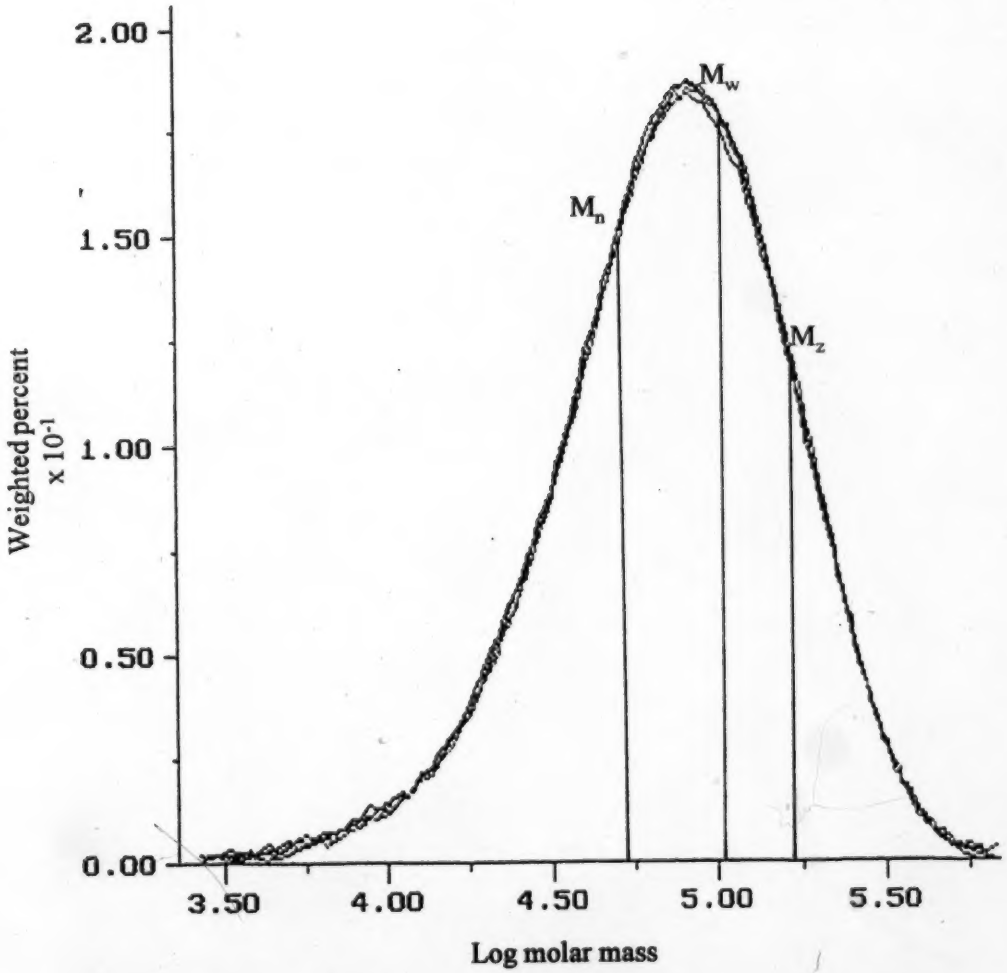

Figure 2.1 Typical molar mass distribution curve (GPC profile for LLDPE2o).

Newtonian fluids have been shown to follow a simple relation which states that the rate of strain is proportional to the stress applied on the fluid as fluids have the capability to flow. Polymers, in general, exhibit an intermediate behavior depending on the temperature, their molecular size and structure and the timescale of deformation and are said to be 'viscoelastic' in nature. Viscoelastic properties are measured by dynamic mechanical testing which involves measuring stress as a function of strain that is a periodic function of time.

Rheological testing was carried out on the RMS800 Rheometrics rheometer using 25 mm diameter parallel plate fixtures for shearing the sample. The polymer samples were compression molded into circular plates of 25 mm diameter and 2 mm thickness using a Carver laboratory press at 200°C and 10 kPa pressure. The polymer samples were placed between the parallel plates of the rheometer at room temperature and heated to the desired test temperature. The polymer was deliberately squeezed out upon melting by bringing the plates closer, in order to wet the parallel plates properly. The excess material was skimmed off from the plate edges to avoid end effects.

Two basic dynamic testing routines are possible for studying the response of the polymer to torsional small amplitude shear in a parallel plate geometry. These are : Frequency sweeps - which involve shearing the polymer over a range of different frequencies at a fixed strain; and strain sweeps - which involve shearing the polymer at a fixed oscillatory frequency to different strains to note the viscoelastic response. In order to determine the Newtonian characteristics of the polymer, one must be in the linear response zone and this must be determined from the strain sweep at a low frequency.

2.2.4 Temperature Rising Elution Fractionation

Temperature rising elution fractionation (TREF) is a technique to classify molecules based upon their crystallizability (Wild, 1991). With the commercialization of LLDPE, this method has been gaining popularity for characterizing the branching

distributions in LLDPEs (Wild et al., 1982, Karbashewski et al., 1991, Lacombe, 1995). Wild (1991) has given a detailed review of TREF techniques. TREF is a two step technique consisting of crystallization and elution. The polymer is first dissolved in a suitable solvent at an elevated temperature in order to disentangle the chains and subsequently cooled in a controlled manner. During the cooling, the temperatures at which different molecules crystallize depends on the branching present in each molecule. The linear molecules crystallize at higher temperature, and branched polymers have poor packing capability and crystallize at lower temperatures. The gradual decrease in temperature facilitates a regular crystallization of molecules based upon their crystallinity (Fig. 2.2). Once the material has been crystallized, it is ready for the elution step.

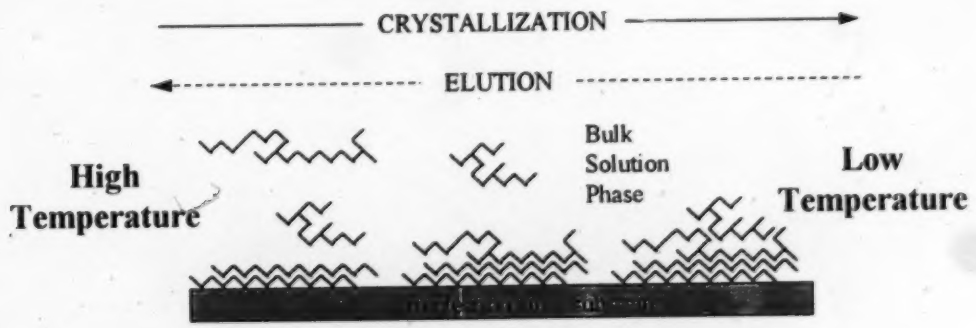

Figure 2.2 : Dynamics of crystallization and elution of polymer molecules.

The procedure for elution is the reverse of the crystallization steps. For elution, the sample is collected in a column and dissolved in a solvent flowing through the column. The elution temperature is increased gradually leading to fractionation of the material based upon the solubility of its crystallized constituents. The eluting solution is passed through an Infrared (IR) detector to measure the amount of material eluting at a certain temperature. This analysis is termed as analytical TREF (ATREF). The term preparative TREF (PTREF) is used when fractions of the polymer eluted at different temperatures are collected for subsequent analysis by techniques such as SEC, FTIR or NMR (Defoor, 1993, Mirabella and Ford, 1987).

The approach adopted in this study was to perform ATREF on the LLDPE samples and measure branching by using the elution temperature - CH_3/1000C calibration curve of Huang et al. (1997), who used the same TREF equipment as the present study.

2.2.4.1 TREF-Experimental Procedure

A polymer sample, typically 5 mg, was weighed using a Mettler HL52 electronic balance and placed in a 15 mL vial. A solvent volume of 1 mL/mg polymer was added to the sample. The solvent used in this case was o-xylene owing to its capability to dissolve polyethylene at lower temperatures than most other known solvents. This ensures a safer experiment along with less degradation of the polymer sample. A disposable Teflon coated stirrer was also enclosed along with other contents in the vials and sealed with a Teflon lined rubber seal and capped with an aluminium cap. In some cases, a small amount (0.6 g) of 100 mesh size glass beads was also added to make the transfer of the precipitated polymer easier. The dissolution of the polymer in o-xylene was carried out for two hours at 125°C in a silicone oil bath placed on a Thermolyne Type 1000 hot plate. The number of vials inside the bath is maximized without obstructing the circulation of heating fluid. The fluid erases the permanent marker labels on the vials thus the vials must bear engraved labels on the aluminium cap for identification. The level of the heating fluid was maintained below the mouth of the vial to minimize chances of sample contamination due to leakage.

The crystallization step was carried out in a temperature controlled bath with diethylene glycol as the circulation fluid, cooled from an initial temperature of 125°C down to -10°C at a rate of 1.5°C/hr (see Appendix A-I (a)). The run took 90 hours to complete. The bath was an Endocal RTE 220 bath/circulator with a M-RS-232 interface connected to a PC for temperature monitoring. The same equipment was used by Chakravarty (1993), Lacombe (1995) and Huang et al. (1997) in previous studies. A special stand was designed to hold the samples in place against the buoyant effects of the

air inside the vials. The level of the heating liquid was again maintained below the level of the mouth of the vials. This is especially critical this time because a vacuum might be created upon reducing temperature if any o-xylene escaped during the dissolution step. The stand was completely immersible inside the bath and this ensured that the lid formed a proper seal. This avoided the loss of the diethylene glycol vapour during the four day long crystallization step, thus avoiding both material loss as well as environmental pollution. The vials were then stored in a freezer at -10°C until subsequent elution.

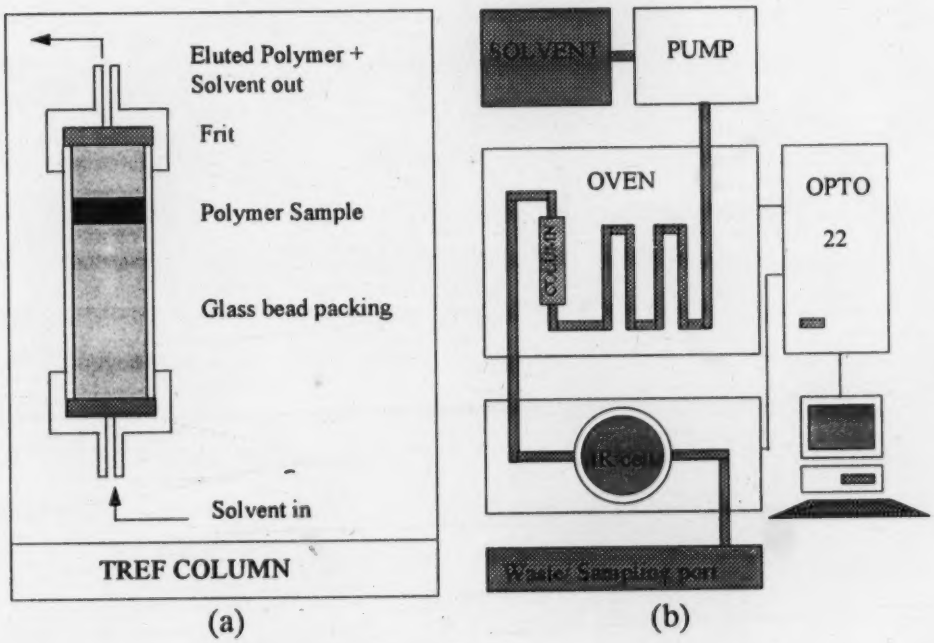

Figure 2.3 : (a) TREF Column. (b) Schematic of TREF elution apparatus.

For the elution step a 10 mm O.D. and 6 mm I.D., 40 mm long stainless steel column with Swagelock fittings was used. Sintered frits of pore size 5 μm and 10 μm were inserted at the entrance and exit of the column respectively (see Fig. 2.3(a)). The fittings had to be machined to allow the frits to sit tight against the union and to form a good seal with the column walls. Glass beads, enough to fill the column, were pre-

measured in the column and set aside. One quarter the amount was added back in the column to form a filter-bed. Cold acetone was used to knock out all the crystallized polymer and wash it out from the vial through a funnel into the column. Mild vacuum was applied using a water jet pump. The funnel had to be sealed to the column with Teflon tape to prevent leakage from the sides. A portion of the pre-measured glass beads was poured into the vial and used as an abrasant to scrape out any polymer crystallized on the wall of the vial. Again, acetone was used to clean out the vial. Low molar mass molecules dissolve at a lower temperature hence can be lost with the solvent while loading the column. This could lead to a reduction in the low molecular weight fraction. This problem can be avoided in the in-column crystallization procedure used by some researchers (see Lacombe, 1995) but the efficiency, both in terms of time and uniformity of crystallization conditions, while processing a large number of samples is much better with the batch off-column crystallization procedure used in the current study. After the crystallized polymer was deposited into the column, the rest of the glass beads were tightly packed into the column and capped with a 5 μm frit and the Swagelock reducing union. The slug remained closer to the exit 10 μm frit to get a uniform flow and avoid channeling and entrance effects. An air jet was used to blow away any glass beads sticking between the threads of the fittings as they caused improper sealing. The column entrance frit pore size is not critical, but exit frit pore size should be such that it allows eluted molecules to pass without hindrance to flow.

The column was attached to a copper tubing inside a temperature controlled oven (Fig 2.3(b)). Details of the equipment can be obtained from Lacombe (1995). An HPLC pump was used to pump the eluting solvent ortho di-chlorobenzene (o-DCB) through a long copper tubing, at a flowrate typically in the range 0.5 - 2 ml/min. A sufficient length of tubing was allowed for the solvent to reach the oven temperature, before solvent entered the column. During the temperature ramping, the light bulb inside the oven acted as a heat source and was used with discretion so as to keep heating uniformly convective. Temperature was monitored by thermocouples inserted at the entrance, at the outer wall of the middle section and at the exit of the column though the exit temperature was used

as the eluting temperature. The eluting temperature range was 25°C to 125°C in most cases, with a heating rate of 1°C/min. While eluting metallocene PEs, the temperature ramping was started at a temperature of 0°C. This was done to avoid loss of low molecular weight, highly branched material eluting at low temperatures.

The eluted polymer solution travels through a short tube connecting the TREF column to an infra red (IR) detector cell equipped with CaF_2 windows. A tape heater wrapped around the tube was used to raise the solution temperature to 125°C before it entered the detector. The IR detector was set to detect the CH_2 stretch wavelength at 3.37 μm. According to Lacombe (1995), this frequency shows the maximum contrast between absorbances of the polymer and the solvent. The absorbance of the IR signal by the solution is a measure of the mass concentration of polymer eluting. The connecting tubing from the column to the IR cell was narrow to minimize backmixing and time lag in measuring the IR signal of the polymer eluting at the oven temperature. An Opto22 interface was used to collect the cell pressure, column and cell temperatures and IR measurement on a PC. Figure (2.4) shows a typical TREF profile of IR signal plotted against the eluting temperature. The profiles were normalized by subtracting the baseline signal and dividing this reduced IR signal by the area under the reduced IR-T curve. The normalized IR signal represents the weight fraction of a particular fraction eluting at a particular temperature.

2.2.4.2 Interpretation of TREF profiles

The branching distribution of the LLDPEs was estimated by comparing the eluted temperature against fractions of known branch distributions. A correlation of the number of methyl groups per 1000 carbon atoms (total) and elution temperature (T_{el}) was given by Huang et al. (1997) for straight chained PEs. The idea of a methylene sequence length (MSL) as the main responsible parameter for crystallization was presented by Bonner et al. (1993). The MSL is the number of bond lengths of crystallizeable sequence between

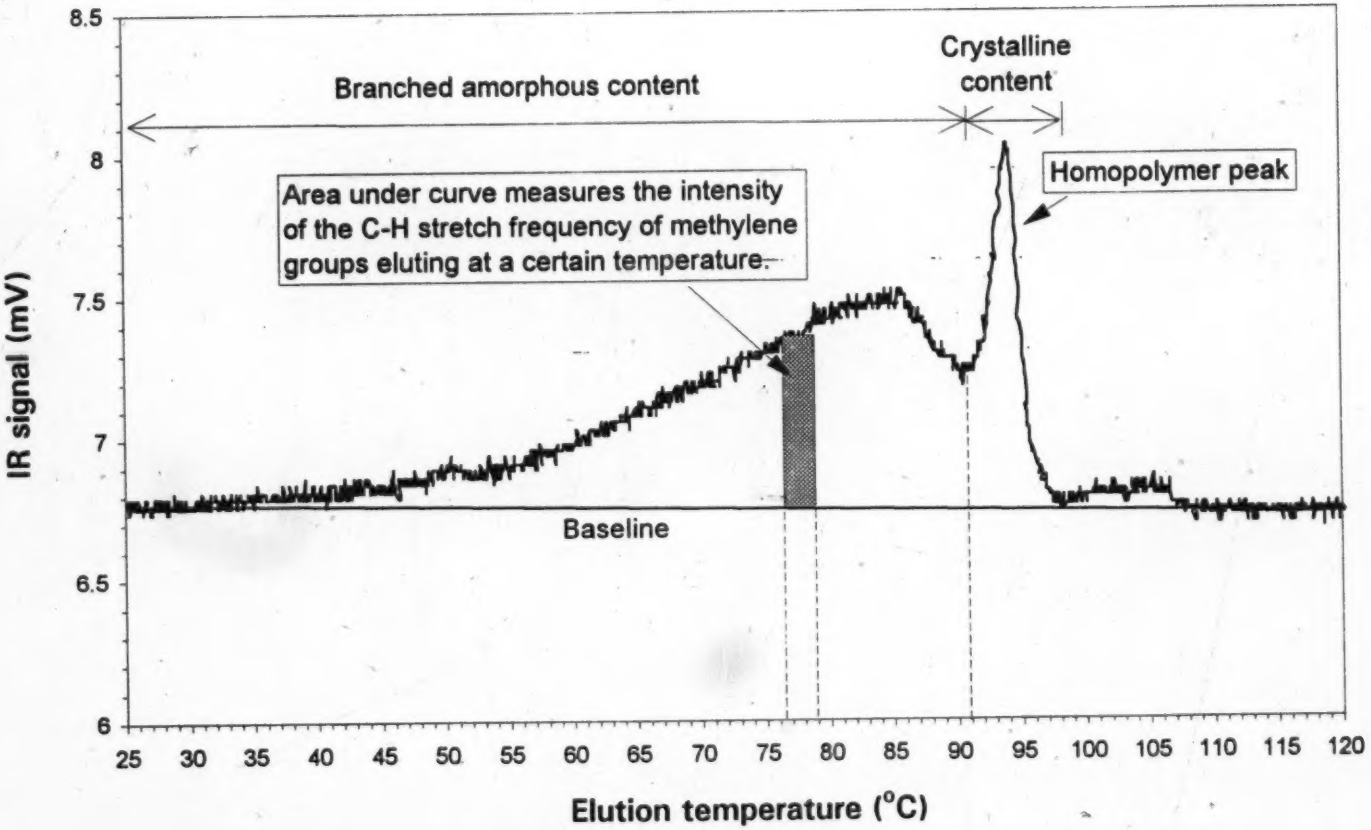
Branched amorphous content
Crystalline content
Homopolymer peak
Area under curve measures the intensity of the C-H stretch frequency of methylene groups eluting at a certain temperature.
Baseline
IR signal (mV)
8.5
8
7.5
7
6.5
6
25 30 35 40 45 50 55 60 65 70 75 80 85 90 95 100 105 110 115 120
Elution temperature (°C)

Figure 2.4 : A typical TREF profile.

short chain branches. This was correlated with the Flory melting equation to obtain an equation of the form:

$$\frac{1}{T_{el}} = \frac{1}{T_o} + c\frac{\ln(MSL)}{MSL} \qquad (2\text{-}1)$$

Huang et al. (1997) reported values of the parameters as T_o= 374.1 K; c=0.006583;

The constants for the above equation were found by Huang et al. (1997) by correlating data from laboratory and commercial samples with the Bonner equation. Furthermore, for straight chained PEs the MSL is related to the CH_3/1000C as

$$\frac{CH_3}{1000C} = \frac{2000}{MSL + 2} \qquad (2\text{-}2)$$

The analytical form for short chain branched PEs changes slightly for different comonomer types but the above correlation (Eq. 2-2) was shown by Lacombe (1995) to describe experimental and literature data reasonably well for most copolymer types. The CH_3/1000C is estimated using these equations for the current set of polymers.

2.3 Results and Discussion

Initially, polyethylenes with varying comonomer content were synthesized using a Ziegler-Natta catalyst provided by Nova Chemicals, in a 1 L reactor using slurry phase polymerization. These polymers had high molecular weight and low yields; hence, it was decided that commercial samples were more suitable for this study. The synthesis conditions and characterization results for these LLDPEs are given in Appendix B.

Eight LLDPEs were evaluated using the methods described above. LLDPE 1 to 4 are obtained with metallocene catalyst while LLDPEs 5 to 8 were obtained with Ziegler-Natta catalysts. The ending letters indicate the type of comonomer (p - propene, b -

butene, h - hexene, o - octene). LLDPE5o was a butene-octene terpolymer. The melt index, number average molar mass (M_n), weight average molar mass (M_w) and the polydispersity ($Pd = M_w/M_n$) are tabulated in Table 2.1 for all the LLDPEs used in this study.

The M_w of all the polymers are in the 85000-110000 range with the exception of LLDPE 4p which had a much lower M_w of 58000. All LLDPEs made with metallocene catalysts, had lower polydispersity than the LLDPEs made with Ziegler-Natta catalysts. The octene copolymer, LLDPE2o, has a very narrow molecular weight distribution with a polydispersity of only 2.0. LLDPE4p shows a much higher polydispersity than the other metallocene LLDPEs probably due to multi-reactor synthesis. Most of the LLDPEs made with Ziegler-Natta catalysts had a polydispersity close to 3.3.

Frequency sweeps were performed from 0.1 to 100 rad/s at a strain of 10%. It was verified that the polymers were in the linear response region for this value of strain. A reliable estimate of $\eta(\dot{\gamma})$ can be obtained by using the Cox-Merz rule (Ghodgaonkar, 1997) which states that $\eta(\dot{\gamma}) \equiv |\eta^*(\omega)|$ with $\dot{\gamma} \equiv \omega$. Scott (1990) has estimated the shear rate to be 65 s^{-1} in the Haake Rheocord batch 600 mixing chamber (Fig. 4.3). The viscosity at zero shear, η_o, and viscosity at 65 rad/s, η_{65}, at different temperatures are tabulated for LLDPEs in Table 2.1. The Cross model (1968) (Eq. 2-3) was fitted to the data for the LLDPEs and the PP used in this study.

$$\eta = \frac{\eta_o}{1+(\tau\omega)^n} \qquad (2\text{-}3)$$

Cross model with parameters τ and n; η : viscosity; ω : frequency;

Complex viscosity ($|\eta^*|$) and elasticity (G') at 220°C for the LLDPEs used have been plotted as functions of frequency in Figure 2.5 and 2.6, respectively. Elastic effects at 0.1 rad/s were negligible as ψ was close to 90°. In the mathematical analysis, $\tan(\psi)$ is

Table 2.1 : Polymer Properties.

Polymer	*Trade Name*	*Mfr. (density) g/cm³*	*MI dg/min*	*M_n gm/mol x 10^{-3}*	*M_w gm/mol x 10^{-3}*	*Pd*	*η_o at 200°C x 10^{-3}*	*η_{65} at 200°C x 10^{-3}*	*η_o at 220°C x 10^{-3}*	*η_{65} at 220°C x 10^{-3}*	*η_o at 260°C x 10^{-3}*
LLDPE1b	Exact 4033	Exxon (0.880)	0.8	51.9	110	2.14	11.7	1.9	9.3	2.7	7.2
LLDPE2o	Engage 8100	Dow (0.870)	1.0	54.0	108	2.00	-	-	7.0	1.7	-
LLDPE3h	SLP9095	Exxon (0.885)	2.2	40.4	86	2.14	-	-	2.3	1.5	-
LLDPE4p	SLP9029	Exxon (0.870)	4.0	18.2	58	3.17	-	-	0.5	0.3	-
LLDPE5o	Sclair 13J7	Nova (0.918)	1.0	28.4	97	3.43	28.7	1.7	11.6	1.8	6.3
LLDPE6b	PF0118	Nova (0.918)	1.0	32.5	107	3.29	8.4	1.9	6.2	1.7	-
LLDPE7h	TF0119	Nova (0.918)	1.0	32.3	106	3.28	8.7	1.9	6.4	1.5	4.9
LLDPE8b	PF0218	Nova (0.918)	2.0	25.9	85	3.29	4.8	1.3	3.9	1.1	3.0
PP1	Escorene 1105	Exxon (0.90)	35.0*				0.30	0.20	0.39	0.3	0.15
PP1c **			-				-	-	0.34	0.2	-
PP2	Escorene 1154	Exxon (0.90)	12.5*				0.66	0.31	-	-	-
PP3	Escorene 1012	Exxon (0.90)	5.0*				0.79	0.33	-	-	-
PP4	3050	Elf Atochem	-		60		3.30	0.84	2.30	0.5	-
PP5	Escorene 1042	Exxon (0.90)	1.7*				13.7	1.14	-	-	-
PS	PS666D	Dow			200		7.1	0.95	2.20	0.6	

η_o : $|\eta^*(\omega)|$ at $\omega \rightarrow 0$ rad/s.

M_w : Weight average molar mass.

MI : Melt Index (decigrams of polymer extruded through a die in 1 minute at 190 °C).

* : Melt flow rate at 230°C / 2.16 kg.

** : PP1 blended with 0.2% (wt) carbon black (from Cabot - Vulcan XC72 GP 2295).

η_{65} : $|\eta^*(\omega)|$ at $\omega = 65$ rad/s.

M_n : Number average molar mass.

Pd : Polydispersity (= M_w / M_n).

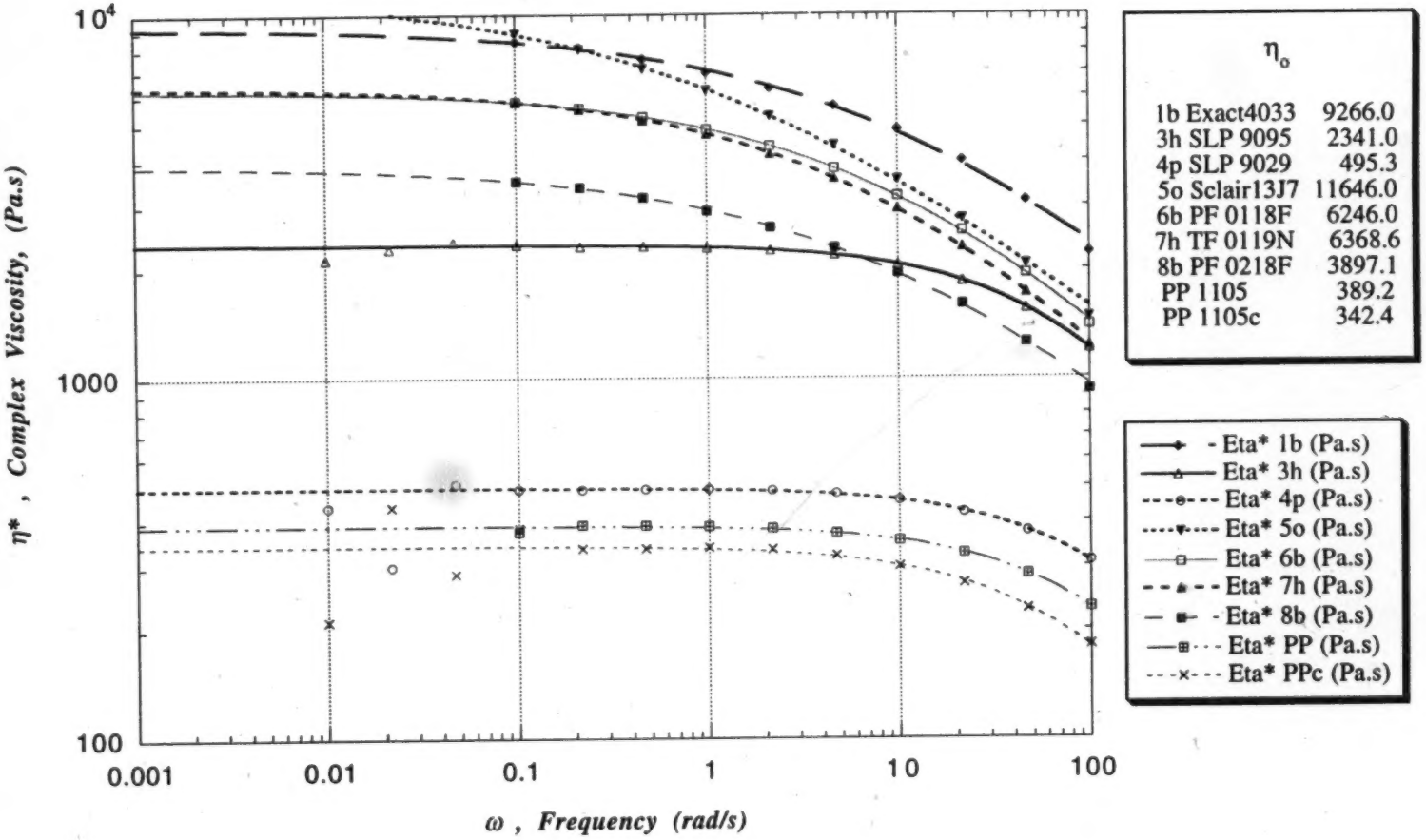

Figure 2.5 Complex viscosity at 220°C as a function of frequency from frequency sweeps at 10% strain. Cross Model (1970) for obtaining zero-shear viscosity.

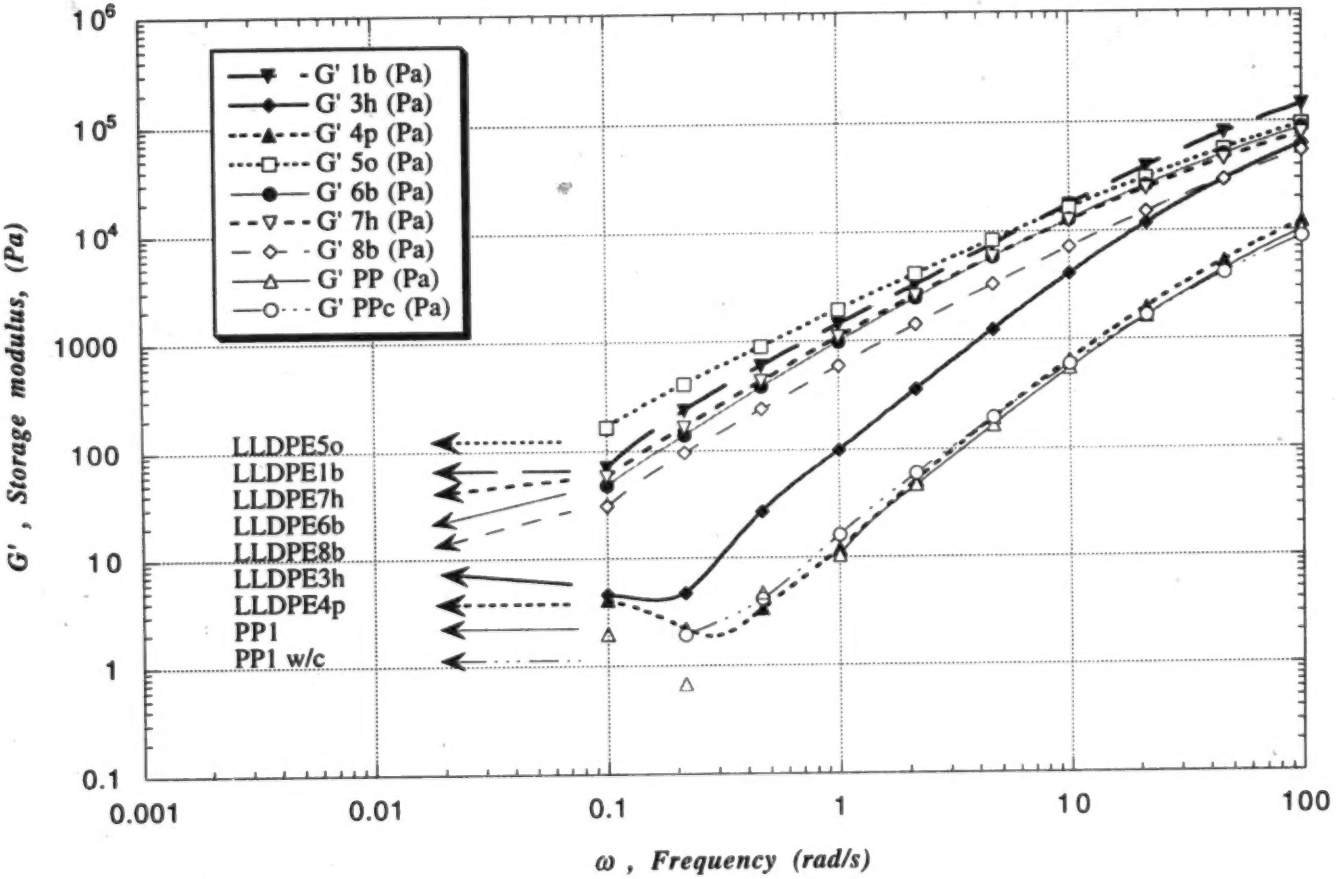

Figure 2.6 Elastic storage modulus as a function of frequency. (Frequency sweep at 10% strain and 220°C)

the ratio of the storage modulus to the loss modulus and a ψ value close to 0° means purely elastic response, while a value close to 90° implies a purely viscous response. This is important for ruling out the presence of elastic stresses at low shear during the breaking thread method which assumes that the polymer behaves like a Newtonian fluid.

The addition of fillers generally increases the zero shear viscosity of pure polymers. In our case, however, the carbon black filled sample, PP1c, had lower viscosity than the pure PP1 sample. Lakdawala and Salovey (1987) have also observed this phenomenon in carbon black filled polystyrene samples. They termed this behaviour as pseudoplasticization and observed that conditions of high temperature, high shear rate and high molar mass of pure polymer along with low concentration and low surface area of carbon black proved favorable for this behaviour. The reason for this phenomenon is still unexplained.

TREF runs were performed for LLDPEs made both with Ziegler-Natta (Z-N) catalysts and metallocene (M) catalysts. The raw TREF data was rather noisy (frequency of data acquisition was 3 s). This short sampling time resulted in noise in temperature and IR signals at low elution rates. The resolution at higher elution rates would however have suffered if the sampling time were increased. A computer program was used to correct this problem by filtering out unreal temperature decreases and averaging the IR signal for repetitive temperature readings. A copy of this program is given in the Appendix A-II (a). Figure 2.7 shows the TREF profiles for M-LLDPEs (1-4) and Figure 2.8 shows the TREF profiles for Z-N LLDPEs (5-8). All the Z-N LLDPEs show greater crystallinity than metallocene LLDPEs.

From Figure 2.7, it can be seen that the hexene copolymer, LLDPE3h, has a higher peak elution temperature than the other metallocene polymers while both LLDPE2o and LLDPE4p have low peak elution temperatures. The lower the elution temperature, the greater the branching. This implies both LLDPE2o and LLDPE4p are highly branched. X-ray results (see Table 2.2) by Mulder (1999) confirm that LLDPE3h has high crystallinity

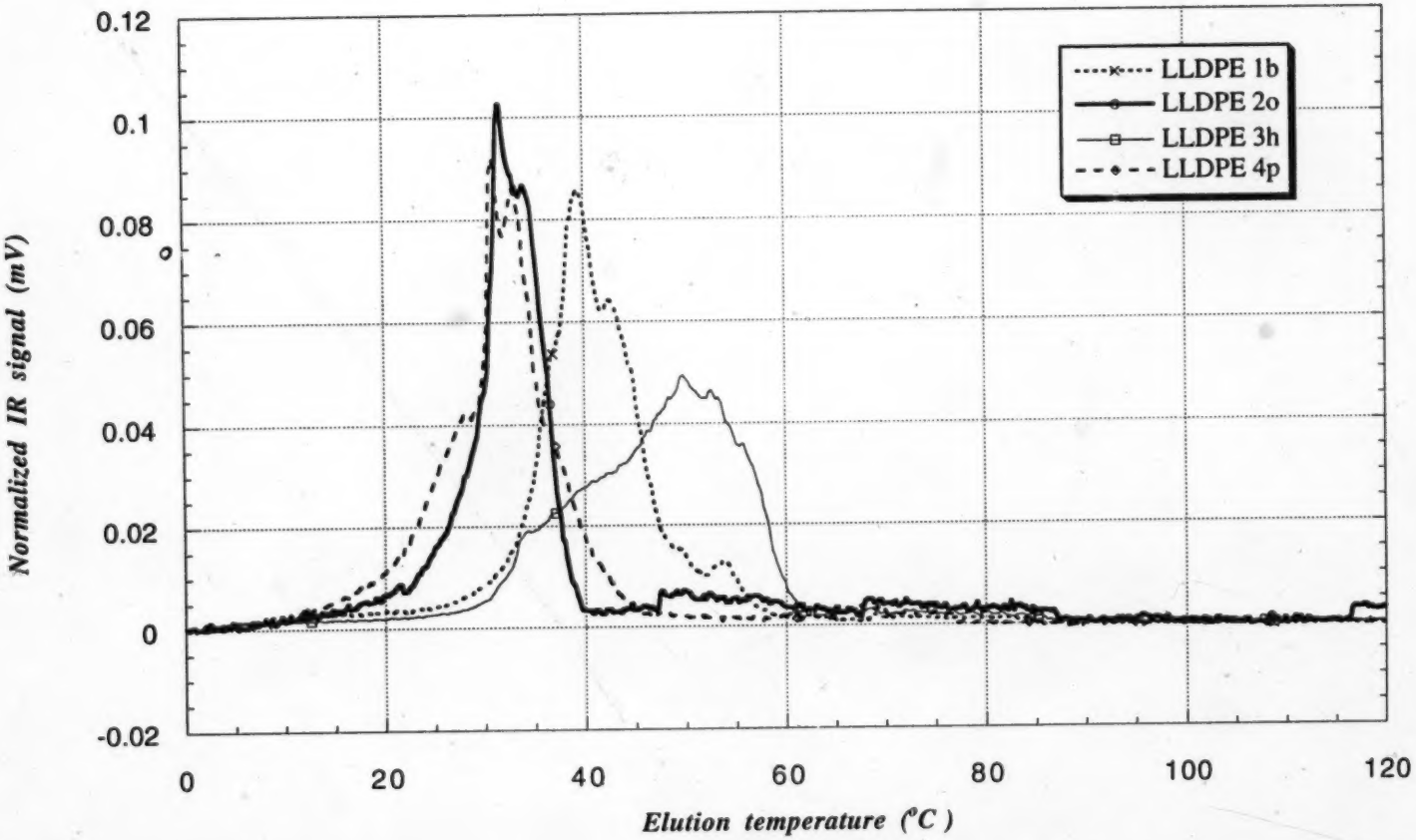

Figure 2.7 Normalized TREF Profiles for Metallocene LLDPEs. Solvent flowrate 1 ml/min; Temperature ramping 1°C/min.

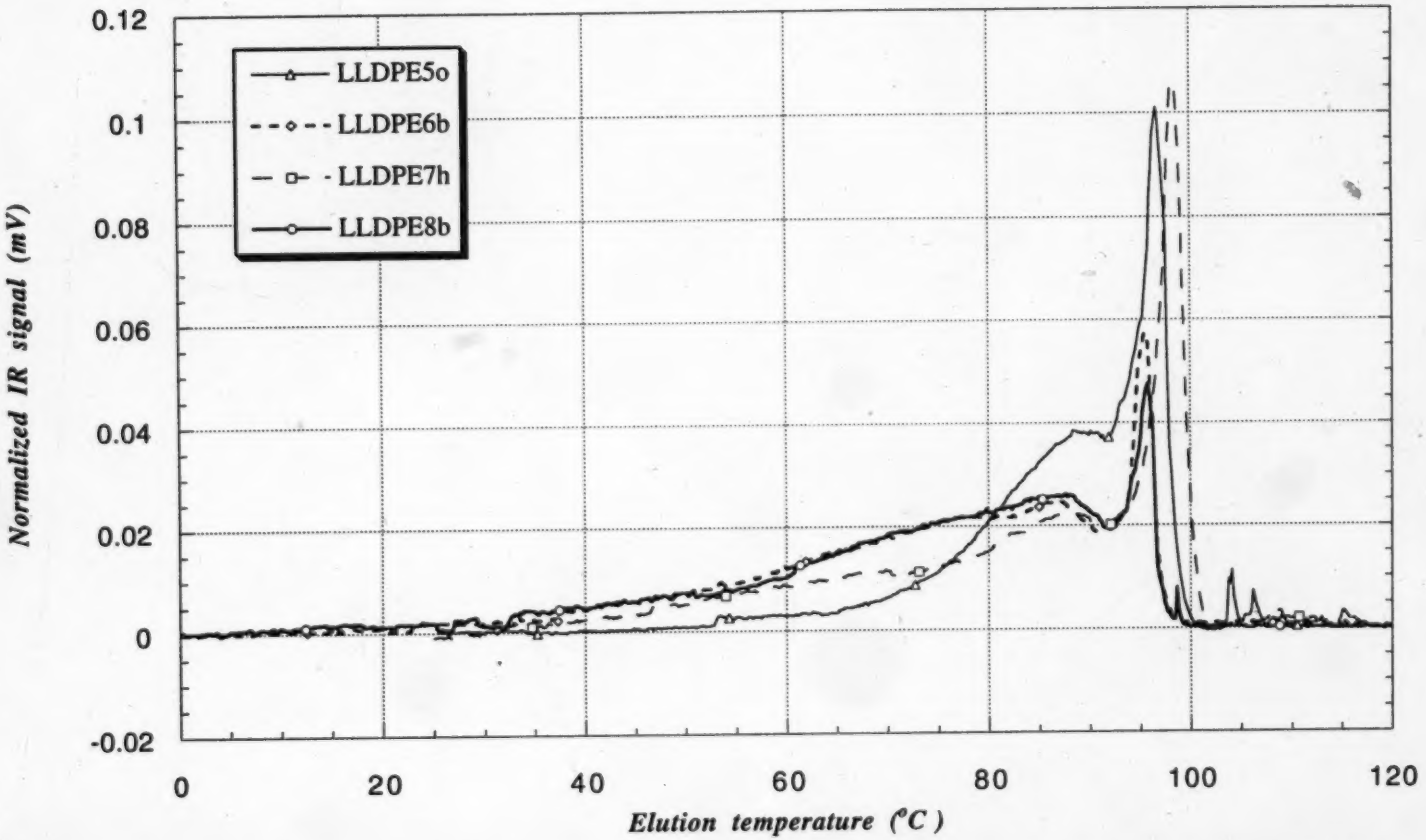

Figure 2.8 Normalized TREF profiles for Ziegler Natta LLDPEs. Solvent flowrate 0.5ml/min; Temperature ramping 1°C/min.

Table 2.2 : Copolymer content and methyl group concentration in LLDPEs.

Polymer	*Comonomer type*	*Synthesis process*	*Coho ratio*	*CH_3 /1000C*	*Dispersity of TREF profile*	*Peak elution temperature (°C)*	*Crystallinity[X] (Xray/density)*
LLDPE 1b	butene		-	36.2	narrow	39	20.9
LLDPE 2o	octene		-	42.6	v. narrow	32	13.3
LLDPE 3h	hexene		-	33.4	broad	50	23.1
LLDPE 4p	propene		-	47.3	narrow	32	24.6
LLDPE 5o	butene-octene	solution	1.3	5.6 (7.9)*	v. narrow**		52.3
LLDPE 6b	butene	gas	4.0	13.4 (20)*	broad**		43.7
LLDPE 7h	hexene	gas	1.4	8.4 (16)*	narrow**		45.1
LLDPE 8b	butene	gas	5.2	14.4 (20)*	broad**		43.5

* Parenthetic values indicate manufacturer's data (# branches/1000C).

** Z-N LLDPEs have bimodal TREF profiles and only the copolymer section has been compared. The comparison of the spread in TREF profiles is again relative to other Z-N LLDPEs only.

X Crystallinity was estimated by X-ray diffraction (Mulder, 1999).

and LLDPE2o has low crystallinity. The propylene copolymer, LLDPE4p, however, shows quite high crystallinity according to X-ray results (Table 2.2) in spite of the low elution temperature. The reason for this is not clear. Even though it has been observed that elution temperature is a weak function of molar mass when M_w is greater than 10000 (Wild, 1991, Karoglanian and Harrison, 1996), it is possible that the lower molar mass of LLDPE4p relative to the other polyethylenes contributes in this observation.

The second most branched species among the metallocene LLDPEs is the octene copolymer LLDPE 2o. As already mentioned, the polydispersity (Table 2.1) of LLDPE2o is only 2.0. The narrow TREF peak indicates a regularly branched polymer, and the low elution temperature indicates high amount of branching. The spread of the remaining metallocene LLDPEs is intermediate. These factors will be important in analyzing subsequent blending and interfacial tension results.

In Figure 2.8, showing TREF profiles for Z-N LLDPEs, all profiles show a bimodal branching distribution. For most of the Z-N LLDPEs, the homopolymer peak, the peak at high elution temperature, is expectedly narrow but the copolymer peak is very broad indicating a broad distribution of side chain branching. This bimodal distribution has been observed in previous studies by Usami et al. (1986) where the narrow elution peak at higher temperature has been attributed to ethylene homopolymer of high crystallinity and the multi modality to the character of the Ziegler-Natta catalyst used to make the polymer. The order of crystallinity predicted from TREF follows the following order: 8b < 6b < 7h < 5o.

Another important parameter for Z-N LLDPEs is the comonomer content. This was estimated by evaluating the copolymer : homopolymer ratio, referred to as the Coho ratio. The lowest point in the valley between the homopolymer and copolymer peaks is used to demarcate the copolymer and homopolymer elution temperatures respectively (indicated by the vertical line drawn through T_{Coho} in Fig. 2.4).

The area under the IR-T curve before and after T_{Coho} represents the fraction of copolymer and homopolymer respectively in the sample. The ratio of these areas, the coho ratio, gives an estimate of the branching present in the polymer. The coho ratios for Z-N LLDPEs (Table 2.2) were evaluated by a computer program using the trapezoidal rule for areas (see Appendix A-II). Metallocene catalysts lack the homopolymer producing active sites and hence produce only copolymer. The crystallinity of the LLDPEs has been investigated by Mulder (1999) and is also presented in Table 2.2.

The difference between the TREF profiles of LLDPE6b and LLDPE8b is merely in the high crystallinity region. The butene copolymers LLDPE 6b and LLDPE 8b show the highest coho ratios with LLDPE 8b exhibiting the highest value of 5.2. They also exhibit a low crystallinity based on x-ray scattering analysis (Mulder, 1999). This indicates a high amount of branching, though the broad copolymer peak indicates that the branching is not regular as in the case of the metallocene LLDPEs. LLDPE5o shows a low amount of side branching and the highest crystallinity. The zero shear viscosity at 220°C (Table 2.1) for LLDPE5o is also the greatest. This implies a large amount of linear polyethylene is present in the sample. Also the spread of the copolymer peak is narrower than the other ZN copolymers considered indicating a relatively regular MSL distribution.

A shift in the homopolymer peak elution temperatures was observed (Fig. 2.8) albeit small in the following order: 6b, 8b < 5o < 7h. Coincidentally, this shift follows the same order as peak shifts observed for the corresponding comonomer type metallocene LLDPEs. It is possible that some kind of interaction between copolymer and homopolymer during crystallization leads to this trend in the Z-N LLDPEs. Defoor et al. (1993), upon blending PTREF fractions, found that even small amounts of amorphous polymer can affect the elution peaks of the homopolymer noticeably. From Figure 2.9 (a) and (b) it can seen that a change in the flowrates can cause a shift in the elution peaks and the IR-T curve over the whole range of temperatures. From Figure 2.9 (b), it can be observed that some of the low temperature elutants are washed away when elution is commenced at 25°C.

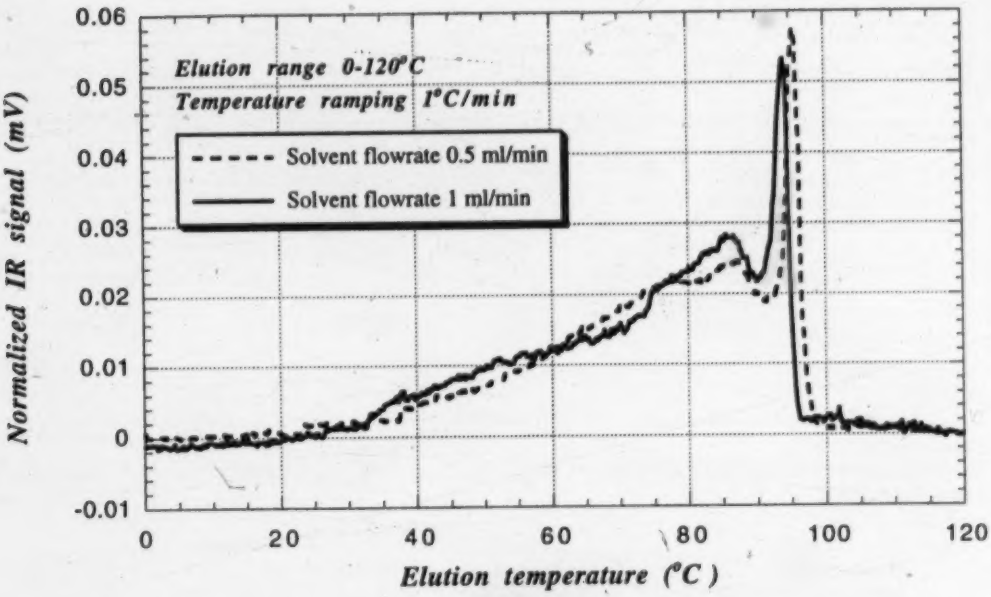

Figure 2.9 (a) Effect of solvent flowrate on TREF profiles of LLDPE6b.

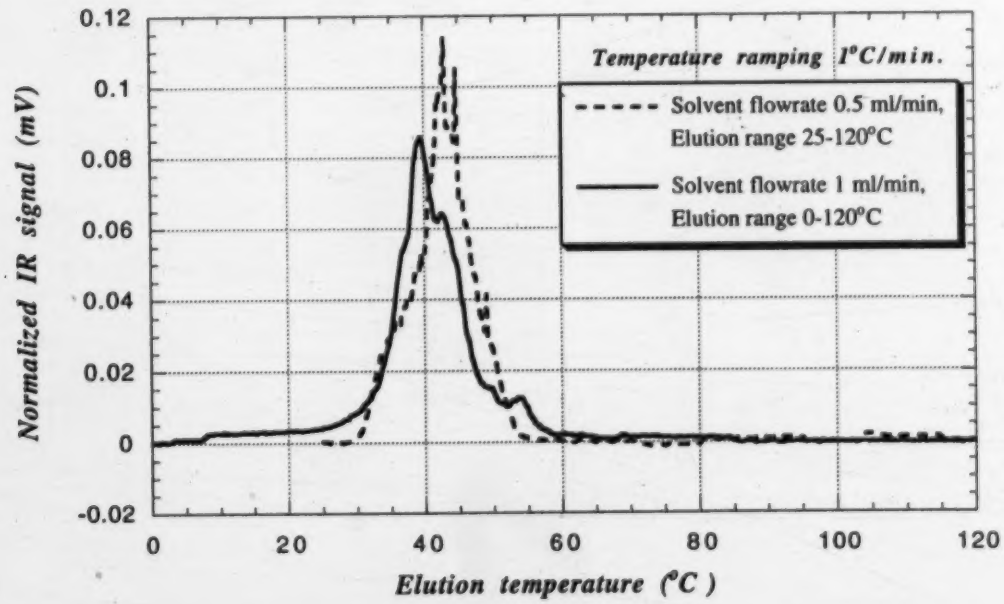

Figure 2.9 (b) Effect of elution range on TREF profile for LLDPE1b.

A factor to consider here is that LLDPEs show only short chain branching and any heterogeneity in the distribution of the short chain branches along the main chain could cause irregular crystallizing behaviour (Fig. 2.2). Molecules may exhibit fairly linear segments marked by sparse distribution of side branches followed by a highly branched segment (Wardhaugh and Williams, 1995). Crystallization of such a sample could cause amorphous zones to get trapped within zones of crystallized linear polymer. The IR signal which indicates amount of eluting polymer would then show unreal bumps at higher temperature indicating an excessive amount of material corresponding to a higher crystallinity than it actually possesses.

The measured values for the methyl groups/1000C is different from the number of branches /1000C quoted by the manufacturer. The explanation for this might be that the calibration curve used to evaluate the branching in the LLDPEs was based on low molar mass homopolymer samples (Lacombe, 1995). The use of this calibration for Z-N LLDPEs of differing comonomer and higher crystallinity might place undue emphasis on certain elution temperatures and exaggerate the branching occurring in other zones. The predictions for the metallocene LLDPEs will suffer from the same effect to a larger extent although the relative trends in both cases is not expected to be affected. A comparison of the manufacturer's data on the branch content of the Z-N LLDPEs shows that the values exceed ours by a constant factor of 1.4 except for LLDPE7h where they differ by a factor of 1.9.

2.4 Recommendations and Concerns:

During TREF, flow irregularities, such as channeling, deadspots and polymer deposition, can affect the dissolution of polymer in the elution solvent and cause unexpected maxima in the IR signal. In some cases extremely high spikes in the IR signal was noticed. This could happen when the polymer melts or dissolves away and releases any trapped bubbles from the interstices of the packing. When these air bubbles pass

through the IR detector a large signal is observed as the absorbance of air is very low. The spikes were removed from the data using the computer program shown in Appendix A-I.

With usage, the windows of the IR cell probably get coated with a film of deposited polymer. This causes reduction in the baseline as well as reduction in the contrast observed in the signal. It is possible that redissolution of this film at higher temperature causes unreal bumps observed in some of the TREF profile.

Another approach to obtain branching data without the use of PTREF has been employed by Pigeon and Rudin (1994), where two detectors were placed in series, one to measure the branch content and the other to measure the concentration of the sample. This accomplishes the same purpose that we are focused on but directly measures the branching at each elution temperature. Although they found that the same signal-to-branching conversion was valid for all the branch lengths they still could not avoid the use of calibrations.

Interfacial Tension and the Breaking Thread Method

Chapter 3

3.1 Introduction

During the mixing of two immiscible polymers, the minor phase deforms and disperses inside the continuous phase. This leads to the formation of an interface between the two phases formed by the respective polymers. The molecules at the interface are influenced by unbalanced molecular forces and therefore possess greater energy than molecules of either bulk phase. This excess free energy at the interface is called interfacial energy and specific interfacial energy or interfacial tension is the excess energy per unit area due to the formation of the interface. When a polymer forms an immiscible blend in another, at high drop diameter the shear forces cause the elongation and deformation of the droplet. The droplet deforms by forming sheets (Sundararaj et al., 1995a). As the sheet grows thin, it develops holes which grow and coalesce to form ligaments. These ligaments or threads elongate further due to shear and at low ligament thickness, interfacial forces take over the breakup process by pinching the thread into droplets via Rayleigh disturbances. When the shear forces no longer exceed the interfacial forces, a stable drop diameter is obtained in the mixing melt. Interfacial tension has been found to have a profound effect on the drop diameter of dispersed phase as well as the morphology of the blend of two immiscible components (Elmendorp, 1986, Elemans et al., 1990). Thus interfacial tension plays an extremely important role in polymer - polymer mixing, and its study can greatly enhance our ability to predict and modify additives to produce superior blends.

Although the LLDPE/PP system has been a topic of several blending studies (e.g. Kryszewski et al., 1973, Chiu and Fang, 1985, Datta and Lohse, 1993, Yu, 1995), little is available in the literature about the interfacial tension of these systems. To fully understand morphology generation in these blends, the interfacial tension value must be known. This study deals with measuring the interfacial tension between different LLDPEs and PP.

3.2 Polymer Interfacial Tension

3.2.1 Experimental Methods for Measuring Polymer Interfacial Tension.

Most methods for direct measurement of interfacial tension of polymer pairs have been derived from techniques used for liquids. These methods can broadly be divided into two categories, namely, static and dynamic techniques. In each of the following static methods, the interfacial force is balanced against another driving force such as gravitational or inertial forces, and the final geometry reached as a result of balance between these forces, gives an estimate of the interfacial force. Luciani et al. (1996b) have recently reviewed various methods for measuring interfacial tension.

The most fundamental method involves measuring the contact angle made at the plane of symmetry of an axisymmetric drop of one polymer lying on the substrate of the other (Kwok et al., 1995, Elemans et al., 1990). The lighter phase forms a biconvex droplet, the contact angle of which depends on the density difference and interfacial tension. However, procedural difficulties such as obtaining the exact plane of symmetry can hinder the accuracy of this method. There is significant uncertainty in these tests since long times are required to attain equilibrium which can lead to oxidation in polymer melts.

Another method based on the same principle is the pendant drop method (Wu, 1969), shown in Figure 3.1 (a). A drop of the polymer with higher density among the two polymers is suspended inside a matrix of the lower one. This is experimentally achieved by injecting a melt of the denser polymer into a chamber containing the matrix polymer while controlling the pressure inside the chamber. Images of the drop are used to obtain

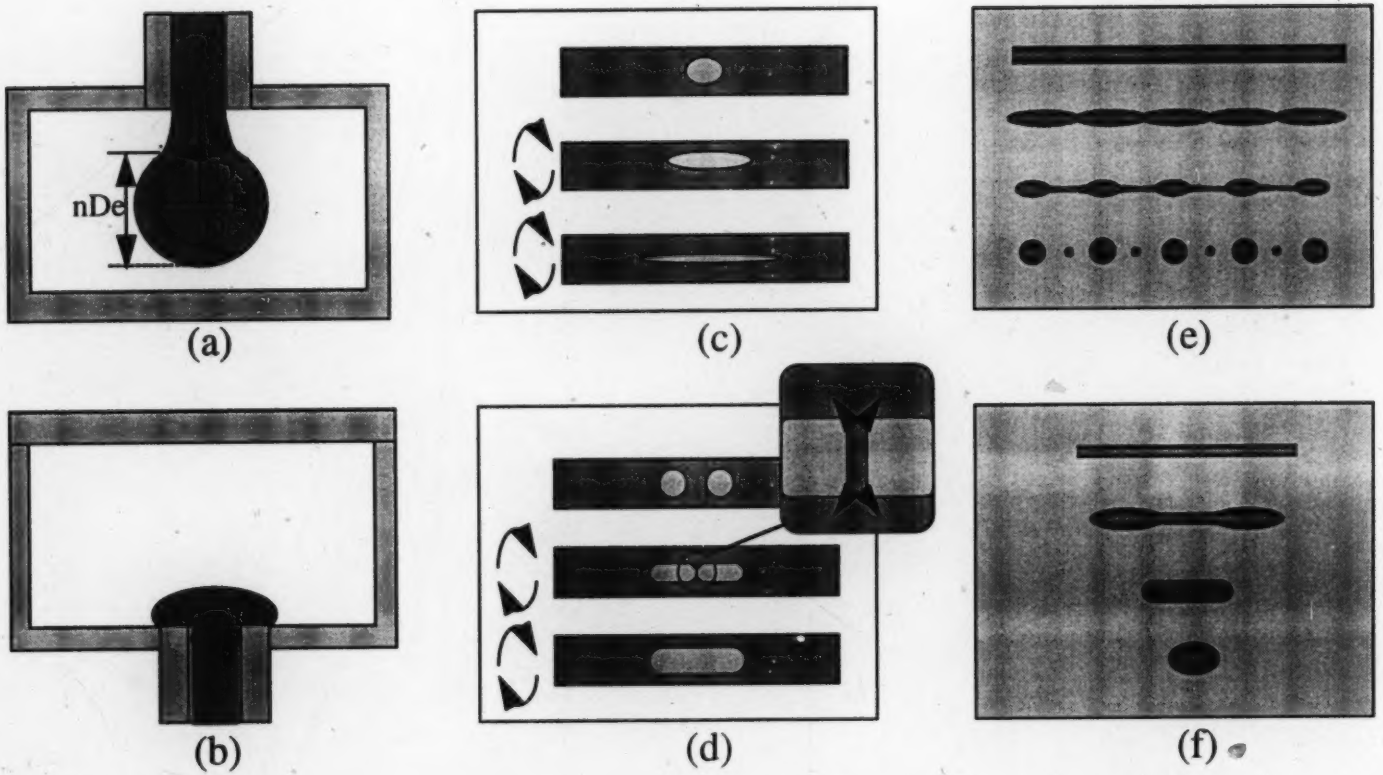

Figure 3.1 : Different methods for interfacial tension measurement : (a) Pendant Drop. (b) Sessile drop. (c) Spinning drop. (d) Coalescence of spinning drops. (e) Breaking thread. (f) Imbedded fibre retraction.

parameters such as the diameter at various heights of the drop, which characterize the shape of the drop. The equilibrium shape of the suspended drop is governed by the interfacial tension, buoyancy and the gravitational pull on the drop. Density data are required for this method. This method has been successfully used for polymer melts by Wu (1971) and Roe et al. (1967). Long equilibrium times, detachment of the suspended drop during measurements and difficulty in accurate determination of the densities are some of the drawbacks of using this method to measure interfacial tension between polymers .

The sessile drop method (Fig. 3.1 (b)), (Staicopolus, 1962) is a variation of the pendant drop method where the denser fluid rests on a solid substrate in a matrix of the less dense fluid. The rate of equilibrium for this method is slower than the pendant drop method as a solid-liquid interface must move, as opposed to a liquid-liquid interface in the case of pendant drops. The problem of drop detachment is however avoided in this arrangement.

The rotating drop technique (Patterson et al., 1971) makes use of centrifugal force as a driving force (Fig. 3.1 (c)). A drop of the lower density polymer is imbedded inside a cylindrical matrix of the other polymer and the system is rotated about the cylinder axis. The drop elongates and attains an equilibrium length which varies with the rotational speed and temperature of the experiment. The time required to achieve equilibrium for this method when used for polymer melts is very high and polymer degradation may occur. Schoolenberg and During (1998) have developed a method based upon the coalescence of two imbedded drops in a polymer matrix in a spinning drop apparatus (Fig. 3.1 (d)). When the sample spins, the two droplets approach each other and the draining of the matrix film governs the rate of the coalescence process. It was claimed that this method gives results as quickly as some of the dynamic methods explained below.

The other class of interfacial tension testing methods are dynamic methods. Recent advances in the pendant drop technique allow estimation of the equilibrium drop profile by studying the transient shape of the interface (Anastasiadis et al., 1986; Demarquette and

Kamal, 1994). This method involves expensive experimental equipment and was not used in our study due to the unavailability of the required equipment.

For this study it was decided that the breaking thread method (Tomotika, 1935) was the most suitable method of determining interfacial tension. Its advantages are: ease of set up, small sample size requirements, low cost and short experimental times, the short experimental times minimizing possible degradation of the polymer sample (Chappelear, 1964). The breaking thread method has been used on a number of systems earlier with and without the use of compatibilizer and is a popular method to measure interfacial tension (Elemans et al., 1990; Watkins and Hobbs, 1993, Sundararaj, 1995a; Cho et al., 1996; Liang and Favis, 1997; Machiels et al., 1997). The breaking thread method involves observing the breakup of a cylinder of one liquid in the matrix of another due to sinusoidal Rayleigh instabilities which develop on the surface of the cylinder (Fig. 3.1 (e)). These instabilities grow and cause necking and subsequent breakup of the thread into spherical droplets. The interfacial tension can be calculated from the rate of growth of such instabilities.

Finally, another method which has been gaining popularity in the last decade is the imbedded fibre retraction method, which was introduced by Carriere et al. (1989). This method (Fig. 3.1(f)) is similar to the breaking thread method in that a thin fibre is embedded in a matrix. The fibre however is of shorter length and the kinetics of retraction of the fibre into a sphere is used to estimate the interfacial tension. However, residual stresses in the polymer may affect the retraction rates and lead to erroneous interfacial tensions (Utracki, 1990). Recently, Carriere and Silvis (1997) have used this method to evaluate interfacial tension between PP and LLDPE. A variant of this method, wherein a droplet is sheared using simple shear into an elongated drop and allowed to retract back to a sphere, has been used recently (Luciani et al., 1997) to study dynamic interfacial tension. An imbedded disk retraction method has been recently proposed by Rundqvist et al. (1996). Sigillo et al. (1997) have recently conducted a study comparing some of these dynamic interfacial measurement techniques.

3.2.2 Theoretical Methods for Predicting Polymer Interfacial Tension

Predictive methods for interfacial tension between polymer pairs have also emerged from techniques used for small molecule liquids. Among the methods developed are the Parachor method introduced by Sugden and later modified by Quayle (1953) to obtain surface tension of liquids. This method can show large errors when used for polymers and polar liquids. Small (1953) introduced a group contribution method to estimate the solubility parameter for a molecule of known chemical structure. Coleman et al. (1994) have refined the parameters used in this method. A technique based on solubility parameters of the individual components from solvent swelling experiments is used to estimate the Flory Huggins chi parameter (χ_{FH}). The information provided by this parameter is the same as that provided by interfacial tension. Two main methods used to estimate the interfacial tension from the Flory Huggins chi parameter are the Helfland and Tagami (1972) self consistent field theory and the Cahn and Hilliard (1958) square gradient theory. Luciani et al. (1996a) have reviewed these methods and Kamal et al. (1997) have evaluated various thermodynamic theories to predict interfacial tension between PS and PP melts. In this study, both the Helfland and Tagami (1974) method and the chi parameter approach have been used to make predictions for comparison with experimental results.

3.3 Breaking Thread Method

3.3.1 Theory

Lord Rayleigh (1879) was the first to study the disintegration of a liquid jet. Rayleigh used linear stability theory to solve the equations of motion for the thread phase neglecting the influence of surrounding fluid (since he studied water jets in air). Tomotika (1935) extended Lord Rayleigh's theory (1892) by considering the breakup of a cylinder of a Newtonian liquid inside another Newtonian liquid in the absence of inertial effects. Rumscheidt and Mason (1962) studied the breakup of highly viscous liquids using this

method. The term breaking thread method was coined by Elemans et al. (1990). Chappelear (1964) was the first to use the breaking thread method for estimating the interfacial tension of polymer melts although his results were found to be unsatisfactory due to the lack of accurate viscosity data. In recent years there has been a renewed interest in this method with the evolution of advanced rheological measurement equipment.

The breakup of the cylindrical thread inside the quiescent matrix is initiated by the propagation of sinusoidal perturbations on the surface of the cylinder resulting in a net decrease of the interfacial area. Kuhn (1953) quantified the size of these initial distortions assuming that they are caused by Brownian motion. A concerted growth of these random perturbations on the surface of the thread assumes a sinusoidal profile at the interface. When the wavelength of these perturbations is greater than the circumference of the thread, wave growth will lead to a reduction in the interfacial area. This interfacial area decrease makes it thermodynamically favorable for the thread to disintegrate into droplets. Only the dominant wavelength grows and leads to the ultimate breakup of the thread. The periodicity of the equi-spaced droplets corresponds to the wavelength of this perturbation. The sinusoidal distortion (α) grows exponentially with time at a rate (q) which is proportional to the interfacial tension (σ) and inversely proportional to the matrix viscosity (η_m) and the initial diameter of the thread (D_o). Tomotika (1935) related these using a distortion function $\Omega(p,\chi_m)$ which is a tabulated function of the viscosity ratio (p) and the wavelength of the instability showing maximum growth (λ_m) responsible for breakup. The average diameter of the thread decreases continuously with the propagation of the disturbance. Its value can be determined by conservation of mass for the thread phase material from initial to final configuration. Polymer behavior is approximated to be Newtonian at the zero shear limit and interfacial tension can be estimated using the following two relations:

$$\alpha = \alpha_o e^{qt} \tag{3.1}$$

α - dimensionless amplitude of perturbation;

α_o - initial dimensionless amplitude of perturbation at t=0;

q - rate of growth of disturbance amplitude;

$$\sigma = \frac{q\eta_m D_o}{\Omega(p,\chi_m)} \tag{3.2}$$

σ - interfacial tension;

η_m - zero shear matrix viscosity;

D_o - initial thread diameter;

$\Omega(p,\chi_m)$ - Tomotika's distortion function;

p - viscosity ratio ($\eta_{thread}/\eta_{matrix}$);

χ_m - wavenumber of dominant perturbation ($= \pi D_o / \lambda_m$).;

It has been observed that the instability of a particular wavelength shows maximum growth depending upon the diameter of the thread and the viscosity ratio of the system. The plot of Tomotika's distortion function Ω and χ_m, as a function of p can be found in Elmendorp (1986) while a more detailed plot, which treats the case of breakup occurring due to wavelengths other than the preferred wavelength, can be found in Chappelear (1964). A sketch of these profiles is provided in the Appendix C (Fig. C-I (a) and (b)). Chappelear's plots have been used to evaluate Ω for most experiments in this study. The corresponding value of $\Omega(p,\chi)$ replaces $\Omega(p,\chi_m)$ in Equation 3.2.

Implementation of the theoretical methods will be explained in section 3.6.

3.3.2 Equipment and Procedure

Threads (or cylinders) were drawn from a bead of molten polymer placed on a glass slide which was kept on a hot plate. The temperature of the bead was kept above the melting point of the polymer. The diameter for threads ranged between 20 μm to 140 μm, with a typical thread diameter of 70 μm. In some cases, streaks were visible on the thread

surface, probably caused by the tweezers used to pinch the polymer for grip while drawing it. Browning occurred at the edges of the molten bead when it was exposed to high temperature for long times. Although threads were not obtained from such degraded samples, it is expected that some oxidation occurs continuously at the melt surface exposed to air. The thread surface would then inherit the degraded products as a coating. Another variable factor was the tension used to pull the thread. Uneven tension can lead to nonuniform diameter and the chances of developing macroscopic curvature upon annealing making it difficult to meet theoretical assumptions. When threads are pulled at a high rate, the thread is thinner, but, the residual stresses incurred are greater and a longer relaxation time would be required to relieve these stresses. The threads were drawn in ambient air and this presented problems such as moisture absorption as well as dust contamination in some cases, not to mention the irregular convective air current around the cooling polymer strand. The threads were therefore scrutinized under a microscope and uniform sections were cut from the thinnest threads obtained and these sections were kept overnight in a vacuum oven at about 40-60°C to remove moisture and relax stresses created while drawing. Residual stresses are believed to delay the onset of the initial distortions on the thread (Bousfield et al., 1986). A higher temperature is desirable for moisture removal but it was found to disrupt the symmetry of the thread. Also, handling with bare hands can severely contaminate the threads which can affect the results drastically. Surgical gloves could leave latex particles sticking to the thread (Sundararaj, 1994); hence, the threads were handled with tweezers at all times.

Two circular plates of the matrix polymer required for the breaking thread method were prepared using a Carver plate press at a temperature of 200°C and a pressure of 1000 psi applied for a period of 3 minutes. In order to avoid entrapping bubbles in the plates, the polymer was allowed to first melt and occupy the shape of the mold by bringing the plates close together without actually touching the mold. Excess polymer was added on top, and after the polymer softened, a preheated Teflon sheet was placed atop the mold and pressure was applied. Dimensions of each polymer plate was approximately 1 cm diameter and 1 mm thickness. A thickness of 2 mm was also tried but it was noticed that

during the experiment, such samples were squashed between the heater plates of the hot stage. The distance between the heater plates was just a little greater than 2mm when the support springs were undeformed. Thus polymer plates of 1 mm each were used to minimize pressure effects. They were kept in the oven overnight at 80°C to relieve any residual stresses and to prevent moisture from adsorbing on the surface. A thread was sandwiched between the plates and placed inside a metal sample holder with glass cover plates on either side and annealed inside a Mettler FP82HT hot stage controlled by a Mettler FP90 processor (Fig. 3.2). The plates are fused to form the matrix by exposing the system to a temperature above the transition temperature (T_g for amorphous polymers and T_m for crystalline polymers) of the matrix phase but below the transition temperature of the thread phase (typically 145-160°C). It must be noted that this method could fail for systems where the T_g of the matrix phase is close to the melting point of the thread phase. Both in-stage and out-of-stage oven annealing were tried. The in-stage annealing procedure was found to be easier and avoided the temperature dip observed during sample transfer into the hot stage. This cooling of the sample could produce unwanted stresses which can distort the uniformity of the thread. Wetting of the thread by the matrix phase drives away most bubbles though sometimes air can get trapped near the middle. This could potentially disrupt the symmetry of the breakup. In most cases however, bubbles were noticed to grow smaller and move away from the interface. Vacuum, when applied while annealing, only increased the probability of the bubbles getting trapped. The molten matrix phase was carefully pressed to assume the shape of the holder thus driving out any air inside the holder. This also ensured that the dimensions of the sample were preserved thereafter. This eliminated the effect of the flow of the molten matrix due to surface tension and external pressure on the breakup. Glass cover slides kept the sample airtight and hence prevented oxidation of the polymer during long runs. Once the thread was imbedded between the two plates and no air pockets were visible, the desired test temperature was imposed. If the threads and plates were not adequately heated before each run, moisture and air adhered to the surface of the polymer and were trapped at the interfaces. We believe that this is one of the causes of uneven thread. Freshly drawn threads increased the chances of successful fusing of the plates without air pockets and

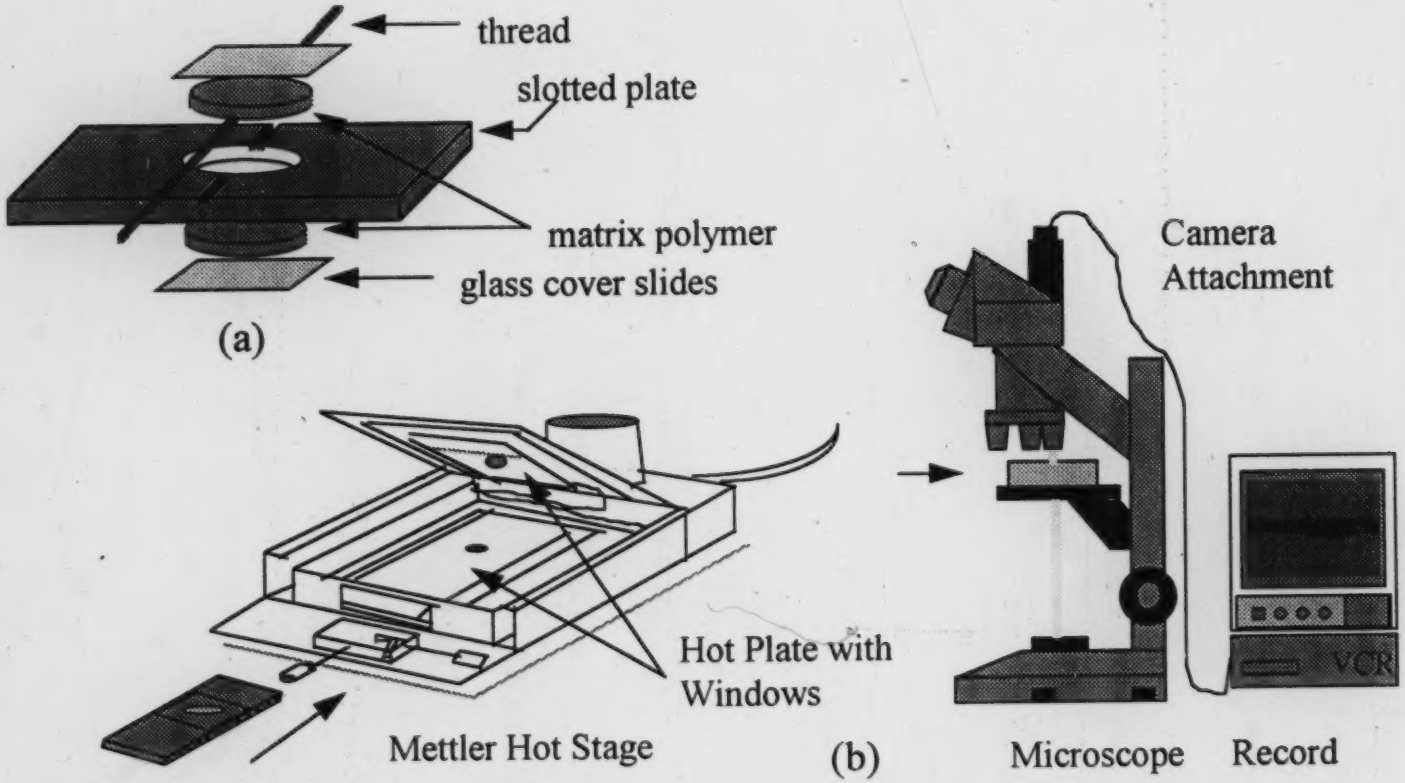

Figure 3.2 : (a) Slotted Plate and sample preparation. (b) Observation Setup for Breakup of the thread.

subsequently obtaining uniform breakup. However, in order to relieve residual stresses, the thread must be stored in a vacuum oven for a minimum amount of time (approximately 30-60 minutes).

The hot stage was placed under an Olympus BH2 optical microscope to observe the breakup of the thread (Fig. 3.2). The microscope was attached with a two way prismatic lens to facilitate recording the breakup with a Pulnix camera. Measurements of the sinusoidal deformation were gathered and used to estimate the interfacial tension of the two polymers.

3.3.3 Calculations

The amplitude of the disturbance was measured as a function of time by measuring "a" and "b", the minimum and maximum diameters of the distorted cylinder (Fig. 3.3), at various times. The variation in $D_{avg.}$ the average diameter across the length of the distorted thread, was neglected in the calculations. The slope of the curve of the logarithm of the dimensionless amplitude α ($2A/D_o$) plotted against time (Fig. 3.4) gives the rate constant q for breakup (Eq. 3.1). In many cases the observed breakup was asymmetric and the average of the interfacial tension values was obtained from measurements of either side of the crest of the sinusoidal disturbance where possible.

For threads with large diameters, the wavelength of disturbance λ is also large and two consecutive crests were sometimes out of view of the TV monitor screen. In such cases, only one crest and trough were used for measuring a and b. The distance between the crest and the trough, $\lambda/2$, was measured and doubled; this is a possible source of error in the calculated interfacial tensions.

The values of breakup function $\Omega(p, \chi)$ were obtained by interpolation using Figures 1 and 2 of Chappelear (1964), the sketches of which are shown in appendix C-I.

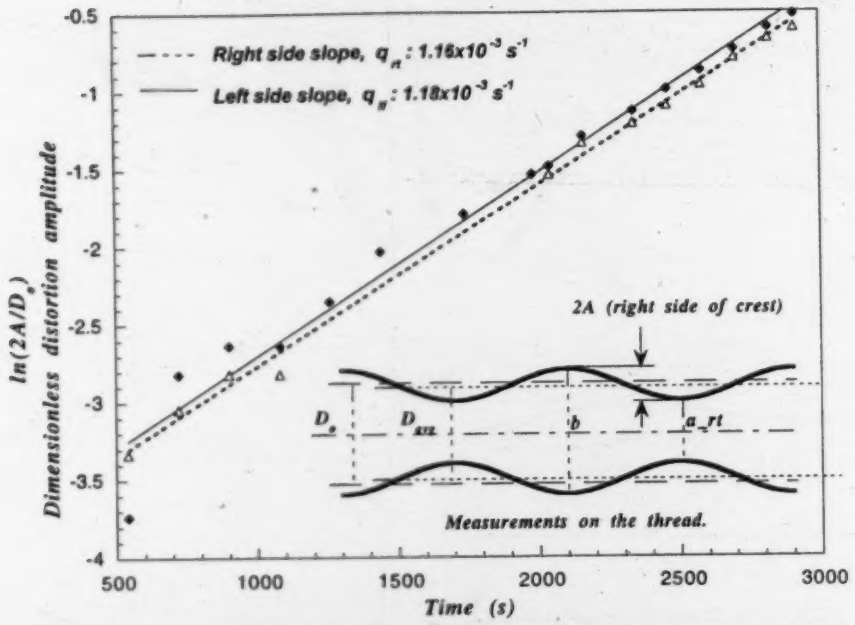

Figure 3.3 : Dimensionless distortion amplitude as a function of time. Linear breakup profiles on left and right sides of the chosen crest indicate uniform breakup. (system : PP1 thread, LLDPE2o matrix, Run 10)

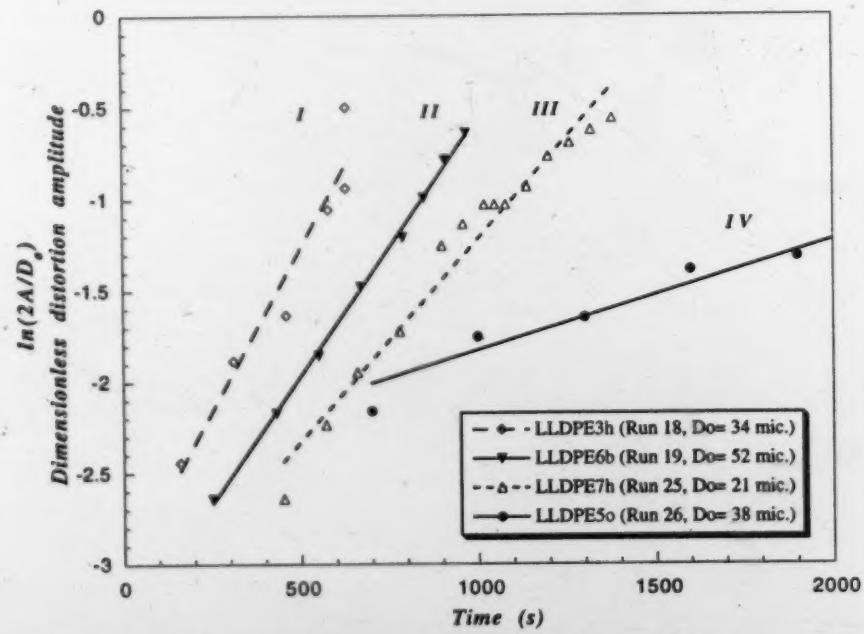

Figure 3.4 : Logarithm of dimensionless distortion amplitude as a function of time for various LLDPEs used in the breaking thread method with a PP1 thread. (Nonlinear breakup profile was observed in some runs.)

These were compared with χ_m and Ω_m, Tomotika's predicted breakup wavenumber and distortion function (shown in Fig. C-I (a)). Equation 3-2 was used to compute the interfacial tension. The interfacial tensions for runs which showed a distortion wavelength close to the dominant wavelength predicted by Tomotika for Newtonian liquids were chosen and averaged to obtain σ_{mp}, the most probable value of interfacial tension.

3.4 Results

Two sets of breaking thread experiments were carried out - the first to see the effect of polypropylene molecular weight and second to see the effect of branching of the polyolefins on interfacial tension. For the first set, an amorphous phase, polystyrene (PS), was chosen as a reference, and used as the matrix phase. The thread phase was composed of isotactic polypropylenes (iPP) with different melt flow rates (see Table 2.1) so that the molecular weight dependence of interfacial tension could be observed. Although the molecular weights of the polypropylenes were not evaluated, the melt viscosities are closely related to the molecular weight and any trends with increasing M_w would be reflected by increasing the melt viscosity. A detailed list of different PP/PS runs can be found in Appendix C, Table C-II (a). The interfacial tension values measured for PP/PS systems show large variations from run to run because improvements to the experimental technique were still being made during the experiments. No clear systematic dependence of the interfacial tensions on the viscosity of the PPs, was observed from the data.

The second set of experiments were conducted with the same PP thread phase and different LLDPE copolymers for the matrix. The lowest viscosity PP, PP1, was chosen so that breakup times could be reduced. Yu (1995) pointed out that such low viscosity polypropylenes were more difficult to impact modify and hence the secondary focus is on how the properties of these PPs can be improved with the addition of LLDPE. The LLDPEs were made with either metallocene (LLDPEs 1-4) or Ziegler-Natta (LLDPEs 5-8) catalysts using different comonomers such as 1-butene or 1-hexene as explained in Chapter 2. The samples were first annealed so that the matrix phase could wet the thread

completely. While the sample temperature was raised to the test temperature, it was observed that at temperatures around 160°C the thread phase was no longer distinguishable from the matrix phase when viewed under the optical microscope. The similarity of the refractive indices in melt state is not surprising since the structures of the two polymers are very similar.

The contrast between the PP and LLDPE phases was very low. During the experiment, any deviation in focal settings due to the sample expanding due to flow made it extremely difficult tracking the thread again. In some cases, it was difficult even to see the thread after both phases had melted. In order to impart contrast between the phases and observe whether breakup occurred, the thread phase (PP) was blended with 0.2 wt% of both a phthalocyanine dye and fine carbon black. It was observed that the dispersion of carbon black was more even in the blend than the dye. The carbon black colorant particles were much finer than the dye globules.

Carbon black additives are known to improve strength of many elastomeric materials and could have some effect on the interface properties. Recently Nesterov and Lipatov (1999) have reported the compatibilizing effect of fillers in binary polymer mixtures. To see the effect of the additives, the interfacial tensions of PS/PP1 with and without additives was measured, assuming a negligible change in the melt viscosity of PP1. These are given below in Table 3.1.

Table 3.1 : Effect of thread phase additives on the interfacial tension between PS and PP1 at 200°C.

Additive	Interfacial Tension σ_{mp} (mN/m)
No Additive	6.5
Carbon Black	6.3
Phthalocyanine Dye	10.7

The results of the PS/PP1 experiments (Table 3.1) show that there is no major effect introduced by blending 0.2% carbon black and interfacial tension is also quite close to that obtained without it. The PP viscosity increased less than 10% with the addition of carbon. The thread phase viscosity does not affect results as much as matrix phase viscosity does and hence the effect of increased PP1 viscosity on the results would be negligible. The dye however led to an increase in the interfacial tension value suggesting that it was incompatible with the polyolefinic phases. This was also evident from the poor dispersion of the dye in PP1. Threads were thereafter consistently drawn from a 0.2% carbon black blend and used instead of pure PP1 to observe the breakup (Fig. 3.5) in the PP1/LLDPE runs.

PP/LLDPE interfacial tensions obtained at different temperatures are presented in Table 3.2. Most of the runs conducted at 220°C. The range of interfacial tension at 220°C ranges from 0.2 mN/m to 4.2 mN/m (see Appendix C-III (b)). Additionally, some runs were carried out at 200°C and 260°C and are also included in Table 3.2.

Table 3.2 PP1/LLDPE Interfacial Tension results

Matrix phase	Interfacial Tension σ_{mp} (mN/m)		
	200°C	220°C	260°C
LLDPE1b	-	0.6*	0.70*
LLDPE2o	-	2.0*	-
LLDPE3h	-	1.9*	-
LLDPE4p	-	2.0*	-
LLDPE5o	0.8	0.8*	0.05
LLDPE6b	-	2.6*	-
LLDPE7h	1.3	1.9*	0.64
LLDPE8b	0.4	0.7*	0.34

* : runs where slotted plate was used.

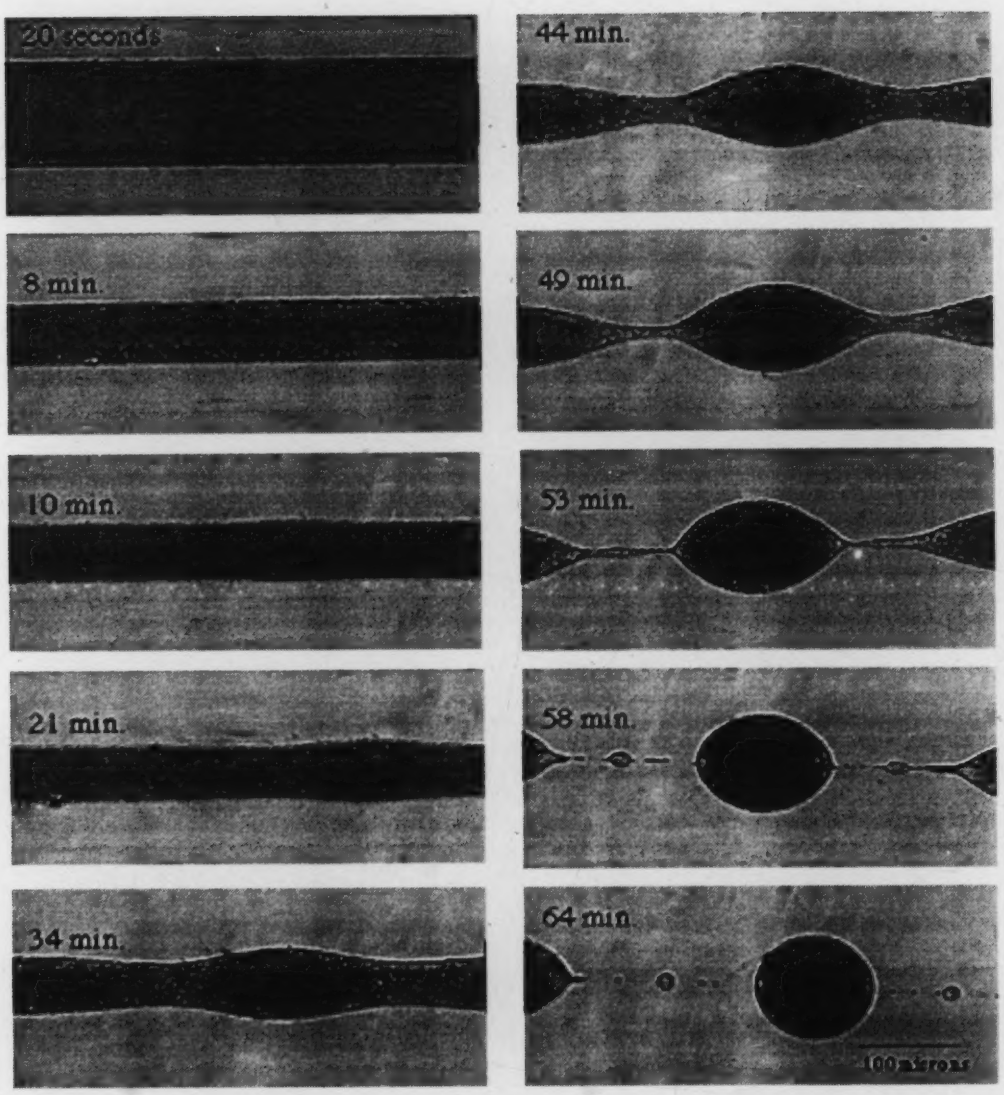

Figure 3.5 : Symmetric breakup observed for the PP1 (thread) - LLDPE2o (matrix) system at 220°C (Run 10). The stages of breakup are a. transient thinning due to flow (20 s - 8 min.); b. growth of Rayleigh instabilities (10 - 49 min.); c. elongation of neck (53 min.); d. breakup and development of satellite droplets (58 - 64 min.); e. retraction of polymer segments into spheres (not shown).

The starred (*) values in Table 3.2 indicate that those runs were conducted with the slotted plate which will be discussed later. In Appendices C-II and C-III, the most probable interfacial tension for each system is listed alongside the individual interfacial tensions calculated for each run.

3.5 Discussion

The Tomotika theory for filament breakup of Newtonian liquids has been used in this study to evaluate polymer interfacial tensions. This has been carried out successfully in many previous studies, as already mentioned. However, this is the first time it has been used to study low interfacial tension systems like PP/LLDPE. The theory assumes that both fluids are purely viscous and the matrix is quiescent. It appears that in the above mentioned experiments with PP/PS systems, some of these assumptions might have been violated. This is reflected in the relatively higher interfacial tensions obtained as compared to that reported in literature. For a Newtonian system, Tomotika's theory predicts the most probable wavenumber χ_m for distortion to occur, and the corresponding distortion function Ω_m is based solely on the viscosity ratio p. These functions have been plotted by Chappelear (1964), Elmendorp (1986) and Elemans et al. (1990) as shown in Figure C-I (a). The χ values obtained for PP/PS systems (Appendix C-II) show large deviations from the predicted χ_m values for the same viscosity ratio. The results could therefore involve effects of degradation and flow. In their study, Elemans et al. (1990) reported inaccuracies in estimating interfacial tension when such differences between χ and χ_m occurred. A close examination of the interfacial tension results shows that as the viscosity ratio increases, the chances of breakup occurring at χ_m reduces and hence it is difficult to obtain the true value of interfacial tension using Equation 3-2. In other words, the theory is inadequate for the accurate prediction of the interfacial tension in the presence of extraneous factors such as elastic forces and flows. In addition to the χ values different from χ_m , other factors, such as end pinching can effect the interfacial tension calculated. Most of the above runs were carried out before the use of a specially designed slotted sample holder was used in the

experimental procedure. The merits of the sample holder will be discussed in the following sections. Only those experiments for which χ is close to χ_m have been used to determine the interfacial tension σ_{mp} (where the subscript mp stands for most probable).

The first set of experiments involved interfacial tension measurements of different PP threads inside a PS matrix (given in Appendix C-II). The measurements for the PS/PP systems were conducted before standardized curing procedure had been adopted for the threads and plates used in the experiment. This is the main cause for the large variation observed in these preliminary experiments. There was no systematic variation of the interfacial tension with viscosity ratio. Both PP2 and PP3 showed unusually high interfacial tensions. PP4 did not follow this trend probably because it was from a different supplier and its molecular architecture (e.g., % isotacticity) might be different from the rest. An increase of interfacial tension with molecular weight followed by a gradual leveling off has been reported before by Kamal et al. (1994) for a PS/PP system as well as by Nam and Jo (1995) between polystyrene and polybutadiene. A value of 5.1 mN/m has been reported by Sundararaj (1994) for a similar PS/PP system at 200°C, while Escudie et al. (1986) have reported a value of 5.8 mN/m at 220°C for this system. Thus the values of the PS/PP interfacial tension obtained in this study are in fair agreement with cited literature values, in spite of the variation in annealing procedure, at least for two of the PPs.

The PP/LLDPE runs were carried out at three temperatures 200, 220 and 260°C (see Appendix C-III (a)-(c)). Initially samples were simply sandwiched between two glass coverplates and kept inside the hot stage. Due to low interfacial tension, coupled with large thread diameters, the initiation of breakup took a very long time at 200°C. Subsequently a higher temperature of 260°C was tried. It was discovered later that some gelling or crosslinking was occurring, at both temperatures, due to oxidation so that the distortion was unable to grow after the first 45-60 minutes. Tomotika's theory (1935) treats the breakup of a viscous thread in the absence of a flow field. It was observed that the sample would get squeezed out until its thickness was reduced to the contact distance

between the plates of the hot stage. This flow was further amplified by surface tension between the glass slides and the matrix polymer. A sample holder, simply a slotted plate with a channel for placing the thread, was designed to remedy this problem. Upon placing glass coverslides on either side of the slotted plate, a closed chamber resulted in which the run could be conducted without the effects of flow or oxidation due to air, during the experiment. The curvature in the thread if any could be corrected to a certain extent before annealing, by placing the thread in the channel.

The thickness of the plate was machined to slightly more than the contact distance between the heating plates of the hot stage. If the thickness of the sample were greater than the contact distance, then closing the hot stage top (Fig. 3.2) would create pressure in the polymer melt and result in flow. When the viscosity ratio of the system was very low ($p<<1$), the thread phase would run out of the sample first and the thread diameter would reduce drastically before the ends got pinched off. In the absence of the slotted plate this occurred frequently. Upon introduction of the slotted plate, however, a distinct flow of thread phase was observed immediately after the thread had melted. The diameter of the thread reduced for some time, after which it stabilized. The initial diameter and initial time for the calculations were measured once this stable diameter was attained. Care was taken to melt the matrix phase first and press out the excess material after filling in the empty space in the slot. Only then, the temperature was raised above the melting point of the PP thread phase (~163°C). A concern about introducing the slotted plate is whether any pressure buildup occurs in the sample. Although most of the excess polymer flows out from under the coverslide, the initial flow of the thread phase indicates that polymer flow occurs through the channel as well. This is also apparent when small beads of polymer collect at the ends of the channel. Whether the initial pressure has an effect on the breakup, will have to be investigated in more detail in future work.

From Table 3.2, the butene copolymers, LLDPE1b and LLDPE8b as well as the butene-octene terpolymer, LLDPE5o, show the lowest interfacial tensions of the chosen group of polymers. LLDPE6b on the other hand, shows the highest interfacial tension of

the studied set of polymers. From the TREF results of Chapter 2 (Figure 2.8), we can see that the copolymer branching distribution is the same for both LLDPE6b and LLDPE8b. However, LLDPE6b shows a greater homopolymer peak than LLDPE8b. Both the melt index (Table 2.1) and molar mass show their effects. The lower value of the measured interfacial tension for LLDPE8b leads to the conclusion that the unbranched segments of the homopolymer interact poorly with the polypropylene phase. Some researchers (Alamo et al., 1997), have argued that the branched fractions when blended with linear polyethylenes, phase separate, when the branch content exceeds a certain amount. This can lead to an alternative explanation that a higher amount of homopolymer in the case of LLDPE6b might hinder the migration of short chain molecules to the interface which are responsible for lowering the interfacial tension, owing to the higher crystallinity even in the melt. Hussein and Williams (1998) have indicated the possibility of liquid crystals in high density polyethylene by observing high temperature phase transitions in the melt. More studies must be conducted to explore the reason governing this difference in interfacial tension.

Molar mass does not seem to control the interfacial tension in the current set. The generalized form (Equation 3-3) of the Gaines equation (see Ellingson et al., 1994) is :

$$\sigma_{12} = \sigma_{12}^{\infty M} - C_1 M_n^{-z} \qquad (3\text{-}3)$$

This was found by Ellingson et al. (1994) to yield constants for a polystyrene /polymethylmethacrylate systems as: $\sigma_{12}^{\infty M} = 1.2$ and $z = 0.73$. Ellingson et al. (1994) also reported that for M_n values above 48000, the interfacial tension was independent of M_n. In this set of data, LLDPE7h, LLDPE3h and LLDPE2o have a constant interfacial tension of approximately 2 mN/m. If the M_n values of the LLDPEs are used in Equation 3-3 and the generalized curve is regressed through some of these points, it was observed that LLDPE1b, LLDPE4p and LLDPE6b do not fit the curve (Fig. 3.6). LLDPE1b shows abnormally low interfacial tension, while LLDPE6b shows a value higher than the trend.

Although this dependence can account for the low interfacial tensions of LLDPE5o and LLDPE8b, the poor fit of the remaining points could indicate that the interfacial tension is either independent of M_n for all the LLDPEs studied or that there are inconsistencies with some of the measured interfacial tension values.

The butene-octene terpolymer, LLDPE5o also has a large homopolymer content but still exhibits an average interfacial tension of 0.8 mN/m. The branch distribution as well as molecular weight distribution in metallocene catalysed polymers are known to be highly regular owing to the stereospecificity of the catalyst. The comonomer branches lead to good inter-phase penetration and thus low interfacial tension. A more intimate knowledge of the synthesis conditions for the two polymers would be needed to make a statement about the difference in their chemical structure.

The observed trend in interfacial tensions for the different comonomers for the LLDPE produced with metallocene catalysts is butene < hexene < propene < octene. The low interfacial tension of the butene comonomer LLDPE compared with other comonomer LLDPEs is remarkable. Again this pattern seems to be governed by the penetration and steric effects of each comonomer. The single methyl side group of the propene copolymer seems to be too short to have significant penetration into the PP, while the six carbon side chain of the octene copolymer might be too bulky to allow effective interaction between the two phases. Carriere and Silvis (1997) have obtained a somewhat similar trend with copolymer type (pentene < octene < butene < propene) in polypropylene - polyolefin elastomer systems but their results show a minimum interfacial tension for the pentene comonomer instead of the butene comonomer as in this study. The interfacial tension between PP1 and the Ziegler-Natta polyethylenes used in this study show an opposite trend i.e. the interfacial tension decreases as the number of carbons in the side chain increases. The trends indicated by this data must be treated with caution since all the polymers are commercial samples produced by different manufacturers and different methods. A study involving systematic variation of branch type keeping all other material properties constant would be insightful but it is difficult to obtain such polymers.

As the run temperature was increased, a modest maximum in interfacial tension was noticed at 220°C (Table 3.2). This was noticed for all three polymers tested (see Fig. 3.7) at other temperatures, namely, LLDPE5o, LLDPE7h and LLDPE8b. Pham and Carriere (1997) have reported a trend similar to this study for a polycarbonate - polyethylene system. Their system also shows a maximum interfacial tension at 220°C. However, in other studies (Kamal et al., 1997, Anastasiadis et al., 1986), interfacial tension has been observed to decrease with temperature. Kamal et al. (1994) have theoretically shown that interfacial tension between PP/PS should decrease with increasing temperature. The short chain molecules become more mobile at higher temperatures and can migrate to the interface with graeter ease, leading to this effect. From Table 3.2 and Figure 3.7, it is also conspicuously evident that all the runs carried out using the slotted plate result in higher interfacial tension. A possible reason is that enclosing the melt inside a chamber prevents flow and any possible oxidative crosslinking which slows down the breakup of the thread.

A fascinating phenomenon was observed at the interface of a PP thread in a LLDPE5o matrix while undergoing cooling after the breakup had almost been completed (Fig. 3.8). Upon cooling from 220°C to 160°C, crystallization was observed to initiate at the interface. The crystallization follows through into the PP1 (thread) phase. Wang and Liu (1999) have observed the same phenomena when PP transcrystallized on PTFE and Kevlar fibres, although in their case the crystallization occured on the outside of the threads as the phases were in reverse configuration to our system. They based their explanation on thermal stress induced crystallization, the ease of which depended upon the roughness of the thread surface as well as the surface free energy. The matrix in this case was LLDPE5o, an ethylene-butene-octene terpolymer. The fact that this type of crystallization was observed upon cooling in this system is indicative of a low interfacial tension in this system. The low Coho ratio for LLDPE5o (Table 2.2), indicates that the homopolymer content in LLDPE5o is also greater than the other LLDPEs and this might aid the transcrystallization process. Other less likely possibilities include epitaxial crystallization of a highly ordered phase separated layer which segregates from the

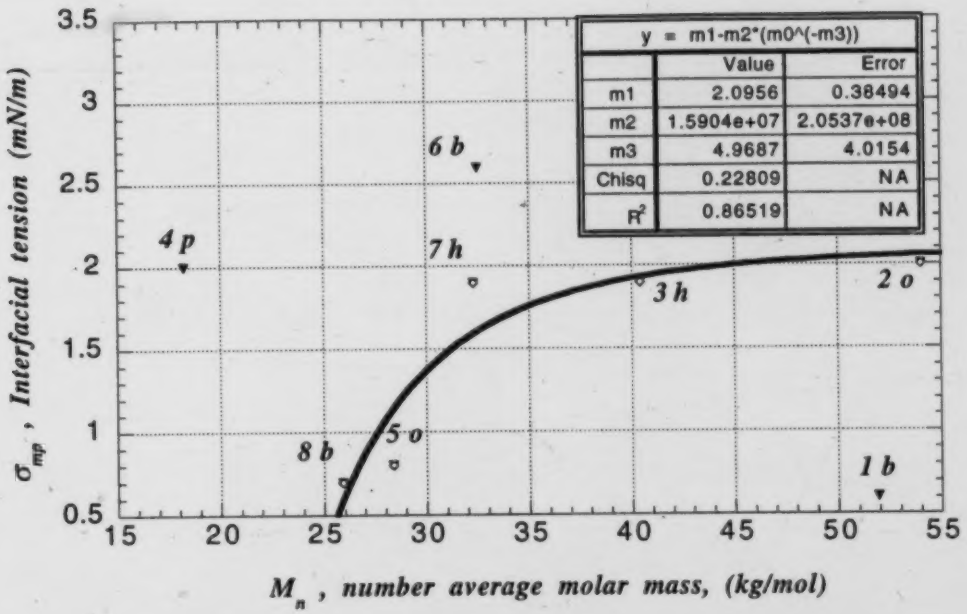

Figure 3.6 Gaines fit for LLDPE/PP interfacial tension data.

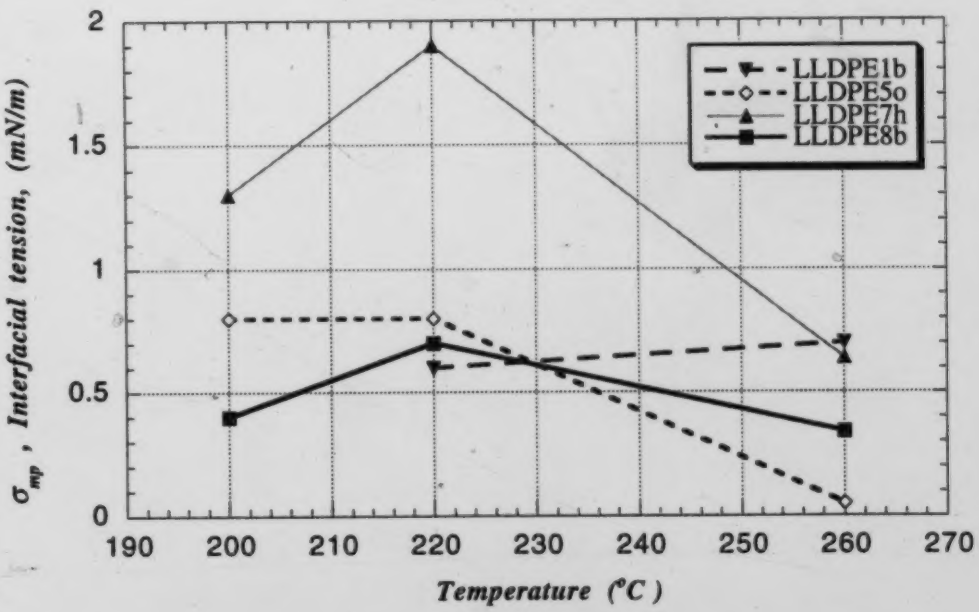

Figure 3.7 Variation of interfacial tension with temperature.

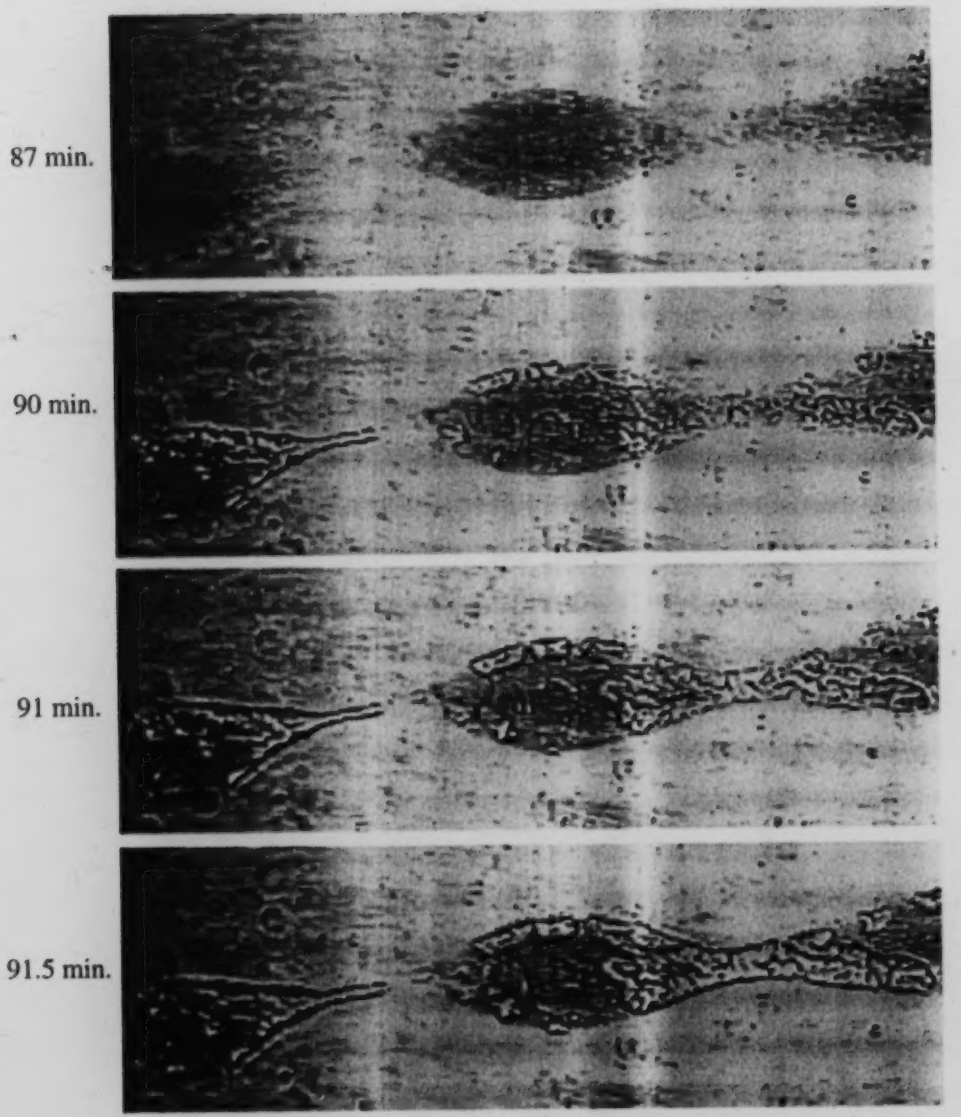

Figure 3.8 : Crystallization observed at interface during cooling of PP1 (thread) - LLDPE5o (matrix) system after breakup.

LLDPE matrix phase to the interface. It has been reported (Alamo et al., 1997) that a highly branched copolymer fraction (>80 branches/1000C) phase separates from a lightly branched (10-20 branches/1000C) majority. Also the incorporation of 1-butene comonomer into the main chain is much higher than that of 1-octene during synthesis and it probably phase separates from the bulk of the low branched octene copolymer. This would, however, still fail to explain the increased crystallinity at the interface to initiate transcrystallization.

In some experiments, especially at the higher temperatures, the breakup did not progress after the first 45 minutes. This is believed to be due to oxidation of the polymer or crosslinking at the interface of the two phases. This has also been observed by Liang and Favis (1997) in the breakup of a PVC thread inside an LLDPE matrix and they termed it 'polymer stiffening'. Experiments indicated that it is observed more often in high molecular weight polyethylenes. However, fewer cases of polymer stiffening were observed with the use of a slotted plate and with smaller diameter of the thread. The slotted plate with the sample sandwiched between glass cover plates eliminated most of the oxidation and also arrested the flow of the polymer after initial flow. This suggests that degradation might be the main cause for hindering breakup.

Breakup was also found to cease in some experiments even at 200°C. Verhoogt (1992) also observed that breakup did not occur in some of the polymer-polymer systems he studied and proposed a criterion for breakup based on the interfacial and elastic forces. Elemendorp (1986) has investigated the role of yield stress in preventing breakup but did not notice any non-Newtonian behaviour with the polymer melts he used. Goren and Gottlieb (1982) studied breakup of jets of polymer solutions, and attributed the delayed breakup of some viscoelastic jets to axial elastic tension. High elongational stresses created during the final stage before breakup lead to increase in the elongational viscosity of the thread phase. This could impede breakup in some cases. This generally manifests as a bead - string shape when the neck elongates but does not break up. Since this shape was not observed for the above mentioned cases, other phenomena such as gelling must be

taking place. LLDPE6b, however, exhibited a bead string shape during final stages of breakup at 220°C. A possible explanation, in this case, might be that the Ziegler-Natta polyethylenes containing long chain homopolymer fractions can store more elastic stresses.

Threads were found to show irregular breakup in many cases (Fig. 3.9). This could be due to insufficient relaxation of the stresses produced while pulling the thread. Higher curing temperatures used to relieve the stresses were found to distort the thread and lead to curling and loss of uniform diameter. Lower curing temperatures on the other hand left traces of moisture absorbed on the threads which would be clearly visible at the melt temperature as engulfed bubbles. According to Machiels et al. (1997) the main factor responsible for nonuniformities is initial distortion imposed by mechanisms other than simple Brownian motion. The surface roughness created while drawing the thread and macroscopic distortion upon annealing to relieve stresses are unavoidable and are probably the main causes for nonuniformities observed in this study. A better method of obtaining thin yet uniform polymer threads is still sought. It is believed that the initial non-uniformity after stress relaxation also contributes towards irregular breakup of the cylinder. Rundqvist et al. (1996) have devised an imbedded disk retraction method which avoids the necessity of producing fibres and the associated problems.

Another reason which could lead to uneven breakup is thermal stresses created during sample heating. A gradual temperature ramp is recommended for the final jump from the annealing temperature to the experimental temperature. In general, at a particular temperature, the distortion with the dominant wavelength grows and subdues the remaining wavelengths from propagating (Tjahjadi and Ottino, 1991). However, when a deformity occurs due to physical stresses, it could suppress the dominant wave from propagating and lead to nonuniform breakup. It is for this reason that annealing temperature must be kept below the melting point of the PP phase since otherwise a dominant wavelength corresponding to the annealing temperature begins to develop and

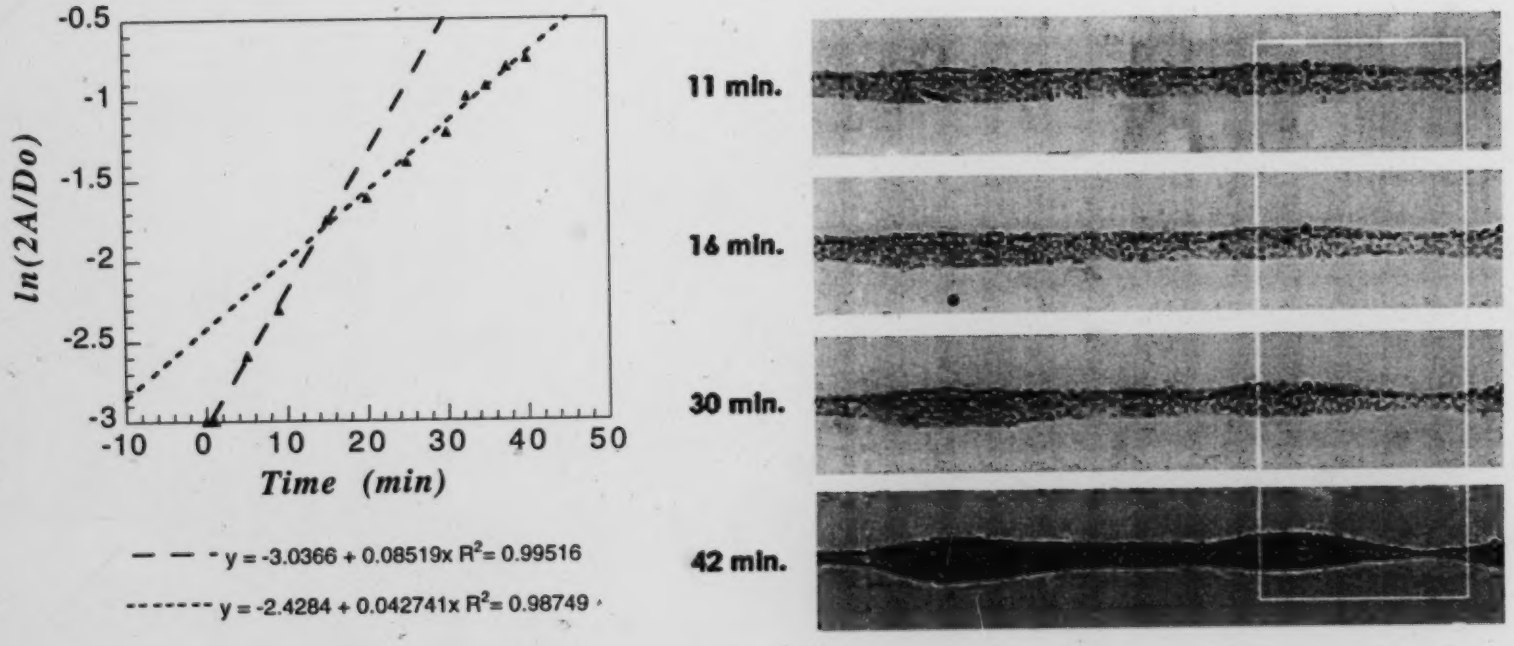

Figure 3.9 : Asymmetric breakup of a PP1 thread inside an LLDPE1b matrix at 200°C shown along with the growth of dimensionless distortion amplitude with time. (Run 21NR2 in Appendix C-II)

interferes with the proper growth of the dominant wavelength when the test temperature is imposed.

Rumscheidt and Mason (1962) reported that the breakup of highly viscous liquids showed simultaneous breakup. Chappelear (1964) found that in polymer melts although the breakup observed was uniform, the perturbations do not progress simultaneously throughout the thread but with some phase lag between successive maxima. Mikami et al. (1974) found that in the case of breakup under extension, the breakup is neither simultaneous over the length nor is the spacing between the principal droplets the same. Schummer and Tebel (1982) reported results of hindered flow of viscoelastic jets which show a similar lag in breakup with length. In this study, even in the case of final uniform breakup, the breakup was observed to successively progress from the ends towards the center, as also observed by Chappelear (1964). Thus, simultaneous breakup on both sides of the crest might not be observed. It is suspected that flow of the whole polymer sample induces extension in the thread which causes this lag.

Small air bubbles on the thread interface were observed for annealing temperatures below 60°C. The effect of these bubbles on the breakup symmetry was insignificant. The wavelength λ of the distortion remained constant until breakup, but the distance between the spheres was greater than λ due to retraction of the distorted droplets into spheres. Thus measurements for λ were conducted while the disturbance was still sinusoidal. Elemans et al. (1990) have studied the effect of addition of diblock copolymers on interfacial tension. Their experiments were similar to ours where they blended block copolymer into the thread phase. They observed that the wavelengths causing breakup were less uniformly distributed along the thread and claims that only wavelengths for which χ_{exp} are close to χ_m should be taken into account for interfacial tension measurements. The most probable interfacial tension values reported in this chapter include only those runs for which χ is close to χ_m.

The spread in the data presented in Appendix C, Tables CI - CIII, could be attributed to several factors. Samples which were not left in the vacuum oven to relieve stresses before the experiment exhibited shorter breakup times and correspondingly higher interfacial tension values, than samples allowed to relax overnight. Insufficient relaxation time, a possible factor for the high value of PS/PP interfacial tensions, would therefore lead to overestimation of the interfacial tension. Retractive effects (Stone and Leal, 1989) in thicker threads might lead to error in measuring the dominant wavelength causing breakup. For the same thread length, a combination of retraction and Rayleigh breakup will occur when a critical thread radius is exceeded. The growth profile of the dimensionless amplitude are shown in the form of log(α) (where α is 2A/Do) plots with time (Fig. 3.4). Most of the runs were found to show exponential growth rates especially with the use of the slotted sample holder. In some cases (e.g. curve III, Fig. 3.4), however, the rate of growth seemed to start out at a low value, gradually rise and then again dip down. If monitored for a long time, the final dip is observed for most cases as it signifies necking before breakup. In some cases stagnation occurs due to increase in elongational viscosity of the neck. After careful examination of the thread profile with the 2A/Do curve (Fig. 3.9) it was determined that the intermediate dips occur due to end pinching. When one end of the thread gets pinched or breaks up, retractive forces come into play and try to average out the diameter between the pinched ends. Thread phase material could either flow into or out of a cylindrical section depending on whether its diameter is less than or greater than the average diameter. In the first case the growth rate starts to rise while in the second it drops. When the diameter stabilizes a linear profile is once again established but this time with a new slope depending on the new diameter. Flow of the polymers due to pressure probably instigates the end pinching in the experiments. This is generally a problem when simultaneous breakup does not occur over the length of the thread. Higher viscosity polymers usually had greater lag between the left and right side (of a crest) breakup and are the candidates for end pinching to pose a problem.

The accurate measurement of the wavelength in the case of asymmetric breakup is very difficult and as the distortion function Ω_m is a very sensitive function of χ_m, the error in the interfacial tension value due to errors in χ_m, is significant. Another cause might be oxidative degradation while pulling the thread. In this case the thread was pulled from a carbon blended sample of polypropylene. The degradation occurring within the blender itself would lead to local differences in properties of the blended material. Cases of end pinching (Stone et al., 1986) occurring outside the field of view of the camera might have led to incorporation of inaccurate values of the initial diameter of the thread before distortions start to grow in the calculation of σ.

3.6 Predictions of Interfacial Tension

One of the common methods of predicting the interfacial tension between immiscible polymer pairs includes the self consistent field approach proposed by Helfland and Tagami (1972). They concluded that the surface free energy varied with χ_{FH} , the Flory Huggins chi parameter, as $\chi_{FH}^{1/2}$, while interfacial thickness varies as $\chi_{FH}^{-1/2}$. They also claimed that surface properties are independent of molecular weight when there is little or no solvent present. The chain ends of long polymer molecules rather than the middle linear segments are more concentrated at the interface and small molecule third components preferentially adsorb at the interface.

The measure of the change in chemical potential when the surroundings of Polymer A molecules is changed from A to B is represented by χ_{FH}. It is a measure of the degree of repulsion felt by the adjacent molecules at the interface. Solving self-consistent equations, Helfland and Tagami found that interfacial tension could be expressed as

$$\sigma = \left(\frac{\chi_{FH}}{6}\right)^{1/2} \rho_o BkT. \qquad (3\text{-}4)$$

where k and T are the Boltzmann constant and the temperature respectively, ρ_o is the number of monomer units per cm^3 and χ_{FH} is the Flory Huggins interaction parameter given by

$$\chi_{FH} = (\delta_A - \delta_B)^2 / \rho_o kT. \tag{3.5}$$

Here δ is the Hildebrand solubility parameter and b is the effective length of the polymer unit, evaluated as

$$B = m^{1/2}\left(r_o / M^{1/2}\right). \tag{3.6}$$

m is the mass of the monomer segment and M is the molar mass of the polymer and r_o is the unperturbed mean end to end distance.

In the absence of experimental data on the unperturbed mean end to end distance r_o for the polymers used, the $r_o/M^{1/2}$ values tabulated in the Polymer Handbook by Brandrup and Immergut (1989) for iPP in 1-chloronaphthalene were used. For the LLDPEs, data was interpolated from values found in Fetters et al. (1994), where the unperturbedchain dimensions for different (ethylene - 1-butene) copolymers has been evaluated. Fetters et al. (1997) found the $r_o/M^{1/2}$ values to follow a linear decreasing trend with ethyl (side) branch content for copolymers of ethylene and 1-butene. The difference in the dimensions though, is only noticeable for a larger difference in chain branching. The geometric mean of ρ for PP and LLDPEs was used to calculate ρ_o.

The solubility parameters of the polymers were evaluated based on the group contribution method. This method was first proposed by Small (1953). A refined form of the same method evaluated by Coleman et al. (1994) has been used in this study. The parameters used to evaluate δ have been listed in Table 3.3. In order to calculate the

solubility parameters, the sum of molar volumes and sum of attraction constants are calculated and substituted into Equation 3.7.

$$\delta = \frac{\sum_i F_i^*}{\sum_i V_i^*} \qquad (3\text{-}7)$$

Table 3.3 : Molar Volume and Attraction Constants for Equation 3-7

Group	*Molar Volume Constant* V^* $(cm^3\ mole^{-1})$	*Molar Attraction Constant* F^* $((cal.cm^3)^{0.5}\ mole^{-1})$
$-CH_3$	31.8	218
$-CH_2-$	16.5	132
>CH-	1.9	23

The structure of the molecule must be known in order to use this relation. The CH3/1000C information available from TREF has been used to hypothesize the structure and calculate δ for each of the LLDPEs. A basis of 1000 carbon atoms (total) was chosen of which i carbon atoms belonged to methyl groups (CH3/1000C) in the polymer. Two methyl groups per molecule are located at the ends of the molecule; the remaining (i-2) methyl groups are due to short chain branches which were assumed to be uniformly distributed along the chain. The remaining carbon atoms constituted part of the main chain and were assigned to either -CH2- or >CH- groups depending on the number of copolymer branches. The results obtained are listed in Table 3.4 and a comparison with experimental results is shown in Figures 3.10 and 3.11.

It is clear that the theoretical predictions are not able to capture the variation in interfacial tension due to branching. The predictions made from the theory proposed by Helfland and Tagami (1972) shows a very good comparison with the average experimental values (Fig 3.10). The Small method (1953) places lesser influence of branching on the solubility parameter δ. The average radius of gyration for the different LLDPEs has been

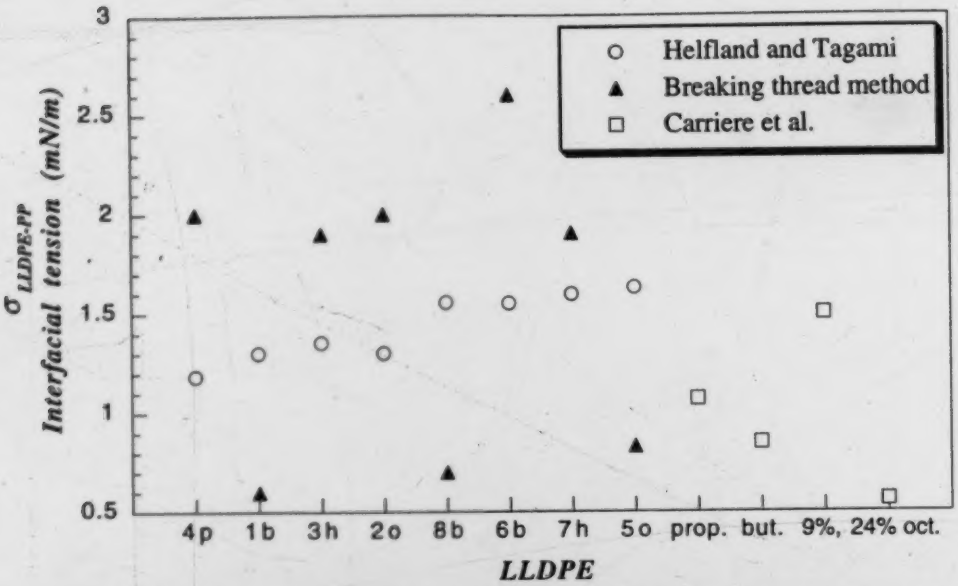

Figure 3.10 : Comparison of interfacial tension measurements (breaking thread method) with values reported by Carriere et al. (1997) and predictions obtained by the Helfland and Tagami method (1972).

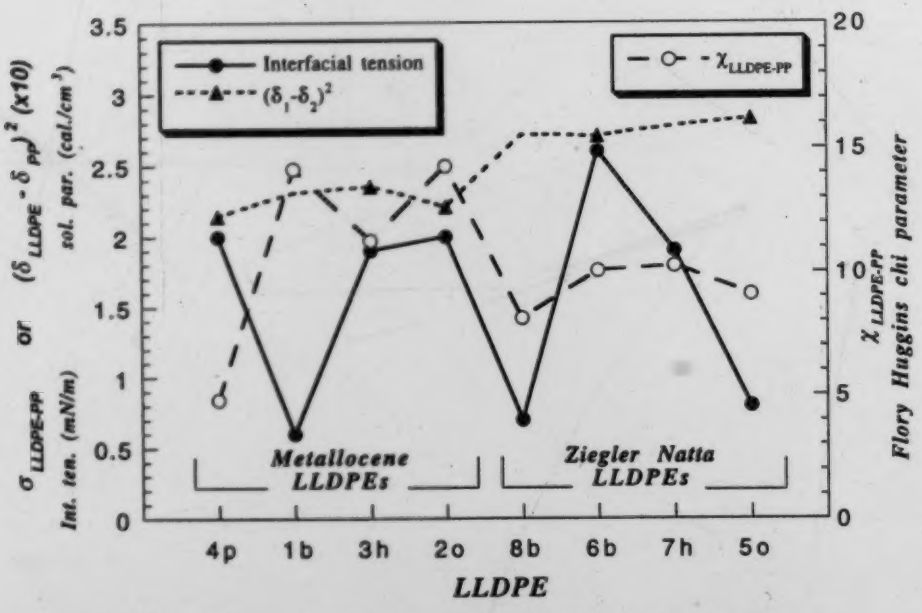

Figure 3.11 : Comparison of trends predicted by Flory Huggins theory with experimental results from the breaking thread method.

evaluated based on linear interpolation of data for Poly(ethyl butenes) of varying butene content at 413 K by Fetters et al. (1994). Dharmarajan and Yu (1996) report the value of solubility parameter of LLDPE1b based on SANS as 16.59 $MPa^{1/2}$ at a temperature of 225°C and the interfacial tension with PP1 based on that value was calculated by them to be 1.68 mN/m.

Table 3.4 : Prediction of LLDPE-PP interfacial tensions (σ) from group contribution method. Comparison of the Helfland and Tagami (1972) (H&T) method in combination with the Small method (1953), the Parachor (Quayle, 1953) method with Antonoff's rule and the breaking thread method (BTM).

LLDPE	*CH_3/1000C*	*δ* $(cal.cm^3)^{0.5}$	*$\sigma_{H\&T}$* *(mN/m)*	*$\sigma_{Parachor}$* *(mN/m)*	*χ_{AB}* *eqn. 3.8*	*σ_{BTM}* *(mN/m)*
1b	36.2	7.9546	1.52	0.83	14.2	0.6
2o	42.6	7.9443	1.51	0.81	14.3	2.0
3h	33.4	7.9592	1.58	0.84	11.3	1.9
4p	47.3	7.9367	1.36	0.80	4.8	2.0
5o	5.6	8.0059	1.97	0.91	9.1	0.8
6b	13.4	7.9925	1.90	0.89	10.0	2.6
7h	8.4	8.0011	1.94	0.91	10.2	1.9
8b	14.4	7.9908	1.90	0.89	8.0	0.7
PP1	335	7.4270	-			

The second method, the Parachor method (Quayle, 1953) does not represent the experimental data very well. This can be attributed to the fact that the branches are not distributed evenly on the main chain as assumed above. The distribution could depend on such factors as stereospecificity of catalytic sites towards comonomers, distribution of the sites on the catalyst and chain configuration of the polymer in the melt. This difference in configuration of the short chains is able to generate large local differences in the representative interacting monomer length of the two phases. The actual interfacial

configuration of the side branches is not known and cannot be expressed in a simple manner assumed here. This probably causes the large difference in measured interfacial properties observed for different copolymers. Luciani et al. (1996) provide a good critique of the different theoretical methods available for estimating interfacial tension and their merits.

$$\chi_{AB} = \frac{V_r}{RT}(\delta_A - \delta_B)^2 \qquad (3\text{-}8)$$

Equation 3-8, similar to Equation 3-5, derived for polymer solutions (Coleman et al., 1994), uses a reference volume V_r to account for the interacting segment of the molecules. When this volume is replaced by the ratio of molecular weight (M_n) to bulk density of each LLDPE, a better prediction of the trend was observed (Fig. 3.11). Except for LLDPE4p and LLDPE1b, the trend in the other LLDPEs is replicated quite successfully by this equation. The other system studied i.e. PS/PP system was not evaluated theoretically since the emphasis was only to determine whether molecular weight had any effect on the interfacial tension. Kamal et al. (1997) have reported the applicability of different theories for determining PS/PP interfacial tension.

3.7 Conclusions

The success of applying Tomotika's theory to the experiments was evident from the linear plots of ln(2A/Do) and time (Fig.3.4) for most polymers with the use of the slotted plate. Tjahjadi et al. (1994) used numerical simulation and the profile of the interface to solve for interfacial tension. The boundary integral method used by Tjahjadi et al. (1994) was used to confirm the interfacial tension value obtained for run (LLDPE1b-PP1). The agreement was within 10% and this justified the use Tomotika's linear stability theory for the analyses.

Threads, when not allowed to relax adequately, resulted in a higher value of interfacial tension. Flow of the polymer was also found to affect the experiment adversely by inducing uneven breakup. The use of the sample holder restricting the flow of polymer due to pressure and surface tension created an effective seal preventing oxidation of polymer due to air. This improved the reproducibility of the runs and eliminated the nonlinearity for most cases. It is believed that the cases of nonlinearities occurring with the slotted plate also occur due to flow when the volume expansion of the polymer is greater than the void space in the cell. Careful design of the slot for each polymer, depending on its volume expansivity, could probably remedy the occurrence of such nonlinearity in the dimensionless distortion growth profiles in future experiments.

The lowest interfacial tension with PP was observed for 1-butene copolymers LLDPE1b (0.6 mN/m) and LLDPE8b (0.7 mN/m). The error in estimating interfacial tension for LLDPE1b/PP is quite large since the breakup was not uniform (Fig. 3.9) in some of the runs. Another 1-butene copolymer, LLDPE6b (2.6 mN/m), had the highest interfacial tension with PP in the set of LLDPEs used. Based on the observation that the only difference between the TREF profiles (Fig. 2.8) of LLDPE6b and LLDPE8b was the homopolymer fraction, it was concluded that the long chain crystalline fraction of polyethylenes plays a key role in interfacial tensions. The linear polyethylene fraction probably interacts poorly with the polypropylene chains. The ethylene-octene-butene terpolymer, LLDPE5o also shows a low interfacial tension. Transcrystallization in the PP1 thread was also observed (Fig. 3.8) while cooling the LLDPE5o/PP sample after breakup. The remaining LLDPEs showed an interfacial tension close to 2.0 mN/m.

The LLDPE/PP interfacial tensions decreased with temperature (with $\sigma_{260^\circ C} < \sigma_{220^\circ C}$) although, at 220°C, a peak was observed (Fig. 3.7). The measurements at 220°C (Table 3.2) were carried out using a slotted plate which sealed the sample while, most of the other measurements were conducted before the slotted plate was introduced. This is believed to be responsible for the slightly increased values although the exact mechanism could not be identified.

Interfacial tensions for the current set of polymers did not vary systematically with molar mass. The effect of elasticity in the breaking thread method manifests in the form of final breakup resembling a bead-string configuration (Elmendorp, 1986, Mikami et al., 1974). This shape was observed for LLDPE6b. This LLDPE also shows a higher interfacial tension than other butene copolymers considered. Again, the higher molecular weight homopolymer fraction is probably responsible for this behaviour.

No clear trends were observed with respect to LLDPE branch length except that 1-butene copolymers showed lower interfacial tension versus PP than did LLDPEs with longer branches. If the octene-butene terpolymer LLDPE5o were to be considered as a 1-butene copolymer, the butene copolymers show an average interfacial tension approximately half that of other comonomer types (Fig 3.11). The trends predicted from theory (Fig. 3.10) indicate that metallocene LLDPEs should possess a lower interfacial tension than the Ziegler-Natta LLDPEs of the same comonomer type based on the higher branching of the metallocene copolymers. The experimental results, however, do not support this prediction. This suggests migration of branched moities to the interface. Experiments indicate that the comonomer chain length and the branch density on the main chain are equally important factors in determining the interfacial tension of the polymer with another. Both of these will vary for LLDPEs from different suppliers and processes. The crystalline fraction in case of Ziegler-Natta polyethylenes, plays a great part in shaping the interaction between polyolefins. The results obtained by Carriere and Silvis (1997) using the imbedded fibre retraction method, which showed that the octene copolymer LLDPE has the lowest interfacial tension was not confirmed in the present study. The propylene copolymer LLDPE in this study does, however, show a greater interfacial tension than the butene copolymers which is in agreement with the results from Carriere and Silvis (1997). These results suggest that the molecular structure of the polyethylenes e.g. the methylene sequence length distribution, plays a key role in the interfacial properties of LLDPEs and PPs. The nature and amount of the comonomer alone cannot be used to predict interfacial tension between two polymers.

Morphology and Impact Strengths of Blends

Chapter 4

4.1 Introduction

The last two decades have seen the advent of synthetic materials for replacing natural materials, thereby achieving lower costs and higher productivity. Newer technology also demands robust performance from a material under a wider range of conditions than ever encountered before. These properties might include lighter weight, better UV resistance, higher degradation temperature, improved low temperature toughness and superior chemical resistance to name a few. However, the chemistry of synthesizing new materials has not been able to keep pace with the growing needs of the industry. For this reason, blending two materials possessing the desired properties provides an attractive alternative to synthesis of a new material. Blending of two materials can broaden the range of products that a chemical plant produces. Blending equipment such as extruders are compact and can be incorporated with minimum demand on space and resources. In a world with growing environmental awareness, the need for recycling and conservation has also provided an incentive for the academic world to study polymer blends and compatibility.

The last chapter dealt with the measurement of interfacial tension of two polymers. It has been shown by Elmendorp (1986) that the morphology of a blend determines properties such as toughness, elongation and strength of the blend, and it is affected by parameters such as temperature, shear rate and interfacial tension. Micron or submicron dispersions of one material inside the other is usually required to gain synergism in desired properties from the constituents (Datta and Lohse, 1993). Interfacial adhesion has been

shown (Wu, 1985) to be a necessary condition for rubber toughening to occur. Yuan and Wool (1990) have looked at intraspherullitic entanglements formed upon crystallization in hot compression molded samples of LLDPE laminated on PP to explain the enhanced strength of the interface for slowly quenched samples. In this chapter, morphology of blends is examined to uncover some of the major factors affecting LLDPE/PP blend impact strengths.

4.1.1 Factors Affecting the Morphology of the Dispersed Phase

In order to optimize blends, it is useful to understand the factors affecting the morphology of blends. Blends, unlike emulsions, never reach their equilibrium size distribution and can exhibit morphologies other than droplet - matrix morphologies seen in Newtonian systems. Morphology is affected most by factors such as concentration of phases, viscosity ratio and elasticity of the two phases, which will be discussed in more detail in the following paragraphs.

4.1.1.1 Processing Conditions Affecting Morphology

Composition has a profound effect on the dropsizes and dropsize distribution of the dispersed phase, especially in the range of concentrations where dual phase continuity is observed for blends (Favis and Chalifoux, 1987). The dropsize increases with concentration while the polydispersity of dispersed-phase dropsizes decrease with increase in concentration. Phase inversion occurs at sufficiently high concentration of the dispersed phase. This means the minor and major phase revert their roles and become continuous phase and dispersed phase, respectively. A co-continuous regime occurs over a range of concentrations, the morphological implications of which might include interpenetrating networks (IPNs). Jordhamo et al. (1986) presented the following semi-empirical expression for predicting the phase inversion point based on the viscosities of the two components of the blend :

$$\frac{\eta_1}{\eta_2} \cdot \frac{\varphi_2}{\varphi_1} \cong 1 \qquad (4.1)$$

where η_i is the viscosity of component i and φ_i is its volume fraction.

The temperature, an important processing parameter, may not affect the viscosity ratio of the blend and is therefore not expected to have a major effect on the dropsize. Other dependent variables such as interfacial tension also show a weak dependence on temperature.

Higher shear rate has been found by some to produce finer dispersion (Taylor, 1932, Schreiber and Olguin, 1983). Favis (1990) reported that the dropsizes remained unaffected over a wide range of shear rates. The effect of shear rate is strongly dependent on the viscosity ratio of the system chosen. The explanation offered by Favis (1990) for the weak shear dependence of dropsize was that even though the blend component viscosities decreased, the non-Newtonian viscosity ratio could be unaffected. Dispersed phase dropsizes in blends of intermediate viscosity ratio were found to decrease with time. Fortelny et al. (1993) have reviewed the dependence of dropsizes on the intensity and time of mixing and found that dropsizes can also increase with shear rate for some systems. This was attributed to the increased collision frequency at higher shear rates causing coalescence of multiple droplets to give larger dropsize.

Time of mixing has been found to have a significant effect only in the initial period of blending as most of the morphological changes occur during this period. Favis (1990) found the time of mixing to be unimportant after 2 minutes for high and low viscosity ratios.

The effect of pressure on blend morphology has not been widely studied in literature, mainly due to the fact that polymers have memory and any pressure applied during processing can reduce the dimensional accuracy of the molded part made out of the blend as it relaxes. In future studies it would be worthwhile investigating the effect of a

constant volume blend as opposed to a constant pressure blend. In general, the mixer is not filled to full capacity hence the pressure is atmospheric.

The type of blending equipment used will also affect the properties of the blend based on how efficiently it provides momentum and heat transfer to the polymer melt. The dispersion in dropsizes will depend on the flow distribution inside the mixing chamber. Twin screw extruders are used in industry for obtaining effective mixing. The Haake batch mixer used in this study has been observed to mimic industrial mixers quite well (Sundararaj et al., 1995b). In a mixer, the effect of increasing the length of the barrel in an extruder is achieved by increasing the mixing time.

Quenching time after blending is a parameter which has an effect on the coarsening of the dispersed phase by coalescence. Coalescence effects increase the steady-state sizes of the droplets during mixing (Fortelny et al., 1993) at high enough concentrations. Coalescence is most important at low shear rates with long residence times and large interfacial tension (Serpe et al., 1990). Elmendorp and Van Der Vegt (1986) showed that at low concentrations (<0.5%), the Newtonian dropsize predictions made by Taylor are satisfactory but at higher concentrations coalescence increases the average domain size. They stated that "the coalescence probability is substantial only when the polymer/polymer interfaces show a high degree of mobility". Additives such as compatibilizers and block copolymers are added to provide interfacial stability and reduce coalescence.

4.1.1.2 Material Properties Affecting Morphology

Interfacial tension between the two phases has a very important role in determining blend morphology. Blending of one phase in the other increases the interfacial area, and the reversible energy imparted to the blend via shear is stored as interfacial energy at the interface. For this reason longer shearing times in addition to more viscous heating, gives finer dropsizes. Each stage of polymer dispersion into finer geometries involves interfacial tension as one of the driving forces. The lower the interfacial tension, the finer is the

dispersion of one phase inside the other. Chemical compatibility of the materials is generally manifested as low interfacial tension.

The viscosity ratio of a blend has been found to be one of the most important factors in determining blend properties and morphology. Taylor (1932) studied the effect of simple shear forces on the breakup of a Newtonian drop inside a matrix. A dimensionless number, called the Capillary number (Eq. 4.2), which represents the ratio of viscous forces to the interfacial force, was used by Taylor to model the breakup.

$$Ca = \frac{\dot{\gamma}\eta_m D}{2\sigma} \tag{4.2}$$

where $\dot{\gamma}$ is the shear rate and D is the drop diameter. By balancing the interfacial force to the shear force, Taylor (1932) obtained the following correlation for Ca as a function of the viscosity ratio, p ($= \eta_d/\eta_m$), for the maximum drop diameter that would be stable in that flow field :

$$Ca_{max} = \frac{(8p+1)}{(19p+16)} \qquad p < 2.5 \tag{4.3}$$

No breakup was predicted for viscosity ratio > 2.5. Several researchers (Rumscheidt and Mason, 1961; Grace, 1982) have presented data from simple shear experiments on Newtonian systems which show that there is no breakup for a viscosity ratio of 4. Most early experiments on elongational flow field were generated on a 4 roll mill and rotational or irrotational flow patterns were obtained by adjusting the rotation of the rolls. Grace (1982) showed that breakup was possible in pure extensional flow for all viscosity ratios.

It must be remembered that the flow inside commercial equipment is a complex combination of shear and elongational flows and the polymer melt itself is non-Newtonian. Taking a step in this direction, Van Oene (1972) addressed the role of elasticity in the

deformation process of a viscoelastic droplet. Van Oene defined a criterion for the formation of droplets of phase α in a matrix of phase β based on the dynamic interfacial tension which is defined as:

$$\sigma_{\alpha\beta} = \sigma^{0}_{\alpha\beta} + (\frac{D_{\alpha}}{12})[N_{1,\alpha} - N_{1,\beta}] \tag{4.4}$$

where $\sigma_{\alpha\beta}$ is the dynamic interfacial tension and $\sigma^{0}_{\alpha\beta}$ is the measured quiescent interfacial tension between the two polymers; $N_{1,\alpha}$ and $N_{1,\beta}$ are the dispersed and matrix phase first normal stress differences (elastic properties), respectively. For droplet formation of phase α in phase β, the dynamic interfacial tension has to be a positive quantity. This is satisfied when either of the following conditions are satisfied:

$$(1) \quad [N_{1,\alpha} - N_{1,\beta}] > 0 \quad \text{or} \tag{4.5}$$

$$(2) \quad \sigma^{0}_{\alpha\beta} > \frac{D}{12}[N_{1,\alpha} - N_{1,\beta}] \text{ i. e., } \sigma_{\alpha\beta} > 0$$

In our case, the blends were prepared with LLDPE dispersed in the PP matrix phase. The interfacial tension measurements for PP dispersed in LLDPE can be assumed to be the same as that for the system with the phases reversed, i.e. LLDPE as dispersed phase and PP as the matrix phase. Sundararaj (1995) has confirmed this for a PS/PP system. Fortelny and Kovar (1992) have suggested the use of an approximation for determining the first normal stress difference from rheological measurements when the shear rate is nonzero:

$$\frac{N_1(\dot{\gamma})}{\dot{\gamma}^2} = \frac{2G'(\omega)}{\omega^2}\left[1 + \left(\frac{G'(\omega)}{G''(\omega)}\right)^2\right]^{0.7} \qquad \text{for } \dot{\gamma} = \omega \tag{4.6}$$

According to Van Oene, if the dynamic interfacial tension is positive, a droplet - fiber morphology is predicted. Otherwise a stratified morphology of minor phase results. In essence, if the normal stress difference is large enough, then it can override the effect of interfacial energy in determining the morphology of the dispersed phase. Due to the difficulty in accurately estimating the shear conditions in mixing equipment, there are significant errors in predicting the local normal stress differences. The application of single drop results on a system with an average dropsize and dropsize distribution are also not accurately known and hence Van Oene's theory has neither been confirmed nor refuted (Fortelny and Kovar, 1992).

Wu (1987) studied the role of viscosity ratio in the formation of dispersed phase in immiscible polymer blends. Wu (1987) obtained a master curve of Ca plotted against the viscosity ratio p for blends made with different combinations of immiscible polymers in a twin screw extruder. He found that the dispersed dropsize was directly proportional to the interfacial tension and the +/- 0.84 power of viscosity ratio. This was expressed as

$$Ca = 2p^{\pm 0.84} \qquad \begin{matrix} +0.84 \text{ for } p > 1 \\ -0.84 \text{ for } p < 1 \end{matrix} \qquad (4.7)$$

where Ca is given by Equation 4.2 and p is the viscosity ratio (in this case, $\eta^*_{LLDPE} / \eta^*_{PP}$ at 65 rad/s). A viscosity ratio of 1 was observed by Taylor to give the smallest dispersed phase particles. Bains et al. (1994) have reported a dramatic improvement in the solid-state tensile properties of LLDPE/PP blends when the viscosities of the two phases were closely matched. Favis and Chalifoux (1987) have also shown that the dropsize shows a minimum at a viscosity ratio close to 0.3 but at very low concentrations of the dispersed phase, the dropsize becomes relatively constant at low viscosity ratio.

4.1.2 Development of Blend Morphology

Mixing of one phase inside the other is determined by two mechanisms - distributive mixing and dispersive mixing (Golba and Seeger, 1987). Distributive mixing can be affected by factors such as mixer dead spaces, flow patterns (Scott, 1990), initial phase distribution (Ghodgaonkar, 1997) and other parameters which effect the movement and distribution of particles of one phase inside another. The other mechanism which governs blend properties is dispersive mixing. The deformation of the minor phase by this mechanism occurs by transfer of stress across the interface causing breakup of the minor phase into smaller particles which are then able to counteract the applied stress with interfacial forces. The mechanical stress across the interface can be imparted by shear or elongational stress.

The mixing of one component inside the other proceeds through various transient stages of morphology as explained by Scott and Macosko (1995), and Sundararaj et al. (1995). Mixing inside the blender typically involves melting of one phase before the other. The phase to melt first engulfs the unmelted pellet phase. Depending on the viscosity ratio and volume fractions of the two components, a variety of final morphologies are possible. Elemens (1989) has shown the systematic effect of viscosity ratio and volume fraction on the blend morphology of HDPE/PS blends. According to the mechanism proposed by Scott and Macosko (1995), shearing stretches the polymer pellets into sheets (Figure 4.1). As the shearing continues, the sheets either show a fingering mechanism and split into elongated threads or become thin enough for initiation of holes in them.

Digressing to the topic of sheets, Lahoti (1997) observed that under quiescent conditions, the velocity of hole growth in a polymer film embedded inside another polymer was a strong function of interfacial tension and matrix viscosity, but it did not depend on the film thickness within the range of thicknesses he studied. The holes grew until they intersected each other giving rise to a polygonal arrangement of threads, which further disintegrated into droplets by Rayleigh breakup. Under conditions of flow, it is possible

that thicker sheets allow the formation of fingers while the thinner sheets disintegrate rapidly, directly to droplets.

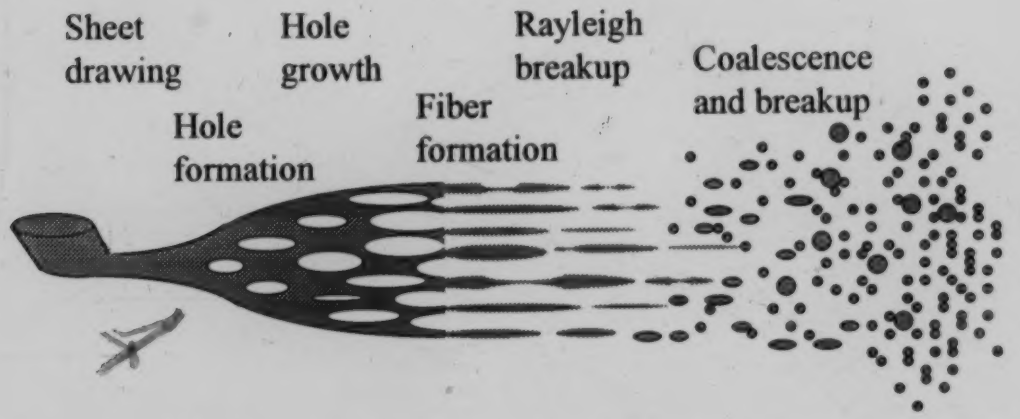

Figure 4.1 : Morphology development in a polymer blend via dispersion. (Adapted from Scott and Macosko, 1991)

The threads formed by the fingering mechanism, elongate and breakup into a series of droplets by the mechanism of Rayleigh breakup, the quiescent version of which has been reported in Chapter 3. Tjahjadi and Ottino (1991) have studied breakup of threads in conditions of shear flow. If the shearing continues, the larger droplets can again elongate into threads and breakup into droplets of smaller size. This process repeats itself until the interfacial forces balance the shear forces on the droplet and prevent further breakup.

4.1.3 Fracture Surface Development

Hobbs (1980) pointed out three morphological regimes in fracture surfaces of moderately ductile rubber toughened blends depending on the speed of the crack propagation (as shown in Figure 4.2).

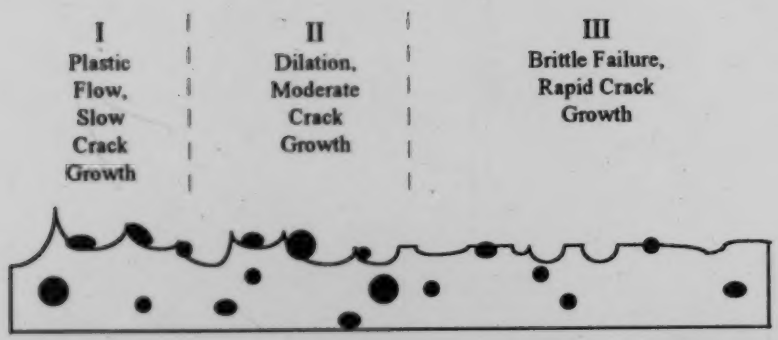

Figure 4.2 Morphological zones in a rubber modified blend. (Adapted from Hobbs, 1980).

According to Hobbs (1980), the crack propagates at slow rates in the first regime causing plastic flow and deformation. The second regime is a zone with moderate crack growth. The matrix phase observes some plastic deformation while the minor phase gets separated from the surrounding matrix relatively undeformed. The third regime explained by Hobbs (1980) is a rapid growth crack which dislodges and severs droplets making it difficult to characterize them. Most of the zones observed in this study correspond to the third regime.

4.2 Experimental

4.2.1 Blending Procedure

A Haake Rheocord 90 torque rheometer equipped with a Haake 600 series batch mixer (Fig. 4.3) was used to prepare the blends. The mixer had programmable temperature as well as programmable rotational speed and was air cooled. The roller blades were shaped (Fig. 4.3) to provide good kneading action similar to that obtained in a twin screw extruder. The rotational speed of one blade was 66% of that of the other blade connected to the drive shaft. This is believed to enhance the distribution of the polymer into both chambers and enable intimate mixing. The mixer was preheated to the start temperature before loading the polymer pellets. Most blending was carried out at 220°C but some investigative torquing, discussed in later sections, was also carried out with programmed temperature ramping. The pellets were dried overnight typically at 80°C to remove

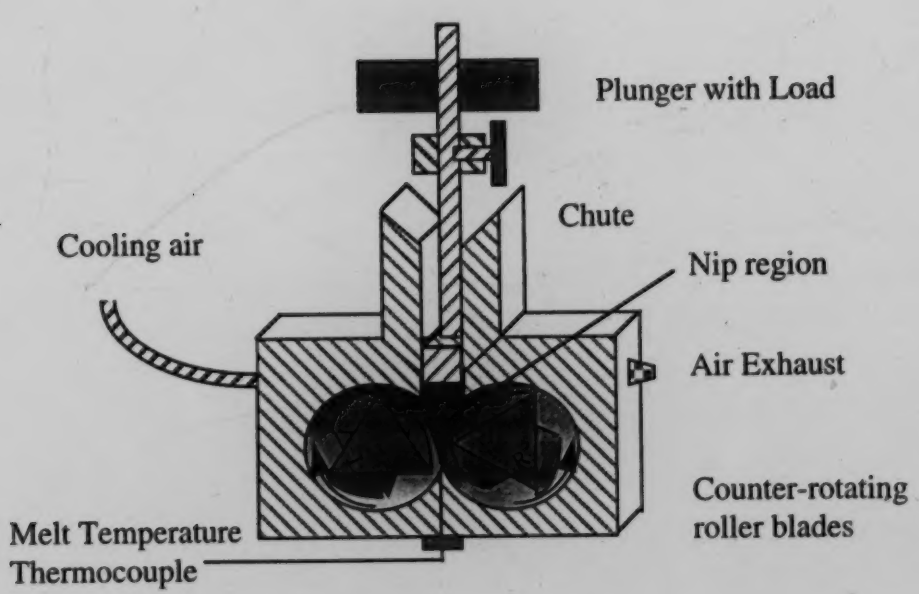

Figure 4.3 : Haake Rheocord 600 mixing chamber and roller blades.

volatiles. Pellets of metallocene LLDPEs softened at 80°C, and hence were dried at 60°C. The polymer pellets were weighed using a Mettler PC2000 weighing scale with an accuracy of 0.01 g. In order to obtain optimum dispersion, the mixing volume should be set to be 78% of the total mixer volume. This volume has been shown by Scott (1990) to minimize stagnant areas in the mixer due to overloading and avoid segregation of the phases around the mixer blades in the case of under-loading. The weights of the individual components to obtain the 78% volume loading were then determined based on the pellet densities. A rough estimate for the melt densities can be arrived at by using data provided by Van Krevelin (1990), but errors due to different crystallinities cannot be avoided. The polymer pellets were premixed in a beaker and loaded onto a hopper. The pellets were loaded into a chute leading to the mixing chamber and a plunger attached with a 5 kg load was used to guide the polymer into the chamber. A spring loaded latch locked the plunger in place, thereby creating a constant volume chamber during the mixing. A nitrogen blanket was used while loading the polymer pellets into the mixer to avoid possible degradation due to oxidation. The polymers, however, were observed to expand upon melting and drive out any gas inside the mixer. A blend time of 5 minutes was determined to be sufficient to get a stable dispersed phase drop size.

Once the blend time was over, the rotor blades automatically stopped rotating. The mixer face plate was removed as soon as possible followed by removal of the plate comprising the mixing chamber. A sample of the blend was scooped from different zones of the mixer and either directly quenched in liquid nitrogen for dropsize analysis via SEM or used to prepare Izod specimens on a Carver plate press as explained in the following sections.

4.2.2 Izod Impact Test Specimen Preparation Procedure

Blends of PP and LLDPE were tested for the improvement in impact strength of PP using ASTM D256-93. For this method, the sample is either molded or machined into strips of standard thickness and notched along the side of least thickness. A pivoted

pendulum which is loaded with an appropriate weight strikes the specimen, the lower half of which is firmly clamped. The velocity of the pendulum in this case was 3.4 m/s. The Izod impact strength is measured by calculating the loss of kinetic energy of the pendulum after it strikes and fractures the specimen along the notch.

The standard strips for measuring Izod impact strength are conventionally obtained by injection molding. The small quantities of blends (approximately 40 g) produced by the batch mixer forced a modification of the test specimen preparation. The blend, still molten from the mixer, was transferred to a preheated mold on a Carver plate press. A plate of dimensions 89 mm x 71 mm x 3 mm was molded at 220°C (same as the blending temperature) and 4.65 MPa for a period of 1 minute. The plate obtained from the mold was machined to obtain five test specimen of dimensions 63.5 mm x 12.5 mm x 3 mm. Details of test specimen dimensions are furnished in Appendix D. Frequently, the polymer plate made in the Carver press contained bubbles. Sufficient amounts of bubble-free regions were usually available for cutting 5 specimen. In the case where insufficient bubble-free regions were available, the specimen were machined so that the bubbles were far away from the Izod fracture zone, i.e., there were no bubbles close to the notch. This problem with bubbles is rarely faced when samples are prepared by injection molding.

4.2.3 Scanning Electron Microscopy of Blend Samples

The main optical methods available for analyzing the microstructure of polymer blends include scanning electron microscopy (SEM), transmission electron microscopy (TEM) and light microscopy. Vasely (1996) has reviewed different techniques to study polymers. Reviews by Hobbs (1980), and Michler (1996) focus on electron microscopic methods and address the merits and limitations of these techniques for polymers. In view of the fact that the size of microstructures in the blend, which could include spheres, voids and fibers, were typically expected to be in the 0.1-10 μm range, SEM was chosen as the prime tool for characterization. Sample preparation for SEM analysis is also less cumbersome than sample preparation for TEM. The microscope used was a Hitachi S-

2700 SEM equipped with a Canon camera with a Polaroid attachment. After analysing the SEM pictures it was clear that a distinction had to be made as to how the samples were prepared. The samples for morphology analysis by SEM could be divided into three categories based on the technique used to expose the fracture surface and amount of processing undergone by the blend as shown in Figure 4.4.

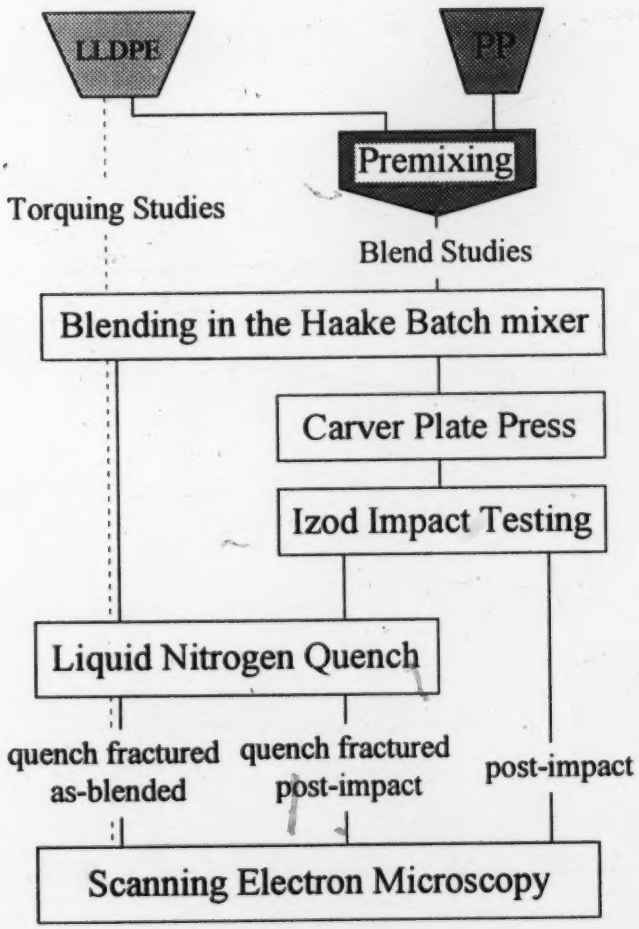

Figure 4.4 Schematic of fracture surfaces originating from different procedures.

The first category, which will be termed as "quench fractured as-blended" samples, abbreviated as "QFAB" samples, consisted of samples obtained from the mixer, directly

after the completion of blending. Most of the preliminary analysis of the LLDPE/PP blends and some PP/PS blends were carried out on QFAB samples. The transient shapes of minor phase can still be captured at this stage if the sample is quenched quickly in liquid nitrogen.

Blend samples were scooped from different zones of the mixer and quenched in liquid nitrogen. The time elapsed between stopping the mixer and quenching the melt was less than 30 s. During the quenching, the polymer melt rapidly cools from outside towards the core and due to the mechanical stresses created, the polymer chunk breaks into fragments. To facilitate easy retrieval of the polymer fragments, a wire metal sieve cup was designed. If the polymer sample did not fracture in the liquid nitrogen, then it was impacted upon by a hammer and fractured while still cold. Fragments of the blend were glued onto a conducting SEM stub with the help of double sided adhesive tape. The opposite plane was trimmed so as to keep the fractured surface as close to a horizontal position as possible. Skewing of the fracture surface can lead to errors in perceiving the morphological features on the polymer fragment. The polymer samples were then coated with a thin layer of carbon in an evacuated cathodic chamber with a graphite rod as the anode. The coating provides a conductive path and prevents charging and overheating of the sample during SEM examination. The stubs were then mounted on a brass sample holder which slides into a dovetail slot in the chamber. The height of the samples was kept at 5 mm to permit easy placing and maneuvering of the polymer samples via an intermediate quick insert vacuum chamber into the SEM chamber.

The second category of SEM samples, which will be termed as "post-impact Izod" samples or simply "PI-Izod" samples, comprised of broken pieces obtained from the Izod test apparatus after impact strength measurement. The morphological features of these samples might be shadowed by the effects of coarsening, because of undergoing the extra molding step on the Carver press. Fracturing at room temperature is also expected to bring in extra effects of plastic flow of the phases. The mode of fracture initiation in this case is more reproducible because the sample is impacted upon with the same velocity

each time and the presence of a notch directs all the impact along a plane whereas in the QFAB case the impact initiates a crack randomly.

The Izod specimen broke cleanly into two pieces for all but one of the 150 total specimen tested. The fractured pieces of PI-Izod samples of each blend were grouped together and bound with copper tape and then coated with carbon. The bundle was gripped in a special spring loaded metal sample holder. The sample height was approximately 30 mm hence it had to be inserted into the SEM chamber through the main opening.

At the initial stages, after SEM analysis of some of the Izod specimen by the above method (all the 5% LLDPE/PP blends as well as the 10% and 20% LLDPE1b/PP1 blends), it was felt that the phase boundaries were not very sharp for some of the blends. In order to obtain sharper boundaries for dropsize estimation, the broken pieces of the remaining PI-Izod samples were quenched in liquid nitrogen, clamped on vicegrips and fractured with a hammer. The fracture direction in this case (thickness-wise) was perpendicular to the (width-wise) fracture direction obtained by the Izod test apparatus. SEM samples obtained thus comprised the third category termed "quench-fractured post-impact" samples or simply "QFPI-Izod" samples. The height of these samples was typically 15 mm and in most cases they could be inserted into the main SEM chamber using the quick insert vacuum chamber.

A beam voltage of 10 kV and a beam current of approximately 6-8 mA was used in most of the SEM examinations to get good resolution. A beam voltage of 20kV was also used in some cases with good results but was not used routinely as overheating of the sample was a concern.

4.3 Results

4.3.1 Torque Profiles in the Haake Mixer

Blends were prepared at three different mass fractions (5, 10 and 20%) of the dispersed phase. The Haake mixer was equipped with torque transducers which measured the resistance felt by the mixer blades during blending. The torque versus time curves for two of the systems, namely, LLDPE1b/PP1 and LLDPE2o/PP1 are shown in Figures 4.5 and 4.6 for different concentrations of LLDPE.

4.3.2 Results of Impact Strength Testing using ASTM D256

Detailed tabulation of the results of the impact strength testing are given in Appendix D (Table D.1). These measurements were conducted at Nova Research and Technical Centre. A summary of the results is presented in Table 4.1. In Figure 4.7, the impact strength is plotted as a function of the viscosity ratio for various dispersed phase concentrations at the blending temperature and shear rate. Figure 4.8 shows the impact strength of PP1 as a function of concentration of LLDPE.

Pictures of PI-Izod pieces taken using a stereomicroscope are presented in Figure 4.9, for a sample of 10% LLDPE2o/PP1 blend, blended at 220°C, 50 rpm and 10 minutes. The impact strength of each specimen is listed at the bottom of the figure. The PI-Izod surfaces shows three zones (Fig. 4.9). The first zone was a stress whitened zone at the notch tip. This was followed by the second zone, a flat surface indicating brittle fracture, interspersed with white streaks which indicate secondary crazing. As the crack velocity increases, the streaks recede and the surface of the fracture curves owing to the pivoting motion of the upper segment of the Izod sample about the bottom segment, which is firmly clamped. As the crack proceeds to the pivoting point, the white streaks reappear. The second zone was the most promising section for dropsize analysis. The curved shape of the fracture surface can also be seen in Figure 4.9. The impact strength was found to increase with the cumulative whitening due to plastic deformation and crazing.

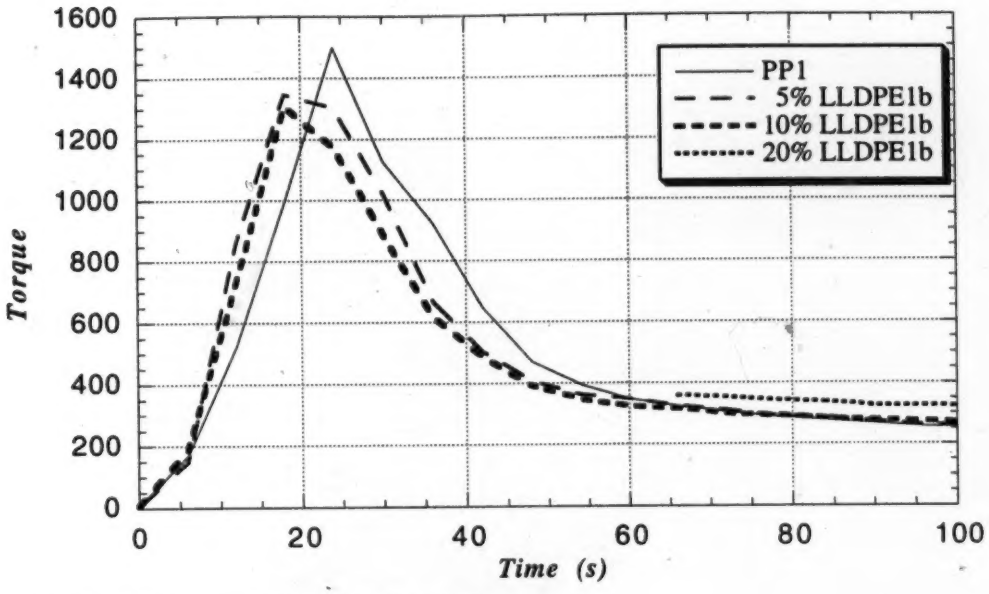

(a) Torque profiles for initial times.

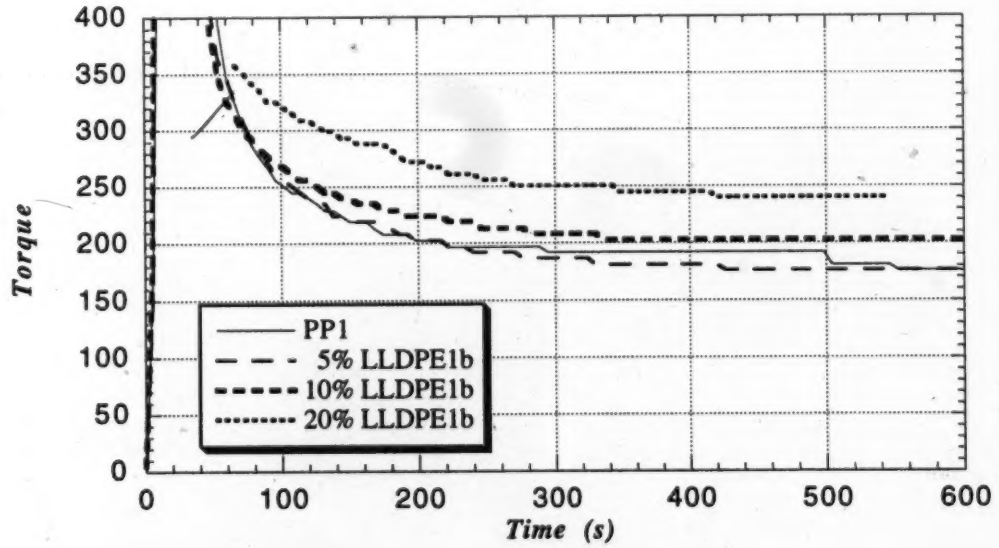

(b) Torque profiles during 10 minute run.

Figure 4.5 : Effect of dispersed phase concentration on the mixer torque for LLDPE1b/PP1 blends prepared at 220°C.

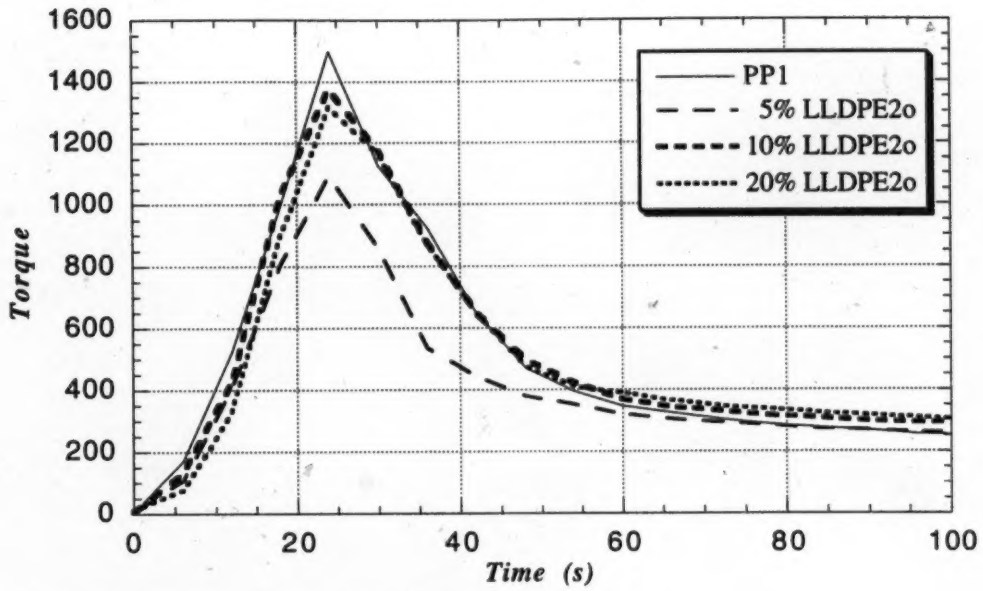

(a) Torque profiles at initial times.

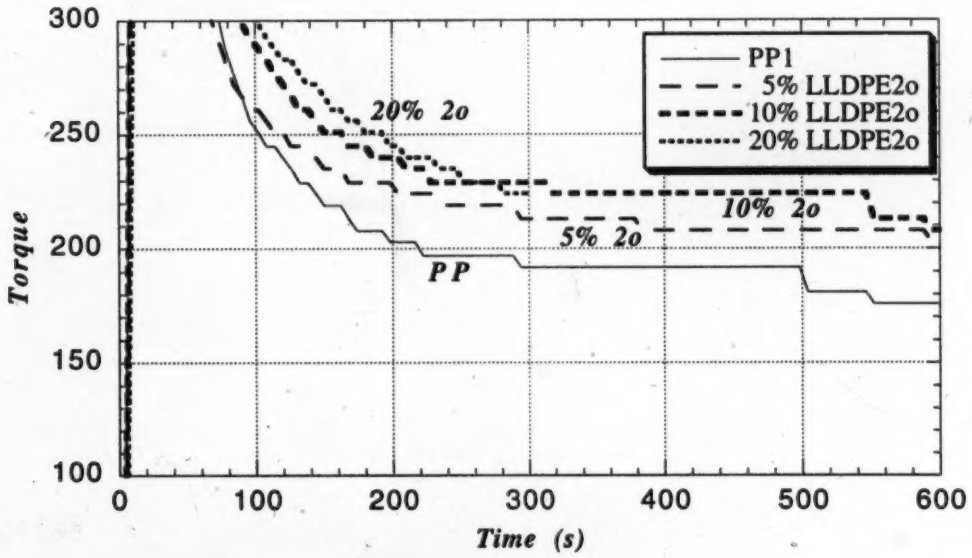

(b) Torque profiles during 10 minute run.

Figure 4.6 : Effect of dispersed phase concentration on the mixer torque for LLDPE2o/PP1 blends prepared at 220°C.

Table 4.1 : Izod Impact Strength of Polypropylene blends at 23°C using ASTM D256-93

Dispersed Phase	wt. (%)	Izod (Nm/m)	STD (Nm/m)
PP1 (as is)	0	30.09	3.63
PP1 (tor. 5 min.)	0	34.89	1.87
LLDPE 1b	5	40.73	3.84
LLDPE 1b	10	46.12	2.82
LLDPE 1b	20	61.07	2.00
LLDPE 2o	5	42.76	3.41
LLDPE 2o	10	51.88	4.00
LLDPE 2o	20	55.09	2.75
LLDPE 3h	5	39.18	3.83
LLDPE 3h	10	48.15	4.69
LLDPE 3h	20	60.69	2.14
LLDPE 4p	5	43.66	3.94
LLDPE 4p	10	48.63	2.97
LLDPE 4p	20	45.16	1.86
LLDPE 5o	5	39.93	4.48
LLDPE 5o	10	42.68	4.43
LLDPE 5o	20	51.78	3.14
LLDPE 6b	5	38.49	3.75
LLDPE 6b	10	42.54	2.46
LLDPE 6b	20	46.60	2.80
LLDPE 7h	5	43.98	3.80
LLDPE 7h	10	46.87	2.31
LLDPE 7h	20	51.14	3.04
LLDPE 8b	5	43.50	4.05
LLDPE 8b	10	46.33	3.67
LLDPE 8b	20	49.48	2.39

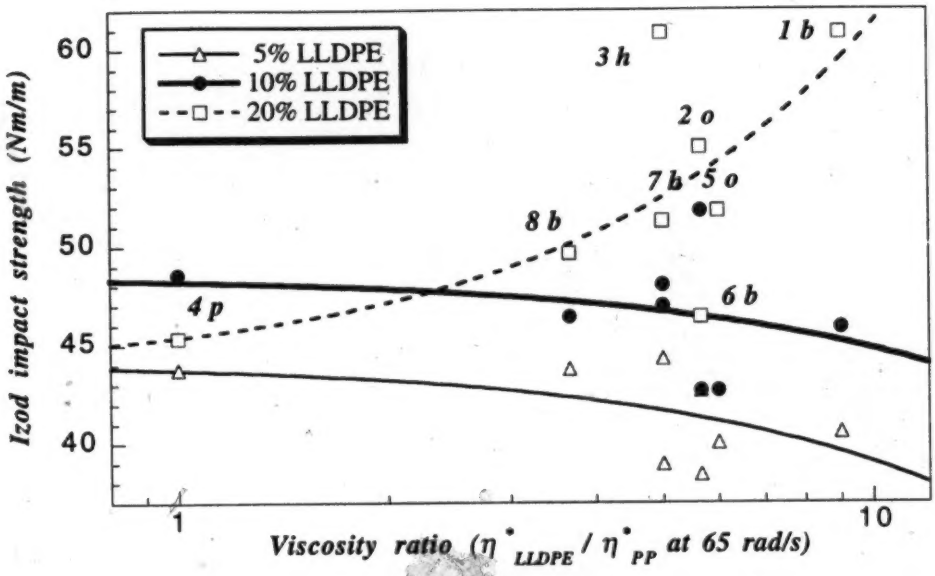

Figure 4.7 : Izod impact strengths (at 23°C) as a function of the dynamic viscosity ratio for LLDPE/PP blends.

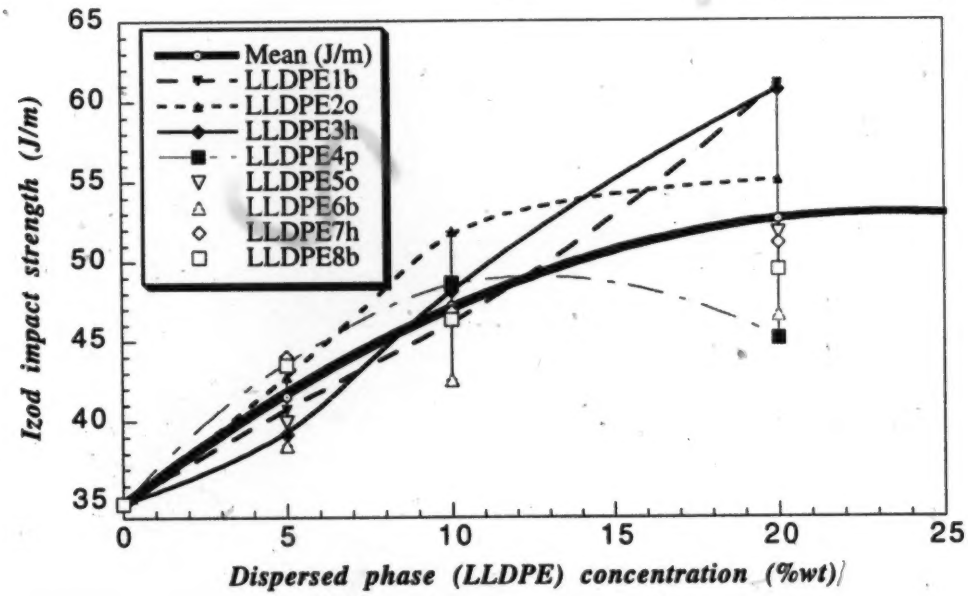

Figure 4.8 : Impact strength as a function of dispersed phase concentration.

Specimen	:	A	B	C	D	E
Impact Strength (Jm^{-1})	:	26.6	53.8	48.4	50.0	47.2

Figure 4.9 : Fracture surface of PI-Izod specimen show increase in strength with amount of crazing for a 10% 2o/PP1 blend. Crazing increases in the order : A, E, C, D, B.

All the 20% LLDPE/PP blends clearly show stress whitening near the tip of the notch. Comparison of the length of the stress whitened zone revealed the following order for 20% LLDPE / PP blends: 1b > 2o > 4p > 7h > 3h > 6b > 8b > 5o. Stress whitened zones for the 5% and 10% blends could not be compared visually.

4.3.3 Results from SEM

4.3.3.1 Morphological Observations

SEM micrographs showing the morphology of each blend were collected for all eight of the systems analyzed (LLDPEs 1-8 / PP1 blends). As already explained in the earlier section, the 5% LLDPE/PP blends were analysed as PI-Izod specimen, while the 10% and 20% LLDPE/PP blends were analysed as QFPI-Izod specimen. Comparison of the SEM micrographs for both methods showed that the dispersed phase drop sizes and shapes were not altered while clarity was enhanced for QFPI samples. A drawback of the later quench-fracturing procedure, discovered only at later stages of the study, was that the particle density was found to be lower for the QFPI samples. This indicates that the crack tended to avoid intersecting the dispersed particles in the QFPI-Izod method of exposing the fracture surface. This was probably an outcome of faster crack velocity in the comparatively more brittle QFPI-Izod samples.

SEM pictures were taken at different positions along the fracture surface of the PI-Izod specimen as shown in Figure 4.10 for a 5% LLDPE1b/PP blend. The crack growth is from top to bottom of each picture and progresses from picture A towards F. The morphology varied from one end to the other. Fig. 4.10 A shows a zone close to the notch. String-like structures are visible along with a few embedded droplets of the dispersed phase indicating significant plastic deformation during crack initiation. Fig 4.10 B is taken in a relatively flat zone of the fracture surface. This zone shows dispersed droplets clearly but also shows distortion of the voids left behind by dislodged droplets in the direction of crack growth. Fig. 4.10 C was taken at the foot of the slope of the fracture surface and shows voids and droplets, both relatively spherical in shape. The

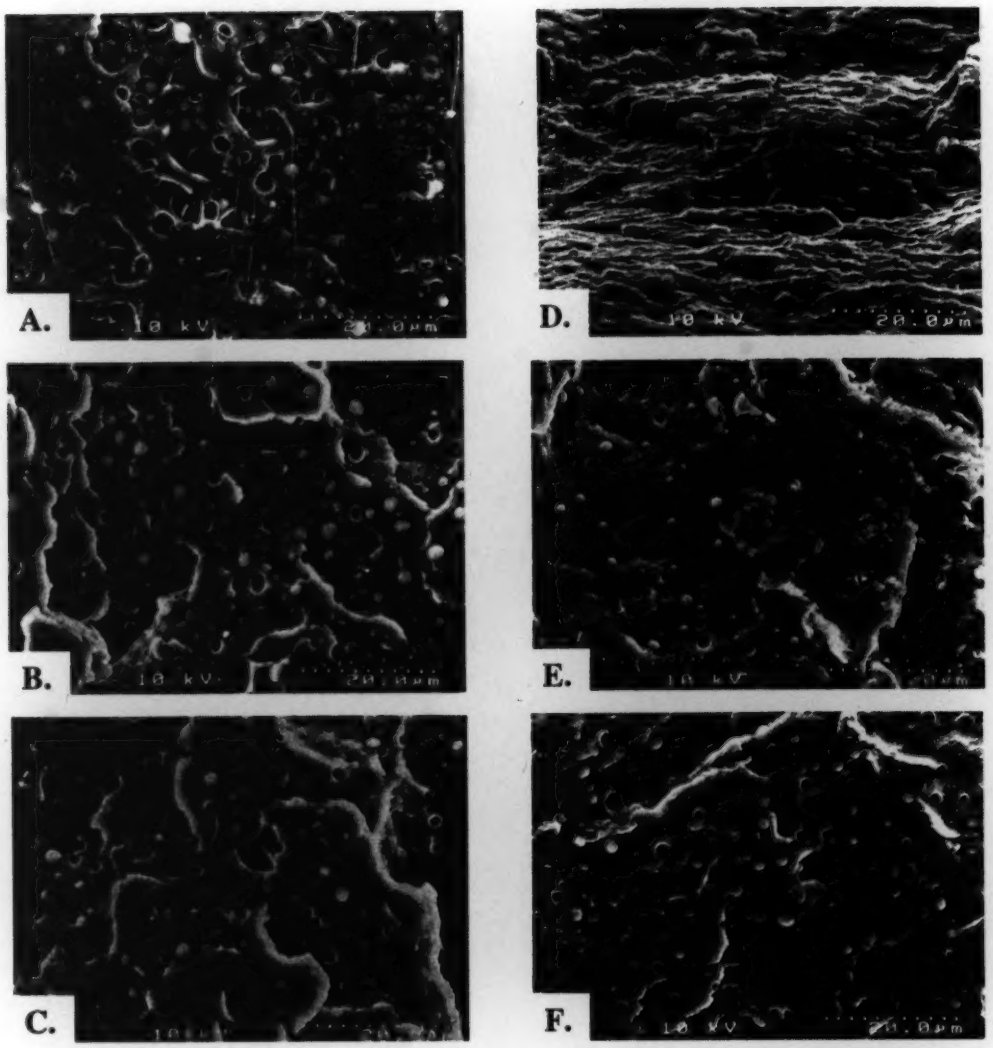

Picture	A	B	C	D	E	F
Position (mm) along Izod fracture surface	2.7	3.6	7	10	10.8	12.6

Fig 4.10 : Changing morphology along the surface of a fractured Izod specimen (#3) of a 5% LLDPE1b/PP blend fractured at room temperature. The location that the SEM pictures were taken, are also listed alongside the fracture profile.

clarity of these structures is poorer compared with Fig. 4.10 B. This indicates more brittle fracture as the crack velocity grows. Fig. 4.10 D shows the sloping surface. Fig. 4.10 E is taken at the end of the slope. There are fewer ridge-like formations than the other zones. There is also some texture visible in the matrix. This could be an indication of matrix cavitation. The droplet and void morphology is similar to Fig 4.10 B and C but with smaller droplets. Fig. 4.10 F is taken close to the edge of the sample where the top piece tears away from the bottom piece of the Izod specimen. The crack velocity appears to be low for this zone as the morphology is similar to Fig. 4.10 B. The promising zone for dropsize analysis appears to be in the flat region between locations of Fig. 4.10 B and C.

SEM of the QFPI-Izod surfaces revealed three zones whose morphology is shown in Figure 4.11. The first (zone I) was a narrow flat zone. Heavy crazing occurred in this zone, as compared with the corresponding notched fractured zone, due to the greater area bearing the impact as well as the absence of a plane of propagation for the crack. The droplets got pulled out and distorted leading to unusual morphology which will be described later. The next zone was a thin bright zone owing to rising topology of the fracture surface. The morphology of this zone was no different than the previous zone but the sloping topology distorts the shape of the particles, hence this zone was avoided for dropsize analysis. This zone was followed by a flat shallow zone (zone II) which probably represented the steady traversal of the crack front along the principal craze. Only a small number of droplets was observed in this zone. The crack, still slow, probably passes predominantly through the matrix in this zone. The last zone (zone III) was rich in particles and the crack velocity is expected to be quite high in this zone as the surface is quite flat and the droplet count is higher than the previous zone, indicating that the crack is forced to pass through all the drops in the plane of propagation. Most of the dropsize measurements were from this zone. A parallel can be drawn between the morphology of PI-Izod samples and the QFPI-Izod samples. Clearly the morphology of PI-Izod samples (Fig. 4.10) also appears to be divided into the three zones described by Hobbs (1980). Fig. 4.10 A falls into zone I, B and F fall into zone II and C and E can be placed in between zone II and zone III. The predominantly zone III type of morphology in the QFPI-Izod

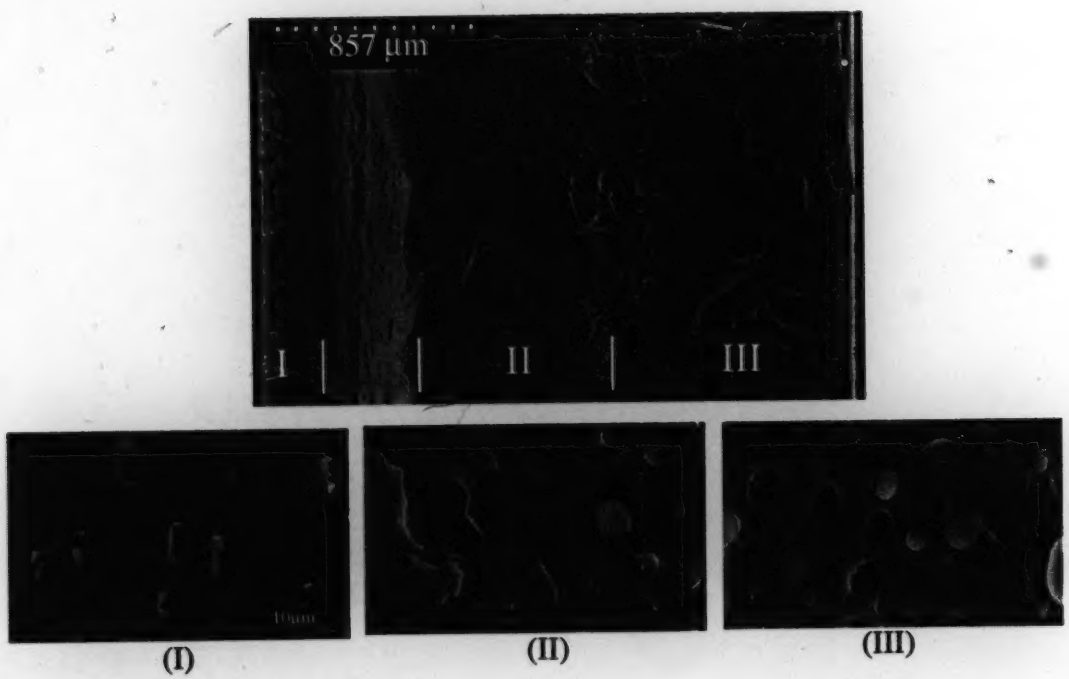

Figure 4.11 : Morphological zones in thickness-wise fractured QFPI-Izod specimen of a 20% LLDPE 8b / PP1 blend observed by SEM.

specimen can be attributed to faster crack velocity owing to the more brittle fracture. Figure 4.12 shows a compilation of the fracture surface morphology for blends with metallocene LLDPEs 1-4 /PP and Figure 4.13 shows the same for Z-N LLDPEs 5-8 /PP.

In Figures 4.10-4.13, the brighter phase is LLDPE and the darker phase is the matrix PP. Most of the pictures showed a droplet-in-matrix morphology which is anticipated since the matrix viscosity is lower than the dispersed phase. Voids are also observed, in the form of dark recesses and these indicate dispersed phase droplets gouged from the surface. The presence of voids indicates that the crack does not pass though the particles but is instead forced to overcome the interfacial adhesion between the droplets and matrix and dislodge the droplets from one of the surfaces.

Particle distribution was not uniform over the fracture surface but, in fact, occured in clusters. Plochocki et al. (1989) also reported the occurrence of clusters in LDPE/PS blends. They observed these clusters to form along flow streamlines in the extruded pellet. The appearance of these droplets on the surface also depends on the path of the fracture.

Qualitative observation of the SEM micrographs (Fig. 4.12 and 4.13) shows that the shape of the droplets varied from system to system. The blends with higher viscosity minor phase show rounder drops while systems with low LLDPE viscosity showed deformed drops, sometimes oval and at other times quite deformed. Sometimes the droplets were veiled by a sheath of matrix phase and were only partially exposed giving the appearence of oval drops even though they were round beneath the surface. The SEM pictures might have been from different zones, thus leading to differences in morphology as already explained. It is not clear what other factors affect the shape of the droplets the most but elasticity, viscosity, molar mass (and hence entanglements) and shrinkage was different for each system.

Several interesting morphological structures were observed in the samples, especially in zone I, where plastic deformation was greatest. The first of such features was

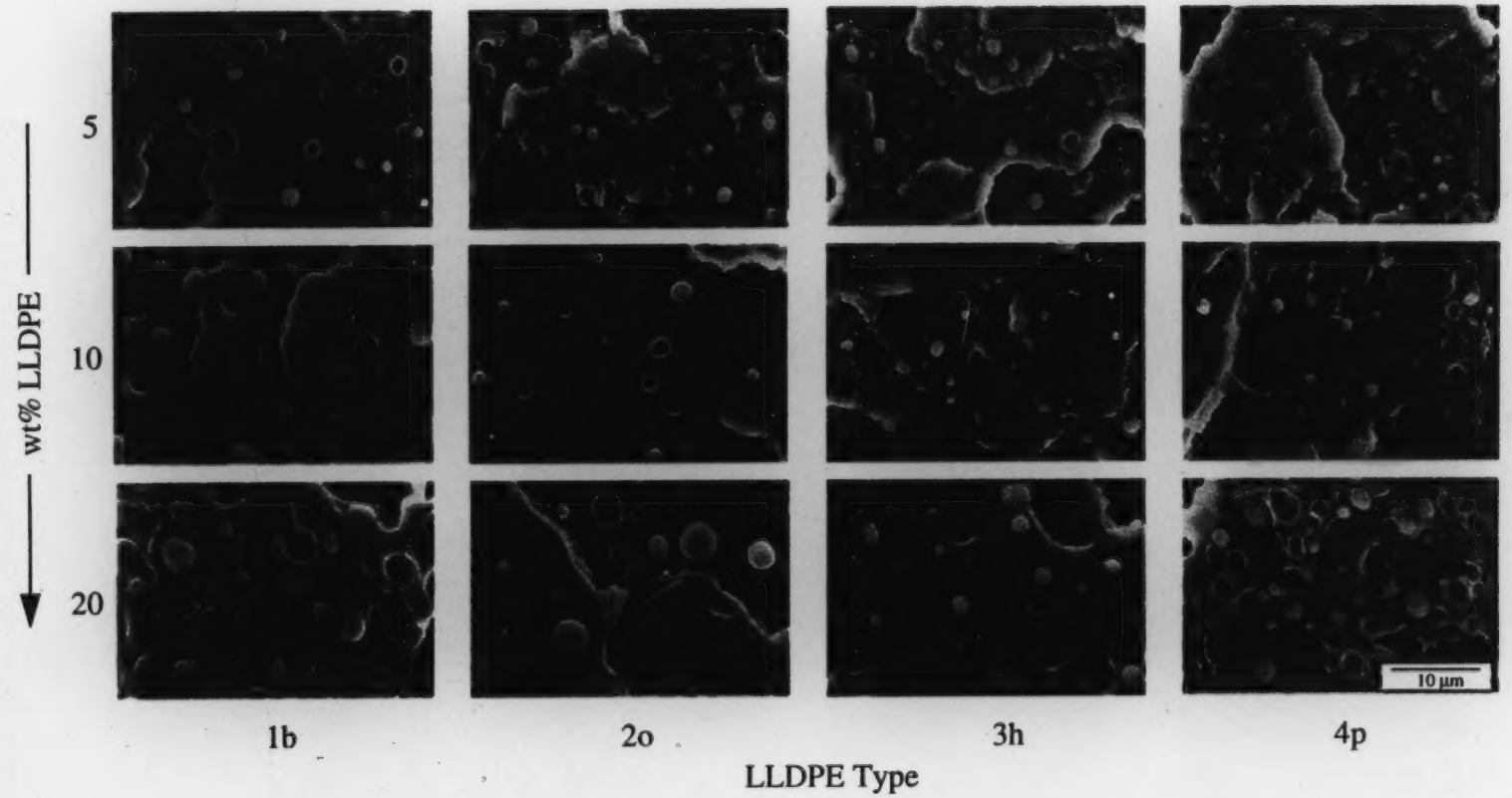

Figure 4.12 : Morphology of fracture surfaces of metallocene LLDPE/PP blends prepared at 220°C.

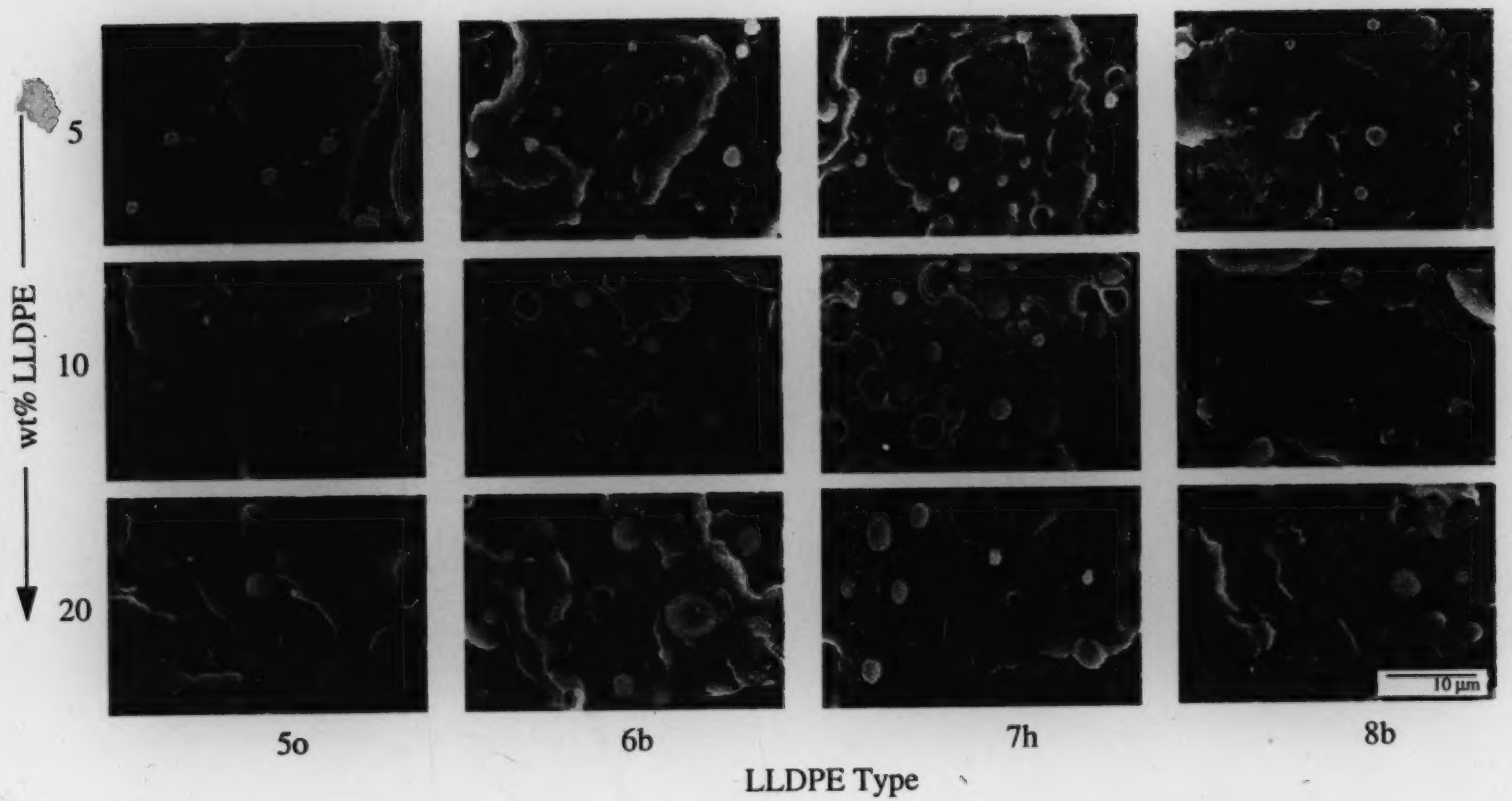

Figure 4.13 : Morphology of fracture surfaces of Ziegler-Natta LLDPE/PP blends prepared at 220°C.

strands originating from a dispersed drop and extending to another droplet or intersecting with a ridge. While some of the strands originate at lower topography and terminate at higher topography (Figures 4.14 A and B, 4.10 D), others appear to connect two droplets below the surface (Figure 4.14 C).

In some of the SEM pictures, shrunken minor phase droplets lay inside the voids formed by the matrix. This is clearly seen for the 10% LLDPE7h/PP1 blend shown in Figure 4.15 A. The shrinkage of the minor phase droplets appears to be responsible for this. In other cases, void space was replaced by interconnecting strands originating from the droplet and terminating at the matrix boundary (Figure 4.15 B). These web-like structures were also observed for LLDPE 4p/PP1 and LLDPE 6b/PP1 blends (shown as Figure 4.15 C and D). In all of these cases the droplet was attached to one side of the inner wall of the void while it was either detached from the other side or connected via thin strands. It is possible the direction of crack propagation is responsible for this. The occurrences of the web-like structures was more common in cases where the interfacial tension was low, e.g. LLDPE5o and LLDPE8b, while, in cases where the interfacial tension was high, e.g. LLDPE7h, mere cavitation was observed without the formation of the strands. The maximum occurrence of web-like structures was noted in LLDPE 8b/PP1 blends. Minor phase shrinkage was found to be a necessary condition for either of these features to exist. All the gas-phase polymerized Ziegler-Natta polyethylenes show shrinkage to some extent. LLDPE 5o/PP1 did not show this and neither did most of the metallocene polyethylenes, which exhibit low shrinkage owing to their amorphous nature. LLDPE 4p/PP1, however, did exhibit this feature.

Another unusual feature observed was a plate-like formation of the matrix phase with several irregularly shaped holes, within which shrunken minor phase droplets were embedded (Figure 4.16). Both LLDPE4p/PP1 and LLDPE6b/PP1 show this feature. Co-continuous phases show sheet-like distribution of one phase inside the other. In this case however, droplets are also observed indicating that the sheet is a meso-phase which might have been created by the diffusion of a miscible fraction of the dispersed phase into the

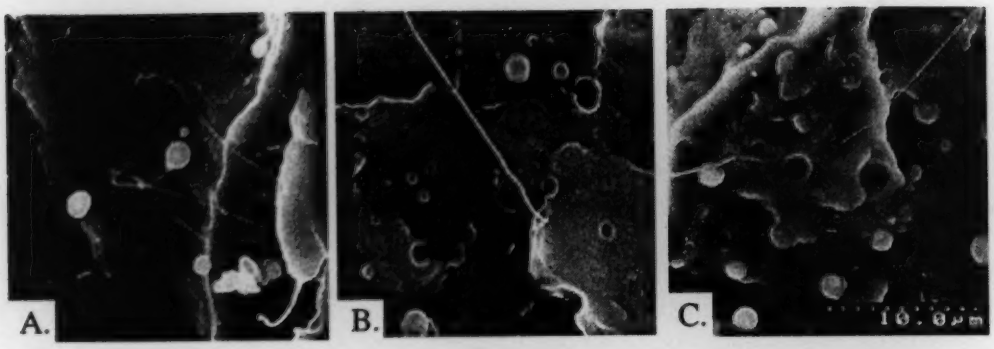

Figure 4.14 : Fiber formation in blends due to crazing or morphology development. A.) 5% LLDPE 5o/PP1 blend. B.) 5% LLDPE 8b/PP1 blend. C.) 5% LLDPE 6b/ PP1 blend.

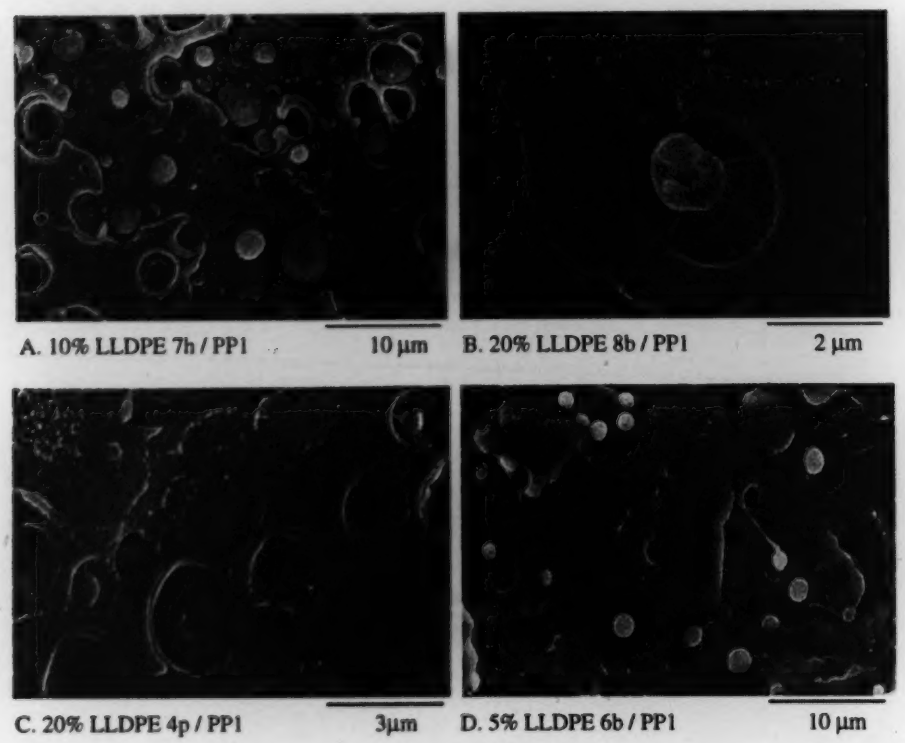

Figure 4.15 : Shrinkage of the minor phase LLDPE causes cavitation in systems with low adhesion and formation of web-like structures in systems with strong adhesion at the interface.

matrix. Mirabella et al. (1988) have also reported the presence of a soft extractable phase inside a hard semicrystalline matrix in their SEM studies on LLDPE resins. The other possibility is that this could merely be a transient sheet breaking up into droplets.

LLDPE 6b/PP1, in Figure 4.17 A, appears to exhibit features similar to those observed in systems exhibiting phase inversion even at 10% concentration. A doughnut shaped minor phase remanant on the fracture surface of 20% LLDPE6b/PP1 blend is also seen on the same picture. Other zones from the same blend however, show clear droplet-matrix morphology. The SEM picture of LLDPE8b/PP1 (Figure 4.17 B) illustrates how plastic deformation of the dispersed phase can lead to these shapes. The strands look as if they are feeding on dispersed phase droplets and draining them. It is quite possible that this was how the doughnut shapes were created. Another explanation is that the adhesion between the two materials is sufficient to cause the dispersed droplet to divide upon fracture, where a ring of the droplet adheres to one surface while the remaining part is yanked away by the other.

In another instance (Figure 4.17 C), the dispersed phase seemed to be coated with precipitated material, which gave the appearence of spots. It is possible that fibrils had extended from the surface of these drops and when they snapped, they collapsed and retracted back forming stubs on the surface.

In one of the SEM pictographs (Figure 4.17 D) for LLDPE8b/PP systems, there is considerable texture observed in the matrix phase. This was attributed to matrix crazing and cavitation. When crazing preceeds the crack, it is possible that fibrils form along with cavitation. The crack sections the craze-induced strands creating this morphology. The other possibility comes from the transient morphology development observed by Sundararaj et al. (1995) wherein a plate of the minor phase deforms inside a matrix giving rise to a band of droplets created via sheet breakup. However, the dropsize was too small for this to be thermodynamically possible. In general, the minimization of interfacial area drives such processes.

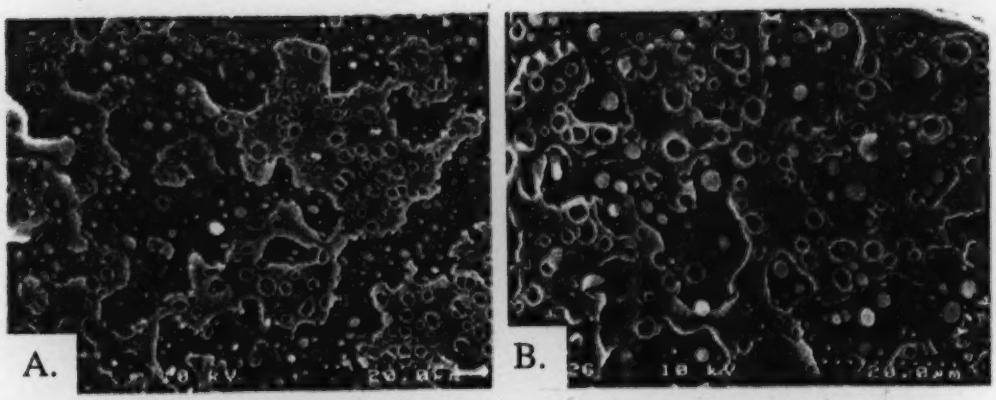

Figure 4.16 : Sheet - like morphology typical of cocontinuous phases observed in A.) 10% LLDPE 4p / PP1 and B.) 10% LLDPE 6b / PP1;

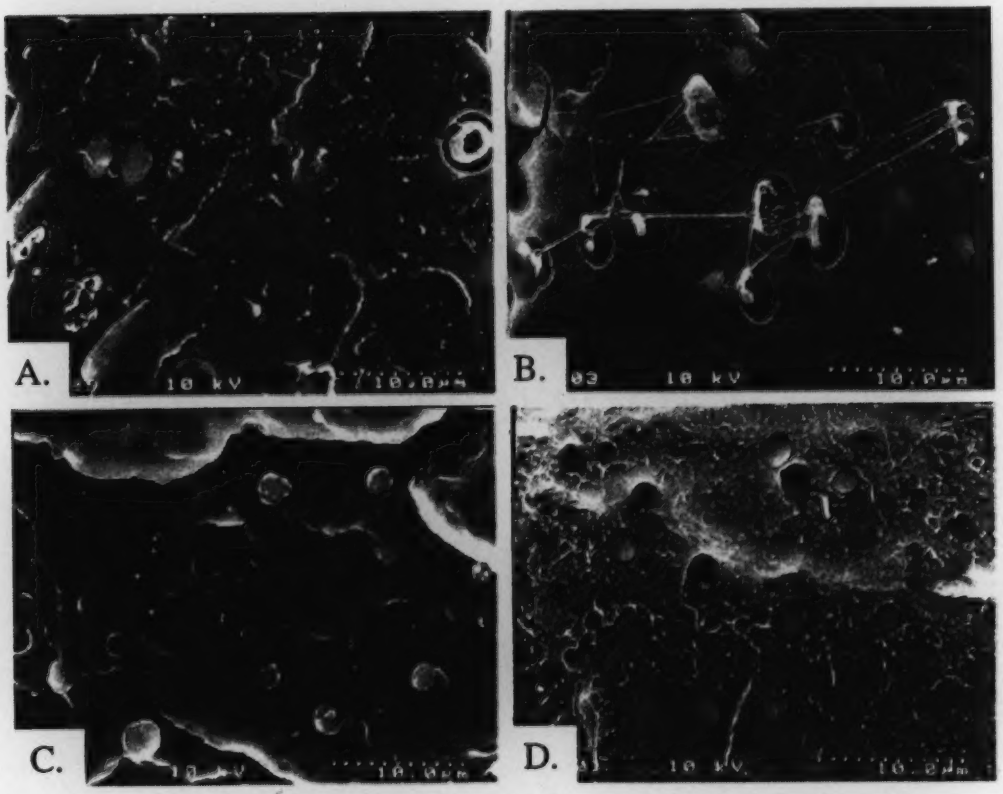

Figure 4.17 : Unusual features observed in some of the blends - Ductile deformation of dispersed phase observed in A.) 20% LLDPE6b/PP1 and B.) 20% LLDPE8b/PP1; Peculiar spots seen in C.) 10% LLDPE 8b/PP1; and Effects of matrix cavitation observed in D.) 10% LLDPE 8b/PP1.

4.3.3.2 Dropsize Analysis

Dispersed drop diameters were obtained for all the LLDPE/PP blends using image analyzing software developed by National Institute of Health. The number of particles analyzed per blend was from 137-580. A step by step procedure is provided in Appendix E to convert SEM pictures to dropsize information. Dropsize data were not extracted for the 10% LLDPE5o/PP blend as the droplets were subsurface and hence their boundaries unclear. Subsurface droplets were observed for 10% and 20% LLDPE5o/PP, and 10% LLDPE7h/PP. The variation of dropsizes with increasing dispersed phase concentration will be discussed in the next section.

Preliminary work on dropsizes of LLDPE 1b with different PPs prepared at 200°C is shown in Figure 4.18. The drop diameter for the LLDPE1b/PP2 blend was measured at concentrations of 3, 5, 7, 10, 15, 20 and 30%. The dropsize appears to vary sigmoidally with concentration. The dropsize is expected to approach the Taylor limit for very low concentrations. There also appears to be an upper limit at higher concentrations above which the impact strength can actually decrease (Wang et al., 1997). The dropsizes measured for all the LLDPE/PP blends, except for the 10% 5o/PP1 blend, are summarized in Table 4.2. A plot of dropsize as a function concentration of dispersed phase is shown in Figure 4.19 for the various LLDPE/PP blends. Blends were only prepared at concentrations of 5%, 10% and 20%. The dropsizes rise rapidly with concentration. Above a certain critical concentration, a co-continuous phase morphology is expected. This was not observed conclusively in any of the samples studied.

In addition to average dropsize, the interparticle distance was calculated assuming the simplest geometric arrangement, a cubic array of the dispersed spheres in the blend (Figure 4.20). Droplets of average radius were assumed to be distributed regularly in the photographed area. The dispersity in dropsizes introduces significant error in the estimation of the interparticle distance. The fractional area of the dispersed drops occurring across a section of such a blend has been tabulated along with the other droplet

Table 4.2 : Dropsize information obtained from SEM micrographs of fractured surfaces of LLDPE/PP blends.

Dispersed Phase (Continuous Phase PP1)	Wt. disp. phase (%)	D (μm) Average Drop Diameter	N Number of Drops analysed	ID (μm) Interparticle Distance	A_{disp} (Fractional area of Dispersed Phase)
LLDPE 1b	5	1.54	352	4.37	4.84
LLDPE 1b	10	1.99	470	3.62	9.04
LLDPE 1b	20	2.76	484	2.77	17.88
LLDPE 2o	5	1.32	186	3.18	6.30
LLDPE 2o	10	2.01	219	6.04	4.30
LLDPE 2o	20	3.03	255	5.30	9.08
LLDPE 3h	5	1.06	231	2.99	5.03
LLDPE 3h	10	1.50	368	5.52	3.19
LLDPE 3h	20	2.65	345	3.02	15.64
LLDPE 4p	5	0.86	334	2.53	4.79
LLDPE 4p	10	1.33	266	2.61	8.38
LLDPE 4p	20	2.15	535	1.85	21.22
LLDPE 5o	5	1.71	137	5.96	3.45
LLDPE 5o	20	3.11	145	6.65	6.80
LLDPE 6b	5	1.43	161	3.94	5.13
LLDPE 6b	10	1.86	582	2.72	12.03
LLDPE 6b	20	2.87	220	5.17	8.77
LLDPE 7h	5	1.78	223	4.99	4.87
LLDPE 7h	10	2.37	372	3.10	13.52
LLDPE 7h	20	2.72	258	5.56	7.41
LLDPE 8b	5	1.07	251	3.27	4.48
LLDPE 8b	10	1.36	187	3.64	5.38
LLDPE 8b	20	3.05	177	4.24	12.21

Note: Underlined quantities indicate samples which show area fractions representative of added dispersed phase content.

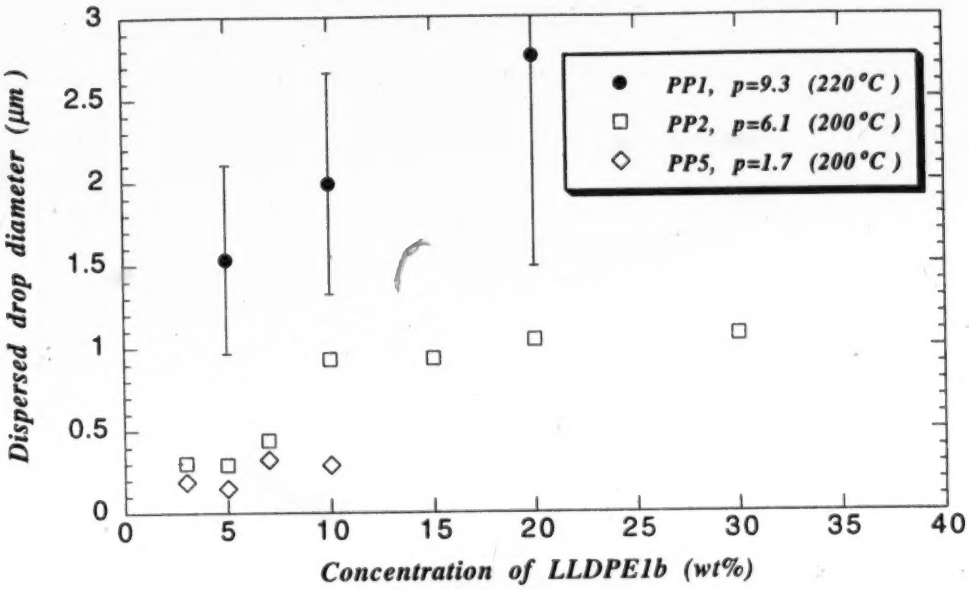

Figure 4.18 : Effect of viscosity ratio (p) on dispersed drop diameter versus concentration plots for LLDPE1b/PP blends. (Data for PP2 and PP5 blends were measured by Larry Unsworth, 1996)

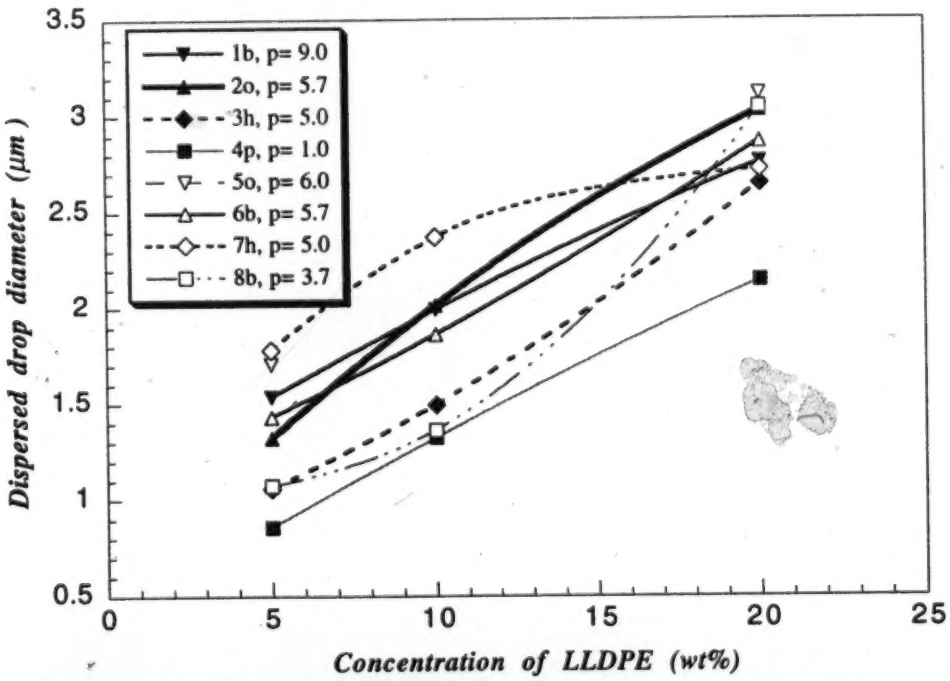

Figure 4.19 : Concentration dependence of dispersed phase drop sizes for different LLDPE /PP1 blends at 220°C .

distribution data in Table 4.2. This gives a rough estimate of the volume fraction of the dispersed phase in the blend and lends credibility to the representativeness of the area analyzed by SEM. If the densities of the two phases are assumed to be the same, the volume fraction will be the same as the weight fraction. Only two of the blends, LLDPE 1b/PP and LLDPE 4p/PP show a dispersed phase volume fraction within 20% of the mass fraction for all three concentrations. The area fraction is approximately equal to the mass fraction for most of the 5% blends.

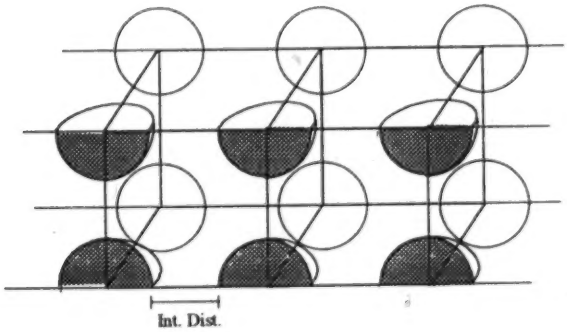

Figure 4.20 : Unit cell chosen to estimate interparticle distance.

The interparticle distance is plotted as a function of the concentration of the dispersed phase in Figure 4.21 (a). From Figure 4.21 (b), it can be seen that the interparticle distance also increases with the viscosity ratio for 5% LLDPE/PP blends. The method of observation (SEM) limits us from making further inferences on this data, because the crack might propagate in any direction and at times bypass the dispersed droplets. In this case, TEM analysis would give a much clearer picture. Starke et al. (1998) have recently looked at the effect of interparticle distance on the fracture toughness of PP in EPR/PP blends. They found that the interparticle distance distribution is also an important factor affecting the strength of a blend and that a narrow distribution of interparticle distances leads to better impact modification than a broad distribution with the same average interparticle distance. This is however an interesting topic for further study.

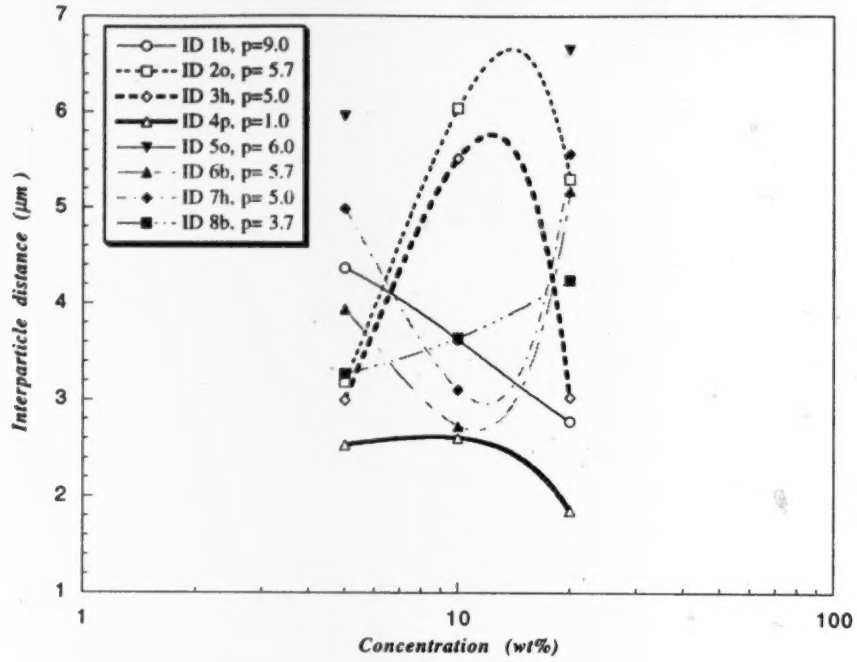

Fig. 4.21 (a) : Interparticle distance as a function of dispersed phase concentration.

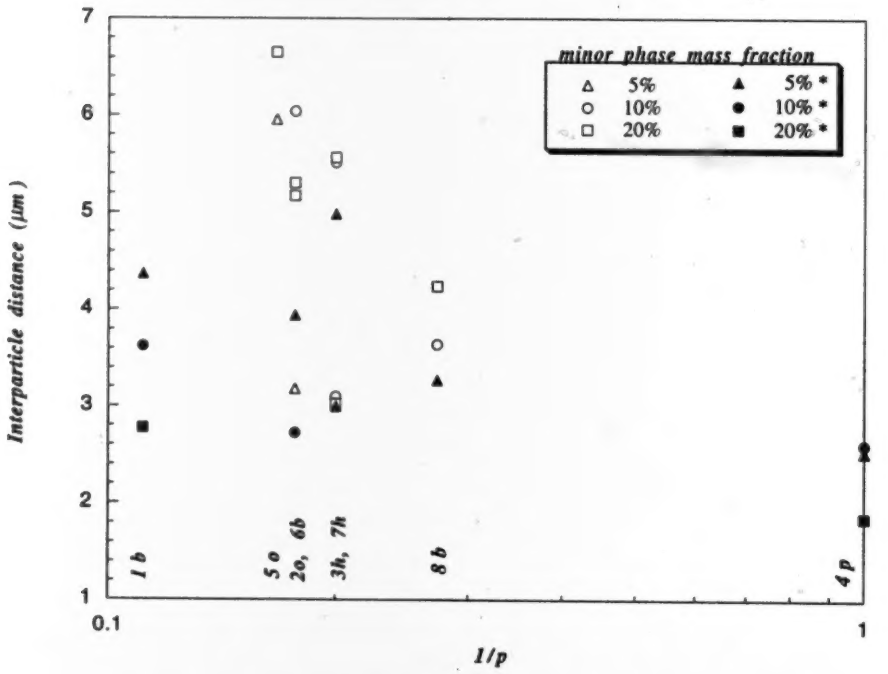

Figure 4.21 (b) : Interparticle distance as a function of viscosity ratio. (The solid symbols (*) indicate samples showing representative area fraction.)

The effect of elasticity was also determined by checking whether Van Oene's criterion for dispersed phase was met for all the polymers (see Table 4.3). The dynamic interfacial tension was verified to be a positive quantity using Inequality 4.5. We assume that $\dot{\gamma} = \omega$ and that at a mixer speed of 50 rpm, the average shear rate is 65 s^{-1}. The rheological properties G' and G" at ω = 65 rad/s were substituted in Equation 4.6 to obtain N_1. The range of frequencies for which ($N_{1,d}$ - $N_{1,m}$) remains a positive quantity is also listed. For LLDPE4p, the first criterion failed LLDPE4p in the frequency range 0.3 - 0.6 rad/s, the second criterion in Inequality 4.5 was verified for where D was replaced by the measured dropsizes obtained from SEM. These results are summarized in Table 4.3. Results of both of Van Oene's criteria support the formation of a droplet - matrix morphology for all the systems.

Table 4.3: Van Oene's Criteria (Inequality 4.5) for drop-matrix morphology.

Dispersed Phase	$N_{1,d}$ x10^{-4} (at 65 rad/s) (Pa)	Range of Frequency ω (rad/s)	Criterion 1 $N_{1,d}$ - $N_{1,m}$ (Pa)	Criterion 2 $\sigma_{d,m}$ (Eq. 4.4) (mN/m)
LLDPE1b	27.6	all ω	+	
LLDPE3h	24.5	all ω	+	
LLDPE4p	1.5	0.3 - 0.6	-	+
		0.1 - 0.3, 0.6 - 100	+	
LLDPE5h	19.5	all ω	+	
LLDPE6b	17.3	all ω	+	
LLDPE7h	15.8	all ω	+	
LLDPE8b	9.8	all ω	+	

N_1 values calculated using Eq. 4.6. For PP1, $N_{1,m}$ (65 rad/s) = 1.4 x 10^4 Pa.

Tested range of ω = 0.1 - 100 rad/s.

4.4 Discussion

4.4.1 Discussion on Torque Profiles

The torque curves show a sharp peak within the first 30 seconds followed by a sharp decline for the next 30 seconds and then the torque gradually drops to a steady value. The rise in torque is due to the melting and deformation of the polymer pellets. Shih et al. (1991) have identified four distinct rheological regimes during the dynamic changes from polymer pellets to a melt. They are:

1. Elastic solid pellets.
2. Deformable solid pellets.
3. Transition material
    A. Fluid with suspended solid particles
    B. Fractured or semi-fluid material
    C. Dough-like material.
4. Viscoelastic fluid.

The first two regimes are not as markedly visible in the torque curves as the latter two. The selected temperature of 220°C is much higher than the typical melting temperatures of either phase. The dispersed phase metallocene LLDPEs, whose blend torque profiles are shown in Figure 4.5 and 4.6, melt rapidly as they are introduced in the mixer. At sufficient concentration, they probably engulf the PP pellets and form the transition material regime with a fluid containing suspended solids.

As mentioned earlier, the mixing time was set as 5 minutes. The torque for PP1, when torqued alone, becomes relatively stable at around 5 min (Fig. 4.5 (b)), and remains at this value until 8 min after the blending commences. This implies that the polymer has melted completely and is well mixed viscoelastic fluid at this stage. Mechanical degradation probably starts to affect the torque after 8 minutes. When the mixer plates were opened to collect the blend, the PP1 film on the mixer plates was observed to brown

rapidly as compared with LLDPE. Degradation of the polymer involves chain scission, which can adversely affect the strength of the polymer. For this reason, the blend time was kept as low as possible and a nitrogen blanket was used while loading the pellets, as already mentioned.

In opposition to the above argument, the torque curves in Figures 4.5 and 4.6 show that the addition of LLDPE to PP1 was observed to delay the inception of this constant torque zone (Fig. 4.5 (b) and 4.6 (b)). Earlier studies by Yang et al. (1995) have also reported that there is no further breakup into finer droplets after a period of 5 min for a 20% PS/LLDPE blend at 180°C. Favis (1990) reported that the most significant particle size deformation and disintegration process occurs within the first 2 minutes. It was therefore unexpected that any significant dispersion should occur after 5 minutes. However, morphological evidence in Figure 4.22 showing the optical micrograph of the fracture surface of an Izod specimen for a 20%LLDPE1b/PP blend, clearly refutes this assumption. A thread of LLDPE1b, approximately 20 μm thick, is observed to breakup into smaller droplets. Fortunately, an examination of the Izod impact strength of individual specimen (Appendix D, Table D.1) shows that this particular specimen had much lower strength (0.86 ft.lb/in) relative to the other specimen (average strength 1.21 ftlb/in) for the same blend. It is possible that LLDPE pellets were segregated in isolated zones, such as the nip region of the mixer chamber, and joined the main stream only at longer times. The interfacial tension for LLDPE1b was among the lowest in all the LLDPEs studied and hence the breakup of transient cylindrical structures into droplets will take the longest time. The dispersion in the blends of the other LLDPEs is expected to be much better because they have a lower viscosity ratio than LLDPE1b/PP1. In future studies it would be advisable to choose a longer mixing time such as 7 or 8 minutes.

There is a reduction in peak torque (Figure 4.5 (a), 4.6 (a)) with the addition of LLDPE to the PP phase for both the systems shown. Shih et al. (1991) have also observed this trend with the addition of PE in nylon/PE blends. The melted polyethylene probably lubricates the unmelted PP pellets and leads to the reduction in deformation and hence

Close-up view of thread.

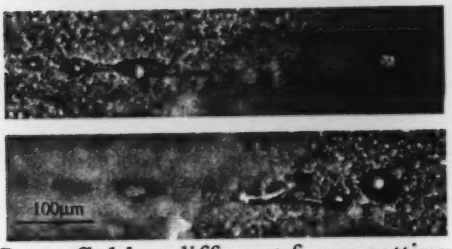

Same field at different focus setting.

Figure 4.22 : Breakup of a thread of LLDPE1b into droplets observed captured in a 20% LLDPE1b / PP1 blend after blending for 5minutes at 220°C.

Figure 4.23 : SEM micrograph of a QFAB 10% PP5/PS blend (p=1.2) sample showing coalescence of dispersed phase droplets . (Blend prepared by Larry Unsworth, 1995)

torque. Also, the molten surrounding phase is a more efficient layer for heat transfer, and can speed up the melting of the PP pellets, thus causing the peak to occur at an earlier time. The LLDPE1b/PP blends, show a decreasing peak torque with increasing dispersed phase concentration. The LLDPE 2o/PP blends also show the same trends for the 10% and 20% dispersed phase blends but show an anomalous reduction in peak torque for the 5% LLDPE 2o/PP blend. It is possible that the feeding of the pellets was not done properly in the case of the 5% LLDPE 2o/PP blend. If the weight of material fed was lesser than the intended amount due to spillage or similar manual errors, a lower peak torque would result. This would then likely affect the dropsizes and distribution of the dispersed phase in the blend.

From Figure 4.5 (a), when we compare the peaks in torque of a pure PP batch to that of the blend containing LLDPE 1b, the peaks occur at earlier time in the presence of the LLDPE 1b phase. The same shift was not observed in the torque profiles for LLDPE 2o/PP blends (Fig 4.6 (a)). The peaks in the latter case occurred at the same time (approximately 25 seconds after loading the pellets), irrespective of the amount of dispersed phase present in the batch and also coincided with the melting peak of pure PP1. From TREF studies, we know that LLDPE 2o has a very narrow branching distribution and is likely to have a sharper melting temperature than LLDPE 1b. In the case of LLDPE 1b, the amorphous fraction, which is present in significant amount, melts at a lower temperature, while the crystalline fraction is not completely mobile. Due to this, the dispersed phase softening occurs over a period of time depending on the heat transfer to the pellet. LLDPE 2o, according to the above argument, will have a sharper melting temperature.

The steady state torque values (Figure 4.5 (b) and 4.6 (b)) increase with the increase in dispersed phase concentration for both the systems. This is no surprise since both the LLDPEs have higher dynamic viscosity than PP1 at the shear rate considered and in general, blends show additivity of properties (Paul and Barlow, 1980).

Some of the nuances which one might expect to find in the torque-time curves might be hidden in the relatively large sampling period of 6 seconds especially in the narrow domain of time where the torque peak occurs. In most studies the volume fraction of each component has been considered as the critical parameter for characterizing morphological changes such as phase inversion. In the absence of density data, this study was carried out on the basis of the pellet densities of the phases at room temperature. The viscosity ratios for all the systems are greater than 1 and hence in the droplet-matrix regime.

4.4.2 Fracture Surface Development

The PI-Izod surface shows three zones as already explained (Fig. 4.9). According to Kambour (1973), when the crack originates, the stress applied at the tip of the notch (which in this case has a radius of 0.25 mm) causes ductile fracture. The propagation of the crack is often accompanied and even preceded by plastic flow. Plastic flow of the matrix can lead to an increase in orientation that can cause such whitening. The whitening at the notch tip can also arise due to another reason. For brittle polymers such as PC, crazes develop in the initial region until the crack tip becomes really sharp and all the stress concentrates along a very thin cross section. The crack growth velocity supersedes the craze growth velocity and a brittle fracture zone results. The formation of multiple crazes at the crack initiation zone is a common feature in tough polymers (Lee et al., 1987, Favis and Chalifoux, 1987). Cavitation which often accompanies this mechanism can also contribute to the scattering of white light. SEM analysis of the QFPI-Izod surfaces also show the dispersed droplets getting distorted. The white streaks observed on the PI-Izod surfaces (Fig. 4.9) are indicative of secondary crazes.

Liu and Truss (1996) observed fractures in notched samples of LLDPE/PP systems. From SEM micrographs of the fractured area, they observed that the notch leads into an area of brittle fracture followed by an area of relatively ductile fracture corresponding to regimes 3 and 2 respectively, of Hobb's (1980) hypothesis (Fig. 4.2).

The blend cited by Liu and Truss (1996) was a 90% LLDPE/PP blend while in our case, PP was the major phase for all blends and both the PI-Izod specimen and the QFPI-Izod specimen mostly show brittle fracture i.e. regime 3. Only the QFAB LLDPE samples used for torquing studies show ductile fracture in some cases.

Cheung and Plummer (1996) have looked at the effect of rubber toughening on polysulfone and poly(phenylene sulfide) blends and reported similar morphological features at similar concentration ranges as ours. Rubber toughening reduced the cavitation observed in the mirror region of the fractured Izod specimen at concentrations above 10%. They also observed a plastic zone immediately following the notch as well as a brittle zone showing secondary cracks. One curious observation by these authors was that annealing reversed the order in which these features occurred after the notch.

The Izod impact strength for the 20% blends follows the order: 1b > 3h > 2o > 5o > 7h > 8b > 6b > 4p. The first three values all correspond to metallocene LLDPEs with the order butene>hexene>octene whereas the following three values are Ziegler-Natta polyethylenes which show the opposite order. The impact strength for both sets vary inversely with the interfacial tension, although one set cannot be compared to the other on the same basis. Exceptions to this trend are LLDPE4p which ended up having the lowest impact strength and LLDPE8b which inspite of low interfacial tension, does not show the corresponding strength. On the basis of interfacial tension, LLDPE4p can still be appended to the first set, but LLDPE8b does not follow this rule.

To see whether the stress whitened zone alone contributed to majority of the toughening, the lengths of the stress whitened zones in PI-Izod specimen were compared for all 20% LLDPE/PP blends. The length of the stress whitened followed the order: 1b > 2o > 4p > 7h > 3h > 6b > 8b > 5o. This does not reflect the impact strengths very well although the first of each series is the same. Figure 4.9 shows the variation of Izod strengths with the appearence of the PI-Izod specimen for a blend of 10% LLDPE2o/PP1. For this particular blend, both the sizes of the whitened zones due to shear and the crazing

in the flat regions of the fracture surface varied proportionally. The impact strength was found to increase with increase in the amount of stress whitening and crazes. Specimen A shows the least number of crazes while Specimen B shows the greatest number of crazes. The impact strengths vary likewise. Yee and Pearson, (1988) also observed that crazing increased the impact strength. Therefore, the physical appearence of the fracture surface of a sample does give a measure of its relative toughness but the important features must first be identified comprehensively.

It is also important to point out that the Izod impact strength values for the 5% and 10% LLDPE/PP blends did not follow the same order as the 20% blends. It has been found that the dispersed phase when present in adequate amount, affects the crystallizability of crystalline polymers. Although a semicrystalline polymer, PP is also affected by the addition of the more amorphous PE phase blended into it. Cser et al. (1997) have shown the spherulitic size of PP domains to diminish with the increase in LLDPE concentration in PP/LLDPE blends. Thus, when drops are closer together, the interdiffusion of phases is greater and a more ductile fracture mechanism is observed. When the minor phase concentration is low, the fracture is likely to bypass the more rubbery dispersed phase droplets and pass through only the brittle matrix zones, thus losing lesser energy to the deformation process. It is possible that for this reason, the Izod trends follow interfacial tension closely only at high LLDPE concentrations and at lower concentrations, the interfacial compatibility is not the main mechanism for improving strength.

The shape of the PI-Izod samples (Fig. 4.9) which is probably governed by the mechanism that the fracture was brought about, is a plateau like structure with a sharp rise followed by a flat summit. In the case of an Izod strength measurement, the fracture occurs under bending strain conditions and hence tensile stress is felt at the crack tip while there is compressive stress at the end of the specimen. The crack grows in the direction perpendicular to the strain and thus the fracture surface rises sharply and tapers off at the end of the specimen as the top segment bends due to impact. Comparison of the shape of

the fractured specimen indicated that it was relatable to the impact strength. When the slope of the fracture plane was low, the impact strength was generally found to be low. Samples which showed higher impact strength, on the other hand, showed sharply curved fracture planes in the third zone. The tougher the polymer, the more curvature it will show owing to greater resistance to the stress and more bending as opposed to more brittle samples which succumb to the crack and cannot alter its direction. Again, in the case of the tougher polymer, since the curvature of the fracture plane is greater, the crack travels through a greater area and imparts more deformation, thereby resulting in a higher impact strength measurement. It may therefore be difficult to predict the performance of the polymer under different strain conditions based on Izod measurements alone.

The QFPI-Izod samples in the absence of any notch to direct the crack propagation, have uneven surfaces with a larger amount of secondary crazing than the PI-Izod surfaces. The surfaces grow flatter as the crack grows indicating a faster, more brittle fracture. While the majority of the samples show a combination of droplets at the surface, cavities or holes left by dislodged droplets, and some subsurface droplets, one of the samples, 10% LLDPE5o/PP1 showed mainly subsurface droplets indicating that the crack bypassed the dispersed phase. The adhesive strength varies as an inverse function of the interfacial tension (Levine, 1964). From Chapter 3 we know that the interfacial tension of LLDPE 5o with PP1 is very low and it is possible that a strong interface formed by the two hinders debonding of the dispersed droplets. The formation of the interfacial layer shown in Figure 3.8 might be an indication of cocrystallization at the interface which then can account for the added strength of the interface. The butene-octene terpolymer LLDPE5o probably has different miscibility characteristics than the other copolymers analyzed owing to its high copolymer content as well as different nature owing to solution phase polymerization. The length of the stress whitened zone in the PI-Izod samples, where LLDPE5o has the smallest length amongst the 20% blends, also reflects that the mode of fracture is brittle. Wu et al. (1994) studied PBT/PC blends and rightly point out that weak interfacial adhesion cannot stabilize the growing crazes and offer no bridging while strong interfacial forces will not promote debonding-cavitation, resulting in high

plane-strain constraint which brings about brittle fracture. For an ideal system the modifier should be such that it maximizes the interfacial adhesion without hindering the debonding-cavitation mechanism.

The first zone observed in QFPI-Izod specimen (Fig. 4.11) showed similar stress whitening as the PI-Izod specimen (Fig. 4.10). It is unclear whether the bright zone corresponds to the acclivity seen in the PI-Izod surfaces. Fracturing the specimen sideways (in case of QFPI-Izod specimen) also left a curved profile similar to that observed for the width-wise fractures of PI-Izod specimen but it was difficult to locate corresponding zones on the two types of fracture. Since the fractures are initiated by manually impacting the sample while it was clamped, there might have been variation in the fracture velocities. The slow velocity fracture will show different morphology than the brittle fast velocity fractures.

Uneven fractures can cause anomolous Izod impact strength. Indications of uneven fractures were - whitening at any point (other than the crack initiation zone) on the fracture plane, bubble entrapment or secondary crack propagation. Uneven droplet dispersion from specimen to specimen can also lead to a large variation in the Izod impact strength. This would be accentuated in cases where coalescence of the minor phase is significant over a small period of time. It is possible that coarsening occurred during the transfer of the polymer melt from the mixer to the hot plate. According to Favis (1990), such coarsening is also highly concentration dependent. The local distribution of the minor phase droplet size and shape as removed from the mixer chamber is another possible cause of the variation in Izod impact strength. As already mentioned, the plates were formed with scoops of polymer melt collected from various locations in the mixer chamber. The distribution of the minor phase from regions close to the mixer blades are probably finer than that nearer to the centre of the chamber and in the blade flutes. The polymer sampled from these regions will have variations in dropsize and density. These variations get transferred to the specimen. Phases segregation of the minor phase has been reported by Plochocki et al. (1989) owing to difference in stress profiles at the centre and the edge of

the blades. Scott (1990) has reported that when the quantity of polymer charged exceeds the optimum value, there are dead spaces created near the nip region between the blades (Fig. 4.3). Since accurate density data was not available, overfeeding in the mixer might have led to poor distribution of the minor phase in the blend.

In case of sparse distribution, cracks may pass only through the matrix phase without causing dispersed phase distortion or interfacial cavitation, leading to low impact strengths. The range of impact strength observed (see Table 4.1) for some of the blends was quite large, e.g., 10% LLDPE3h/PP1 shows a standard deviation of 4.69 J/m for a mean impact strength of 48.15 J/m and 5% LLDPE5o/PP1 shows a standard deviation of 4.48 J/m for a mean impact strength of 39.93 J/m. The standard deviation was lower at a concentration of 20% LLDPE (e.g., 2.14 for 20% LLDPE3h/PP and 3.14 for 20% LLDPE5o/PP). In our case, since all the viscosity ratios of the systems chosen are greater than 1, the dispersion is expected to be coarse. Poor dispersion of the dispersed phase might therefore be held responsible for this variation. As explained by Sundararaj et al. (1995) the morphology goes through stages of droplet elongation into fingers, to thin sheets, to filaments and finally to droplets. If the breakup of minor phase filaments leads to large droplets with generation of a multitude of smaller associated satellite droplets, then the distribution of dropsizes is very broad. With reduced coalescence at low concentrations, the size variation would be very large. This is likely the case with the minor phase being less deformable of the two phases.

4.4.3 Factors Affecting Morphology

The impact tests conducted at room temperature can vary significantly from those at lower temperatures. This is intimately related to the melting point and glass transition temperatures of the constituent polymers. PP has a T_g of approximately -10°C. At room temperature, the ductile flow of the matrix phase can make it difficult to observe the morphological features of the dispersed phase and might even incorporate some artifacts. PP1, which was used as the matrix phase for all the blends, is a low molar mass PP.

According to Avella et al. (1993), fracture toughness of isotactic polypropylene increases with molar mass owing to tie molecules and entanglements. Brittle fractures of the matrix might not be seen for blends of other PPs due to their highermolar masses. On similar grounds, the PI-Izod samples will differ from the QFPI-Izod samples owing to the mode of fracture and regimes of crack speed causing the fractures.

Blend morphology of post-impact Izod specimen are expected to differ from quench fractured as-blended polymer samples due to coarsening of the blend occurring during molding of the Izod specimen at elevated temperatures on the Carver plate press. The low matrix viscosity of the chosen polypropylene (PP1) aids the coarsening process.

There is a significant increase in the dropsize with increase in concentration (Fig 4.18). This has been suggested (Fortelny and Zivny, 1995) to be a result of collision of two or more droplets at the same time, coalescing to produce a single droplet of greater dimension. Morphological evidence for this phenomena was observed with a 10% PP5/ PS blend of viscosity ratio of 1.2 (Figure 4.23, page 108).

One drawback of the procedure used to prepare the Izod specimen is the coalescence occurring in the dispersed phase while the blend is molded into a plate. The disperse phase droplets will show significant coalescence at elevated temperatures especially when there is a high concentration of disperse phase. This is because coalescence lowers the overall energy of the system and lower matrix phase viscosity aids this process. Favis and Chalifoux (1988) found 75% increase in the number average diameter for a PC/PP system of viscosity ratio of 7 kept at 250°C for 85 minutes. The coalescence in the reversed system, however, was found to be negligible. The effects of coalescence in iPP/LLDPE systems, which inherently have low interfacial tensions, have been investigated by Liu and Truss (1996). Their study on remelting blends and keeping them at 200°C for extended periods of time, showed that there is about 40% reduction in the number of dispersoids in 2 hours for 10 LLDPE/ 90 iPP blends. Although in this study, the Izod specimen used for morphological analysis using SEM correspond to the 'as

blended' samples referred by Liu and Truss (1996), the sensitivity of dropsizes to the melt time are a cause for concern and will have to be investigated in future studies.

4.4.4 Morphological Features and their Origin

One of the interesting features observed in many of the samples was the formation of web-like structures at the drop-matrix interface (Figure 4.15) due to shrinkage of the minor phase. According to McEvoy and Krause (1997), these structures occur in high impact strength systems. Westphal et al. (1997) reported that such microfibrils were present in more ultra low density polyethylenes with a greater crystallizible fraction and that the fibrils strengthened the interface and reduced the ductile-brittle transition in blends when compared with homogeneous modifiers of equal density. As one would expect, the more crystalline minor phases show more shrinkage and more manifestation of webs. In cases where the adhesion between the phases is strong, the dispersed phase is stretched to form fibrils which adhere to the interface forming web like structures bridging the droplet to the matrix. It is possible that these strands are caused by the entanglement of the longer chained molecules with the matrix phase. Cocrystallization of the phases at the interface might also be a reason for the interfacial bonding. Yamaguchi (1998) refuted the dependence of interfacial adhesion in PE/PP films on the formation of PE influxes between PP spherulites formed upon crystallization. Entanglements between the two phases was found to be the main factor affecting adhesion. Levine et al. (1964) expressed adhesive strength as an inverse function of the interfacial tension.

In this study, the occurrences of the web-like structures was found to occur more in cases where the interfacial tension was low while in cases where the interfacial tension was high, mere cavitation was observed without the formation of the strands. All the gas-phase polymerized Ziegler-Natta polyethylenes show this to some extent while the maximum occurrence was noted in LLDPE 8b. LLDPE 5o did not show this and neither did most of the metallocene polyethylenes, which exhibit low shrinkage due to their amorphous nature. LLDPE 4p however did exhibit this feature and this was probably due

to better matrix penetration owing to a much lower viscosity ratio as well as better packing efficiency of the molecules due to a shorter side branch. Avella et al. (1993) explored the effect of M_w on the fracture toughness of iPP. They found that tie-molecules are present in high M_w iPP and that they bind the crystallites together. They also saw a more marked plastic deformation zone following the notch tip in fractured specimen and concluded that the greater toughness of high M_w species is due to higher crazing in those samples. They also studied the effect of quenching temperature on the blend toughness and found that a higher temperature range of quenching ensures greater amorphous nature and a higher number of tie molecule binding the spherullitic domains and hence more strength. Whether these strands are composed of a highly deformable low molar mass amorphous fraction or whether they are made of entangled high molar mass molecules is a topic for future studies as this can influence the toughness of the blend, when stretching of these strands is a mechanism for fracture resistance.

Another interesting phenomena observed was strands connecting one particle to another (Figure 4.14). One possible explanation could be that these strands are only on the surface and are a result of dispersed phase crazing. For cases where the droplet adhesion with the matrix is strong, crack propagation through the droplet would cause the droplet to get stretched into a fiber. When the crack develops, the broken strands would collapse back on the surface and fuse with the first point they touch, which would be the nearest ridges in the vicinity. This would explain the routing of these threads from dispersed droplets through higher points to other dispersed droplets. These strands can be also formed when strands stretch and then fuse with a close-by craze strand, followed by simultaneous collapse to the same surface.

The second premise for interconnecting strands, such as those seen for LLDPE8b/PP1 blend (Figure 4.17 B), is that these strands are not on the surface but exist throughout the matrix, much like an interpenetrating network. The explanation in that case would be that collision of droplets occurs during mixing and the droplets are pulled apart without sufficient time for coalescence. The coalesced zone gets stretched into a fine

interconnecting thread. The higher the elasticity and lower the interfacial tension, the longer is the timescale for breakup of these fine threads by Rayleigh breakup (Janssen et al., 1992). Slender threads of highly elastic minor phase have been observed to show retarded breakup via a bead string configuration (Elmendorp, 1986). The interconnections exist for long enough times, they can be captured by rapid quenching. The blend could then be thought to be similar to an interpenetrating network. This could also explain the steep increase in impact strength of PP blends at higher concentrations. Luciani and Jarrin (1996) have proposed a criterion for phase inversion based on the stability of such fibrillar structures in both phases.

Other interesting structures included a doughnut type minor phase remanant on the fracture surface of 20% LLDPE6b/PP1 blend (Figure 4.17 A). This could be caused due to a circumferential ring of adhered minor phase after most part of the drop is pulled out by the other surface. The ring could also be composed of complex material formed by the partial miscibility of the minor phase in the matrix. Dispersed drop crazing is another possibility, although it was not observed in any of the other cases. A three-phase system was visible in the same micrograph located in the lower left corner. Small particles were entrapped in a globular structure which was further encapsulated inside the matrix. This could also be caused by the minor phase particles being pulled away, causing web-like fibrillar structures to snap, leaving behind stumps arranged in a circular arrangement after fracture on one of the surfaces. The same mechanisms could have been held responsible for the morphology seen in the 20% LLDPE 8b/PP1 blend (Figure 4.17 B).

The plate like formation of the matrix phase with several irregularly shaped holes, within which shrunken minor phase droplets were embedded (Figure 4.16) could be brought about by hole formation inside a sheet of polymer exposing the underlying morphology through the holes. This feature was seen only for the LLDPE4p and LLDPE6b blends. It could be indicative of a phase miscible fraction of the minor phase with the major phase.

4.4.5 Effect of various factors on Impact Strength

In Figure 4.7, linear trends have been fitted through the Izod strength versus viscosity ratio data for each of the three concentrations (these look curved owing to the log scale). It is observed that at the low concentrations of dispersed phase, 5% and 10% LLDPE, the impact strength decreases with viscosity ratio. The reason is that at higher viscosity ratio, the dispersion of droplets inside the matrix is coarser. Uneven distribution of dispersed phase is ineffective in inhibiting crack growth. At 20% LLDPE, however, the Izod impact strength increases with viscosity ratio. The reason for this could be that at higher concentrations, molecular entanglements are more prevalent. Entanglements increase the strength between two phases and higher molar mass polymers exhibit more chain entanglements and generally possess higher dynamic viscosities, thus higher viscosity ratios. Another possible argument could be that high viscosity polymers generally exhibit greater elasticity and are therefore expected to show greater individual Izod impact strengths. The character of a particular component can dominate when its concentration in the blend is high enough. However, from the SEM pictures, the crack was never observed to pass through the dispersed phase, suggesting that the fracture mechanism did not involve elasticity of the dispersed phase.

From Figure 4.8, two of the metallocene LLDPEs, LLDPE1b and LLDPE3h show a continuously increasing impact strength with concentration. The Z-N LLDPEs and LLDPE2o seem to reach a steady value of impact strength at a concentration of 20%. In comparison, the impact strength of LLDPE4p was observed to decrease at a concentration of 20% after the initial rise at 10%. Wang et al. (1997) have also reported a significant increase followed by a gradual reduction in the sharp notched Izod impact strength of epoxidized EPDM/PC blends with increase in eEPDM (modifier) content. They explained that increasing local shear yielding is responsible for the reduction. They did not report the viscosity ratio of the system and it is not fair to say that the same factors are active in our blends. Moreover, at higher concentrations of LLDPE, the individual Izod impact

strengths of the LLDPEs will play a greater role in determining the properties of the blend and this will have to be investigated in further detail.

Table 4.1 shows that the standard deviation in the impact strengths from specimen to specimen, for most systems, decreases with concentration. It appears that the dispersion is better at higher concentrations, leading to synergistic increase in strength and better average performance. When the average impact strengths for the metallocene LLDPEs are considered relative to that of the Z-N LLDPEs, a distinct advantage is observed at higher concentrations for the metallocene LLDPEs. This can be seen in Figure 4.24. At lower concentrations, however, the Z-N LLDPEs showed a slight superiority. It is possible that in Z-N LLDPEs, there is phase segregation of the amorphous branched moities from the linear chained fraction which results in poor dispersion.

LLDPE4p shows a maximum impact strengthening at a concentration of 10%. With further LLDPE4p addition, the Izod strength actually decreases. It is possible that at higher concentrations, LLDPE4p meets the criterion for cocontinuity of phases and the reduction in dispersivity causes the reduced Izod strength. The 10% LLDPE4p/PP1 blends show the presence of a two continuous phases as well as dispersed droplets (Fig. 4.16). It is not clear whether this third phase is simply LLDPE in a plate like morphology or whether it is a miscible complex of LLDPE and PP as indicated by Liu and Truss (1996), who studied fracture surfaces of 50% LLDPE/PP blends.

According to the correlation of Jordhamo (1986), Eq. 4.1, the minimum viscosity ratio for which a co-continuous morphology is predicted, using the maximum concentration of 20% and PP and LLDPE densities of 0.90 and 0.88, respectively, is 0.256. This estimate is, however, only approximate, since the densities at room temperature rather than at the melt temperature were used. The closest viscosity ratio is 1.0 which belongs to LLDPE4p. The existence of the plate-like morphology at mass fractions as low as 10% favors the argument that a complex composed of a miscible fraction of LLDPE and PP is formed.

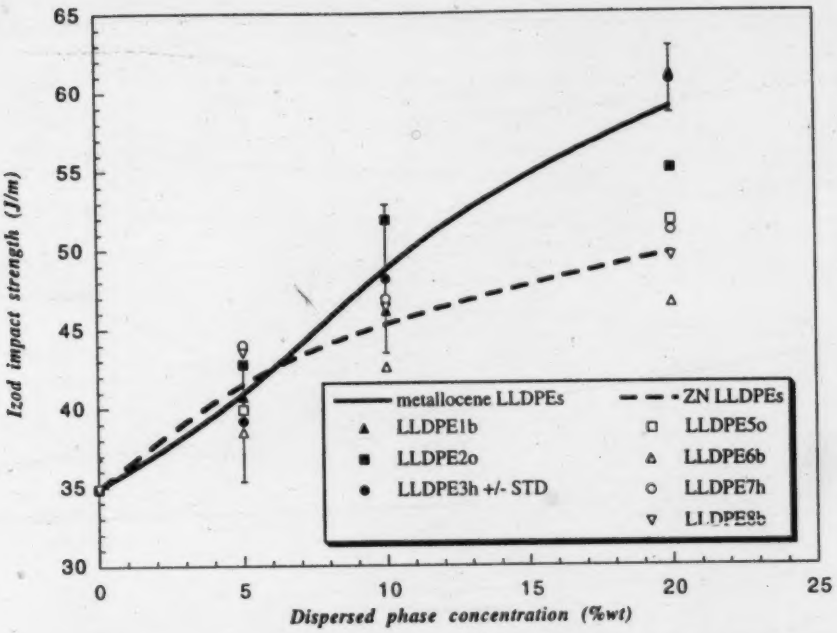

Fig 4.24 : Comparison of metallocene and Ziegler Natta LLDPEs for impact modification of PP.

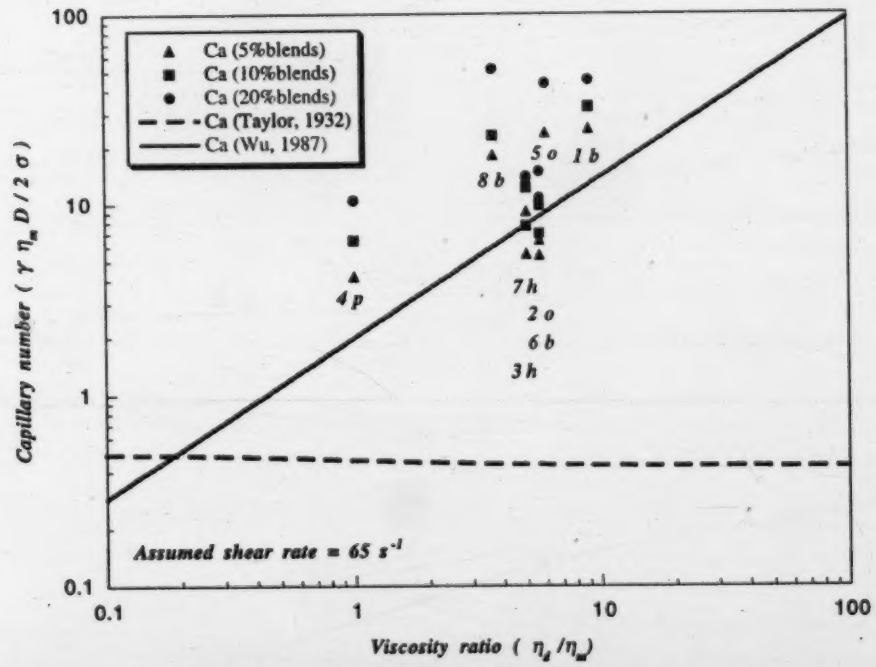

Figure 4.25 : Capillary number as a function of viscosity ratio - Comparison of experimental observation with Newtonian limit predicted by Taylor and correlation given by Wu for blends processed in a twin screw extruder.

The 10% blends LLDPE4p/PP1 and LLDPE6b/PP1, both show plate-like structures (Figure 4.16) in which dispersed droplets are embedded. It is not clear whether this feature is due to the brittle fracture of matrix phase at low temperatures or whether this is due to stratification of the minor phase. Some zones of the 20% blends of the same systems show encapsulated dispersed droplets inside a third phase, suggesting phase inversion, but clear droplet-matrix morphology was also present at other zones.

Using the theory proposed by Van Oene (1972), only LLDPE4p/PP system shows a possibility of stratified morphology according to the first criterion (Inequality 4.5), as the difference in the dispersed phase and matrix phase first normal stress differences is negative (Table 4.3) in the range 0.3 - 0.6 rad/s. The dynamic interfacial tension was evaluated for the 20% LLDPE4p/PP blend, using a drop diameter of 2.15 μm (obtained from Table 4.2). The dynamic interfacial tension was positive and hence no stable stratified morphology was predicted. Moreover, from Figure 4.12, we can clearly see that the 20% LLDPE4p/PP blend has a drop-matrix morphology. The sheet-like morphology observed in the 10% and 20% LLDPE4p/PP blends (Figure 4.16) might just be a result of partial stratification of the dispersed phase inside the matrix phase during the developmental stages of the blend morphology (as depicted in Figure 4.1).

4.4.6 Dropsizes

To determine whether all the dropsize measurements could be related to the rheological and interfacial conditions, the Capillary number, based on the measured interfacial tensions, was plotted as a function of the viscosity ratio for all the blends (Figure 4.25). The solid line in Fig. 4.25 depicts the equation (Eq. 4.7) proposed by Wu (1987) and agrees reasonably well with our data. Since all the blends are in the range $p>1$, the exponent of p in Equation 4.7 is +0.84. Again, if only the two systems - LLDPE1b/PP and LLDPE4p/PP were considered, then the exponent of the viscosity ratio in Eq. 4.7, +0.84, was accurately met although the value of the coefficient preceding the viscosity ratio term was found to be 4 instead of 2.

According to Favis and Willis (1990), the heirarchy of effects controlling the morphology of immiscible blends follows : interfacial tension > viscosity ratio > shear stress. In the present study however, the differences between the interfacial tensions was relatively small and viscosity ratio appeared to play the greater role.

Wu (1985), while studying rubber toughening of nylon, observed a sharp tough to brittle transition in the Izod impact strength as the dropsize of rubber particles was increased, keeping the rubber volume fraction and interfacial adhesion constant. He found that the critical dropsize at which this transition occurs increased with increasing rubber volume fraction. Consequently, the interparticle distance of the rubber particles was found to be a critical parameter in determining the toughness of the blend. Only blends with interparticle distance below a critical value were found to show significant toughening.

In the present study, these transitions were not captured since only three compositions were analyzed. Figure 4.21 (a) shows the interparticle distance plotted as a function of concentration of dispersed phase. There is no clear trend when all the blends are considered together. When a distinction is made between the PI-Izod samples and the QFPI-Izod samples, then we can see that a significant jump in the interparticle distance is observed when samples are fractured at lower temperature. When interparticle distance of the QFPI-Izod samples are examined, the metallocene LLDPEs clearly show a decreasing trend with increasing concentration, which is expected. On the other hand, the Z-N LLDPEs show greater interparticle distances as the concentration increases. This is counterintuitive as one would expect that as concentration of the dispersed phase increases, the interparticle distance should decrease. Possible scenarios where this could occur are that there is partial miscibility of the Z-N LLDPEs with the PP. The second possibility is that coalescence is greater for the Z-N LLDPEs either in forming larger droplets, or other transient structures such as sheets. However, if only those blends showing the representative area fraction are considered, then the interparticle distance is observed to decrease monotonously with concentration.

4.5 Summary and Conclusions

The following general observations and conclusions were arrived at based on the results and observations presented earlier in this chapter.

The impact strength increased with increasing LLDPE content (Figure 4.8). The average Izod impact strength of metallocene LLDPE/PP1 blends was found to be higher than Ziegler-Natta LLDPE/PP1 blends as the concentration of dispersed phase increased. The low concentration minor phase impact strength was greatest for LLDPE 2o/PP blend while at high concentration LLDPE 1b/PP and LLDPE 3h/PP blends, both show high impact strengths. This is attributed to low shrinkage of amorphous LLDPEs, thus avoiding debonding by exerting lesser interfacial strain. Higher crystallinity of the Z-N LLDPEs caused shrinkage and cavitation, eliminating one of the mechanisms of reducing triaxial stress and thus resulting in lower strength.

Viscosity ratio and concentration of LLDPE, both affected the strength of the blend greatly. Interfacial tension only affected the droplet diameter at higher concentrations. It is possible that the mismatch in viscosity of the matrix and dispersed phase led to greater coarsening at lower concentrations.

Morphology of a blend plays an important role in determining the impact strength of the blend. Several morphological features exhibiting plastic deformation were seen in high Izod impact strength samples. Visible features included a stress whitened zone following the notch and whitened craze streaks along the Izod fracture surface. The relative strength of the samples was related to the stress whitened zones and amount of crazing present on the post-impact Izod surfaces for same component blends. However, when the components or compositions changed, the stress whitened zones alone did not relate well with the measured Izod impact strength. Evidence of plastic deformation from SEM pictures were interconnecting strands from the droplet to the matrix and dispersed droplets extending into thin threads stretching from one droplet to another. The presence

of web-like structures at the interface appear to contribute to added strength although they are also accompanied by void space created due to debonding is also quite high. Shrinkage was observed more in the samples with greater crystallinity and this resulted in void formation for systems with poor interfacial strength and web-like structures in systems with strong interfacial strength. The higher molar mass LLDPE systems showed more of these structures, supporting the conclusion interfacial strengthening is enhanced largely by molecular entanglements. Sheet-like morphology observed for a 10% LLDPE6b/PP blend with droplets of an immiscible fraction indicated phase separation of LLDPE and the partial miscibility of a phase separated low molar mass fraction with the matrix. Other uncommon features also included matrix cavitation, dispersed droplet cleavage and formation of a cocontinuous phase.

The temperature of the fracture can significantly alter the fracture mechanism as can the presence of a notch to initiate the crack. The speed of the crack and the interfacial strength both determine the path of the crack and this affected both the morphological zones as well as efficacy of exposing droplets. The crack propagated largely through the matrix phase in the case of low temperature fracture and this was reflected by high interparticle distances (Table 4.2) for these fracture surfaces. Although lower temperature fractures were found to show a sharp interface between the phases, they led to more difficulty in measuring droplet size due to shrinkage and debonding of the minor phase. LLDPE5o was found to show several sub-surface droplets. This was attributed to a strong interface formed by co-cystallization of the interfacial layer.

Three zones were observed in both the room temperature fractured PI-Izod samples and low temperature quench-fractured samples. The first zone showed ductile deformation of minor phase leading to formation of threads. The second and third zones showed more brittle fracture but the third zone bypasses the droplets. The interfacial adhesion due to entanglements led to the formation of web like structures bridging the minor phase particles to the matrix. Samples with these structures show good impact strength.

The dropsizes, for the systems with viscosity ratio > 1, were largely viscosity ratio dependent. The effect of interfacial tension increased at higher concentration. Interfacial tension is responsible for some of the morphological features determining the strength of the blend and might also play a role in the coalescence governed range at high concentrations. In order to clearly see the effect of the interfacial tension, all the compared systems would have to have similar viscosity ratios. The impact strength also depended largely on the viscosity ratios but was also dependent on the concentration of the minor phase. The interfacial tension was internally found to affect the morphology by manifestation in fibrillar stability and interfacial strength in the form of web like structures.

The shrinkage of minor phase and partial penetration of the electron beam leading to only surface details, are two reasons why the droplet boundary was not clearly representative of the true value in some cases. The latter problem can be avoided when preferential dissolution of one phase in a solvent is carried out followed by SEM. This method has been recently used by Luciani and Jarrin (1996) to study the stability of fibrillar structures in some blends. In our case, this would leave clear voids in the matrix phase. The reduction in dropsize due to crystallization upon cooling is still a problem. The hole size may or may not correspond to the void size. TEM is certainly a better method to measure dropsizes for these blends but is more tedious and difficult for this system and the latter problem still exists. Whether the crystallization-shrinkage was due to slow-cooling on the plate press or whether it was imparted subsequently upon quenching from room temperature to very low temperatures, will have to be investigated. Quick - quenching of the melt is likely to preserve the amorphous nature of the melt. The variation of density with temperature might also be an important factor for consideration.

Summary, Conclusions and Future Work

Chapter 5

In the first part of this study the interfacial tensions were measured between various linear low density polyethylenes and a low molar mass polypropylene, namely, PP1. The application of Tomotika's breaking thread method was successfully demonstrated for the LLDPE/PP systems. The problem of low contrast between the thread and matrix phases was solved by the addition of carbon black to the thread phase with minor effect on the interfacial tension. Inadequate annealing, oxidation due to long exposures to air and flow of the molten sample were identified as factors affecting the experimental results adversely. The use of a slotted plate to conduct the breakup solved some of these problems and improved reproducibility of the measurements.

The interfacial tensions from individual runs were all in the range of $0.2 < \sigma < 4.2$ mN/m. The most probable interfacial tension values for these runs, determined by how closely they followed Tomotika's breakup criterion, a measure of how well the Newtonian theory applied to the melts, was in the range $0.6 < \sigma_{mp} < 2.6$ mN/m for the LLDPE/PP1 sytems. The σ_{mp} values were subsequently used to predict blend dropsizes.

One of the aims of this study was to see if there was advantage of using one type of copolymer over another for increasing impact strength in LLDPE-PP blends. Even though the butenes copolymers did not always show the highest impact strength among the set of LLDPEs used, the interfacial tensions indicate that the use of 1-butene LLDPEs is favoured over other comonomer types. Two of the three 1-butene copolymers, LLDPE1b and LLDPE8b, show lower interfacial tension values (0.6-0.7 mN/m) while the other copolymers have interfacial tensions of approximately 2 mN/m. On the other hand,

LLDPE6b, also a 1-butene copolymer had an interfacial tension value of 2.6 mN/m. A comparison of the TREF profiles of LLDPE6b and LLDPE8b showed a difference only in the intensity of the homopolymer peaks. This led to the conclusion that the homopolymer fraction, is responsible for the high interfacial tension. This could either be because the homopolymer fraction, which is generally composed of molecules of high molar mass, leads to greater retraction and elasticity effects during experiments, or because the homopolymer fraction, consisting of unbranched chains, does not interact well with the PP phase. Another possible argument is that if the migration of smaller chained branched moieties is responsible for lowering the interfacial tension of two polymers, then the polymer with the more crystalline structure, LLDPE6b, has lower migration of such molecules. LLDPE5o, a butene-octene terpolymer with a sizeable homopolymer content (Coho ratio = 1.3) also showed a low interfacial tension of 0.8 mN/m. It is possible that migration of molecules is unaffected because of the octene copolymer weakening the continuity of the crystal structure. Thus, there is no clear explanation for the interfacial tension trends and further work in this direction must be carried out.

Another intent of this research was to determine if the LLDPE-PP interfacial tensions of the metallocene LLDPEs differed from those made with Ziegler-Natta LLPDEs. Theoretically, the metallocene polyethylenes were predicted to have lower interfacial tension owing to their higher branch content, but experimental measurements for both systems did not support this prediction. The impact strength for metallocene LLDPE-PP blends was however found to be higher than Z-N LLDPE blends at 20% LLDPE concentration.

The Izod impact strength of all the PP blends prepared with different LLDPEs, showed increases with increases in LLDPE contents. While the increase in strength with concentration was modest for low viscosity ratio blends, it was quite dramatic for systems in which the viscosity ratio approached 10. The dependence of the impact strength on interfacial tension was observed only for the 20% LLDPE/PP blends.

Three morphological zones were observed on the fracture surface of the Izod samples. The first of these showed plastic deformation of the dispersed phase into fibers extending across the matrix. Stress whitening on the fracture surface of Izod samples of a particular blend could be related to the corresponding impact strengths but this could not be extended to samples from different blends. Quench fractured samples showed a lower number of exposed particles than the samples fractured at room temperature. This was evident from the representative areas of minor phase derived from dropsize measurements. This was attributed to the speed of crack propagation which resulted in a brittle mode of fractures at the low temperatures.

In many of the blends, the LLDPE phase was observed to shrink inside the matrix. For systems with good interfacial strength, web-like fibrils extended from the droplets to the void surface and were believed to contribute towards increasing the impact strength. These fibrils were probably caused due to entanglements between the two phases at the interface.

The observation of morphology which resembles phase inversion, in 20% LLDPE6b/PP1 sample, suggests phase separation of the LLDPE6b. Encapsulation of the high molar mass PE fraction inside the more amorphous lower molar mass PE fraction, as a result of vigorous mixing, would explain the partially miscible fraction. The segregation of amorphous phase at the interface would also explain the differences in the interfacial tension of the different polyethylenes composed of the same monomers.

The branching of metallocene polymers is very controlled and the polydispersity is also very low. Therefore, it is not surprising that the metallocene polymers do not show many unusual features. There is therefore a smaller chance of phase separation in the metallocene polymers. On the other hand, the Z-N LLDPEs have a linear homopolymer fraction, which might hinder the migration of low molar mass molecules to the interface, if phase separation occurred. Due to this mechanism of amorphous phase segregation at the

interface, the Ziegler-Natta polyethylenes might actually prove more effective in impact modification. The amorphous fraction then performs the function of a compatibilizer.

Finally, the type of comonomer alone did not determine the properties of the LLDPE/PP blends. Intermolecular heterogeneity and detailed information on the molecular architecture, e.g. methyl sequence length distribution, are required for systematic studies aimed at determining the effects of comonomer type on blend properties.

The structural information on the polymers used in this study was still inadequate for detailed interpretation of the results. Further characterization, such as cross fractionation and DSC analysis of the blend, might be able to uncover some of the synergistic effects coming into play. The effect of elasticity of the LLDPEs on the blend properties was also not dealt with in detail in this study and can form an interesting future study.

The field of view available in the experimental equipment used for the breaking thread method spanned only half a wavelength of the distortion. This prevented observing the remainder of the thread which is needed to ascertain whether the breakup was uniform. Equipment with better resolution and a broader field of view can improve the results significantly and make the experiments less cumbersome. With the use of recent equipment acquisitions in the Department it should also be possible to determine interfacil tension of polymer mixtures by the spinning drop method.

A greater number of repeat measurements for each system would increase the accuracy of the interfacial tension results. Future studies should involve matching the viscosity ratio more closely for more uniform breakup. A detailed examination of the slotted plate for the breaking thread method runs should also be done.

The current study was carried out using fixed processing conditions for all the blends. This resulted in different drop diameters and different interparticle distances. For a blend of a certain composition, a minimum dispersed phase dropsize will exist, limited only by coalescence. Such a blend can be obtained by varying the processing conditions such as shear rate. This will reduce the number of variables affecting blend properties and simplify the study of the effect of interfacial properties of the components on the blend properties.

References

Alamo R.G., Graessley W.W., Krishnamoorti R., Lohse D.J., Londono J.D., Mandelkern L., Stehling F.C., Wignall G.D., Small angle neutron scattering investigations of melt miscibility and phase segregation in blends of linear and branched polyethylenes as a function of the branch content. Macromolecules **1997**, 30, 561-566.

Anastasiadis, S.H., Chen J.K ., Koberstein J.T., Sohn J.E., Emerson J.A., The determination of polymer interfacial tension by drop image processing: Comparison of theory and experiment for the pair, Poly(dimethyl siloxane)/Polybutadiene. Polym. Eng Sci. Mid-Nov. **1986**, 26(20), 1410-1418.

Avella M., dell'Erba R., Martuscelli E., Ragosta G., Influence of molecular mass, thermal treatment and nucleating agent on structure and fracture toughness of i-PP. Polymer, **1993**, 34, 14, 2951-60.

Bains M., Balke S.T., Reck D., Horn J., The compatibility of LLDPE-PP Blends: Viscosity ratio plots. Polym. Eng. Sci., **1994**, 34, 16, 1260-68.

Bonner J.G., Fyre C.J., Capaccio G., A novel calibration of polyethylene copolymers by temperature rising elution fractionation. Polymer, **1993**, 34, 16, 3532-34.

Bousfield D.W., Keunings R., Marrucci G., Denn M.M., Nonlinear analysis of the surface tension driven breakup of viscoelastic filaments. J. Non-Newtonian Fluid Mech. **1986**, 21, 79-97.

Brandrup J., Immergut E. H., Polymer Handbook 3rd ed. Interscience Publishers, **1989**.

Bremner T., Rudin A., Cook D.G., Melt flow index values and molecular weight distributions of commercial thermoplastics. J. App. Polym. Sci., **1990**, 41,1617-27.

Cahn J.W., Hilliard J.E., Free energy of a nonuniform system. I. Interfacial free energy. J. Chem. Phys., **1958**, 28(2), 258-267.

Carriere C. J., Silvis H. C., The effects of short-chain branching and comonomer type on the interfacial tension of polypropylene polyolefin elastomer blends. J. App. Poly. Sci. **1997**, 66, 1175-1181.

Carriere C.J., Cohen A., Arends C.B., Estimation of Interfacial Tension Using Shape evolution of Short Fibers. J. Rheol. **1989**, 33(5), 681-689.

Chakravarty J., Characterization of polyolefins by TREF. M.Sc. Thesis, University of Alberta, **1993**.

Chappelear D.C., Interfacial Tension Between Molten Polymers. Polym. Prepr. **1964**, 5, 363-371.

Cheung M.F., Plummer H.K., Izod impact fracture morphology of rubber-toughened polysulfone and poly(phenylene sulfide) blends. Polym. Eng. Sci., **1996**, 36, 1, 15-22.

Chiu W.-Y., Fang S.-J., Mechanical properties and morphology of crosslinked PP/PE blends and PP/PE/Propylene-ethylene copolymers blends. J. App. Polym. Sci., 1985, 30, 1473-1489.

Cho K., Jeon H.K., Park C.E., Kim J., Kim K.U., The effect of end-sulfonated polystyrene on the interfacial tension of nylon-6/polystyrene blends. Polymer, 1996, 37, 7, 1117-1122.

Coleman M. M., Graf J. F., Painter P. C., Specific Interactions and the Miscibility of Polymer Blends. Technomic Publishing Co., Lancaster, PA 1991.

Cross M.M., Kinetic interpretation of non-Newtonian flow. J. Coll. Int. Sci., 1970, 33, 30-35.

Cser F., Rasoul F., Kosior E., Micro-morphology of compatibilised and noncompatibilised blends of PP with LLDPE. International symposium on polymer blends, alloys and filled systems: Polyblends 1997, SPE RETEC, 9-10 October, 1997, 354-373.

Datta S., Lohse D.J., Graft copolymer compatibilizers for blends of isotactic polypropylene and ethene-propene copolymers. 2. Functional polymers approach. Macromolecules, 1993, 26, 2064-76.

Defoor F., Groeninckx G., Reynaers H., Schouterden P., Heijden B. Van der, Thermal and morphological characterization of binary blends of fractions of 1-octene LLDPE. J. App. Poly. Sci., 1993, 47, 1839-48.

Demarquette N.R., Kamal M.R., Interfacial Tension in Polymer Melts. 1: An Improved Pendant Drop Apparatus. Polym. Eng. Sci. 1994, 34(24), 1823-1833.

Dharmarajan N.R., Yu T.C., Modifying polypropylene with a metallocene polymer. Plastics Engineering, Aug 1996, 33-35.

Dumoulin M.M., Utracki L.A., Farha C., Rheological and mechanical properties of ternary blends of LLDPE/PP?ethylene-propylene block polymers. Polym. Eng. Sci., 1984, 24, 17, 1319-1326.

Elemans P.H.M., Janssen J.M.H., Meijer H.E.H., The Measurement of Interfacial Tension in Polymer/Polymer Systems: The Breaking Thread Method. J. Rheol. 1990, 34(8), 1311-1325.

Elemans P.H.M., Ph.D. Thesis, Eindhoven Univ. Tech., Netherlands, 1989.

Elmendorp J.J., A Study on Polymer Blending Microrheology . Polym. Eng. Sci. 1986, 26(6), 418-426.

Elmendorp J.J., Van Der Vegt A.K., A study of polymer blending microrheology : Part IV. The influence of coalescence on blend morphology origination. Polym. Eng. Sci., 1986, 26, 19, 1332-38.

Ellingson P.C., Strand D.A., Cohen A., Sammler R.L., Carriere C.J., Molecular weight dependence of PS/PMMA interfacial tension probed by imbedded fiber retraction. Macromolecules, 1994, 27, 1643-1647.

Escudie E., Graciaa A., Lachaise J., Pendant drop measurements of the PP/PS interfacial tension between 220°C and 270 °C. Mat. Chem. Phys. 1986, 14, 239-246.

Favis B.D., Chalifoux J.P., Influence of composition on the morphology of PP/ PC blends. Polymer, 1988, 29, 1761-1767.

Favis B.D., Chalifoux J.P., The effect of viscosity ratio on the morphology of PP/PC blends during processing. Polym. Eng. Sci., 1987, 27, 20, 1591-1600.

Favis B.D., The effect of processing parameters on the morphology of an immiscible binary blend. J. App. Polym. Sci., 1990, 39, 285-300.

Favis B.D., Willis J.M., Phase size / composition dependence in immiscible blends: Experimental and theoretical considerations. J. Polym. Sci.: Part B: Polym. Phys., 1990, 28, 2259-69.

Fetters L.J., Graessley W.W., Krishnamoorti R., Lohse D.J., Melt chain dimensions of Poly(ethylene - 1-butene) copolymers via small angle neutron scattering. Macromolecules 1997, 30, 4973-4977.

Fetters L.J., Lohse D.J., Richter D., Witten T.A., Zirkel A., Connection between polymer molecular weight, density, chain dimensions, and melt viscoelastic properties. Macromolecules 1994, 27(17), 4639-4647.

Fortelny I., Kovar J., Effect of the composition and properties of components on the phase structure of polymer blends. Eur. Polym. J., 1992, 28, 1, 85-90.

Fortelny I., Zivny V., Theory of competition between breakup and coalescence of droplets in flowing polymer blends. Polym. Eng. Sci., 1995, 35, 23, 1872-77.

Ghodgaonkar P. G., M.Sc. Thesis, Morphology development and compatibilization in immiscible polymer blend systems. University of Alberta, 1997.

Ghosh T., Huang J. C.-K., Williams M.C., Melt index for molecular weight quality control. Proc. XII Int. Congr. on Rheology, Quebec City, Quebec, Canada, 1996, 85-90.

Gisbergen J.G.M. van; Meijer H.E.H., Influence of electron beam irradiation on the microrheology of incompatible polymer blends: Thread breakup and coalescence. J. Rheol. 1991, 35(1), 63-87.

Golba J., Seeger G.T., Complex blends need both compatibility and SEC. Plast. Eng., March, 1987, 57-59.

Goren S.L., Gottlieb M., Surface tension driven breakup of viscoelastic liquid threads. J.Fluid Mech. 1982, 120, 245-266.

Grace H.P., Dispersion phenomena in high viscosity immiscible fluid systems and application of static mixers as dispersion devices in such systems. Chem Eng. Commun. 1982, 14, 225-277.

Helfland E., Tagami Y., Theory of the interface between immiscible polymers. II. J. Chem. Phys. 1972, 56(7), 3592-3601.

Hobbs S.Y., Polymer microscopy. J. Macromol. Sci. - Rev. Macromol. Chem., 1980, C19, 2, 221-265.

Holz N., Goizueta S., Capiati N.J., LLDPE addition to PP/Elastomer blends: Phase structure and impact properties. Polym. Eng. Sci., 1996, 36, 22, 2765-2770.

Huang J. C.-K., Lacombe Y., Lynch D.T., Wanke S.E. Effects of H2 and 1-butene concentrations on the molecular properties of polyethylene produced by catalytic gas phase polymerization. Ind. Eng. Chem. Res., 1997, 36, 1136-43.

Hussain I.A., Williams M.C., Rheological evidence for high-temperature phase transitions in melts of high density polyethylene. Macromol. Rapid Commun. 1998, 19, 323-325.

Janssen J.H.M., Peters G.W.M., Meijer H.E., Baaijens F.P.T., Mixing of immiscible liquids. Theoretical and App. Rheol., 1992, Proc. XIth Int. Congr. on Rheology, Brussels, Belgium, 369-371.

Jejelowo M.O., Lynch D.T., Wanke S.E., Comparison of ethylene polymerization in gas phase and slurry reactors. Macromolecules, 1991, 24, 1755-1761.

Jordhamo G.M., Manson J.A., Sperling L.H., Polym. Eng. Sci., 1986, 26, 517.

Kamal M.R., Demarquette N.R., Lai-Fook R.A., Price T.A., Evaluation of Thermodynamic theories to predict interfacial tension between polystyrene and polypropylene melts. Polym. Eng. Sci. 1997, 37(5), 813-825.

Kamal M.R., Lai-Fook R., Demarquette N.R., Interfacial tension in polymer melts. Part II: Effects of temperature and molecular weight on interfacial tension. Polym. Eng. Sci. 1994, 34(24), 1834-1839.

Kambour R.P., A review of crazing and fracture in thermoplastics. J. Polym. Sci. : Macromolecular Reviews, 1973, 7, 1-154.

Karbashewski E., Rudin A., Effects of polymer structure on the onset of processing defects in LLDPEs. Polym. Eng. Sci., 1991, 31, 22, 1581-89.

Keroglanian S.P., Harrison I.R., A temperature rising elution fractionation study of short chained branching behaviour in ultra low density polyethylene. Polym. Eng. Sci., 1996, 36, 5, 731-736.

Kesari J., Salovey R., Mechanical behavior of polyolefin blends. Ch. 13, Polymer blends and composite in multiphase systems. Amer. Chem. Soc., 1984, , 211-219.

Kim B.K., Reactive extrusion of polyolefins and their blends. Korea Polym. J., 1996, 4, 2, 215-226.

Kryszewski M., Galeski A., Pakula T., Grebowicz J., Transport phenomena on interfaces in blends of polypropylene and polyethylene. J. Coll. Int. Sci., 1973, 44, 1, 85-94.

Kuhn W., Spontane Aufteilung von Flussigkeitszylindern in kleine Kugeln. Kolloid Z. 1953, 132, 84-99.

Kwok D.Y., Hui W., Lin R., Neumann A.W. Liquid-fluid interfacial tension measured by axisymmetric drop shape analysis: Comparison between the pattern of interfacial tension of liquid-liquid and solid-liquid systems. Langmuir, 1995, 11, 2669-2673.

Lacombe Y., TREF characterization of ethylene/1-butene copolymers produced at various 1-butene and hydrogen pressures. M. Sc. Thesis, University of Alberta, 1995.

Lahoti M. R., M.Sc. Thesis, Adhesion measurement and stability of bulk polymer phases and thin polymer films. University of Alberta, 1997.

Lakdawala K., Salovay R., Rheology of polymers containing carbon black., Polym Eng. Sci. 1987, 27,14, 1036-1041.

Lee L.H., Mandell J.F., McGarry F.J., Fracture toughness and crack instability in tough polymers under plane strain conditions. Polym. Eng. Sci., 1987, 27, 15, 1128-1136.

Levine M., Ilkka G., Weiss P., Polym. Lett., 1964, 2, 915.

Liang H; Favis B.D., Surface modification strategies for multicomponent polymer systems. 2. Study of the interfacial tension and morphology of linear low density polyethylene/poly(vinyl chloride) blends. Ind. Eng. Chem. Res. 1997, 36, 1211-1217.

Liu Y., Truss R.W., Study of dispersion morphologies of iPP and LLDPE blends by scanning electron microscopy. J. App. Polym. Sci., 1996, 60, 1461-1473.

Luciani A., Jarrin J., Morphology development in immiscible polymer blends. Polym. Eng. Sci., 1996, 36, 12, 1619-26.

Luciani A., Champagne M.F., Utracki L.A., Interfacial tension in polymer blends Part 1 : Theory. Poly. Networks Blends 1996a, 6(1), 41-50.

Luciani A., Champagne M.F., Utracki L.A., Interfacial tension in polymer blends Part 2 : Measurements. Poly. Networks Blends 1996b, 6(2), 51-62.

Machiels A.G.C., Van Dam J., De Boer A.P., Norder B., Stability of blends of thermotropic liquid crystalline polymers with thermoplastic polymers. Polym. Eng. Sci. 1997, 37(9), 1512-1525.

McEvoy R.L., Krause S., Impact strength and fracture surfaces of interfaces between polyethylene and polypropylene and some ethylene containing copolymers. J. App. Polym. Sci., 1997, 64, 2221-35.

Michler G.H., Electron microscopic investigations of morphology and structure formation of polymers. J. Macromol. Sci.-Phys., 1996, B35(3&4), 329-355.

Mikami T., Cox R.G., Mason S.G., Breakup of extending liquid threads. Int. J. Multiphase Flow 1974, 2, 113-138.

MirabellaF.M., Westphal S.P., Fernando P.L., Ford E.A., Williams J.G., Morphological explanation of the extraordinary fracture toughness of linear low density polyethylenes. J. Polym. Sci.: Part b: Polym. Phys., 1988, 26, 1995-2005.

Mirabella F. M., Ford E.A., Characterization of LLDPE: Cross fractionation according to composition and molecular weight. J. Polym. Sci. : Part B: Polym. Phys. 1987, 25, 777-790.

Mulder M., M.Sc. Thesis (in progress), University of Alberta, Edmonton, Canada, 1999.

Nam K.H., Jo W.H., The effect of molecular weight and polydispersity of polystyrene on the interfacial tension between polystyrene and polybutadiene. Polymer 1995, 36(19), 3727-3731.

Nesterov A.E., Lipatov Y.S., Compatibilizing effect of a filler in binary polymer mixtures. Polymer, 1999, 40, 1347-1349.

Patterson H.T., Hu K.H., Grindstaff T.H. Measurement of interfacial and surface tensions in polymer systems. J. Polym. Sci.: Part C 1971, 34, 31-34.

Paul D.R., Barlow J.W., Polymer Blends (or Alloys). J. Macromol. Sci. - Rev. Macromol. Chem., 1980, C18, 1, 109-168.

Pham H.T., Carriere C.J., The effect of temperature on the interfacial tension of polycarbonate/polyethylene blends. Polym. Eng. Sci. 1997, 37(3), 636-639.

Pigeon M.G., Rudin A., Branching measurement by analytical TREF: A fully quantitative technique. J. App. Polym. Sci. 1994, 51, 303-311.

Plochocki A.P., Dagli S.S., Curry J.E., Starita J., Effect of mixing history on phase morphology of a polyalloy and a polyblend., Polym. Eng. Sci., 1989, 29, 10, 617-624.

Plochocki A.P., Melt rheology of polymer blends: The morphology feedback., Polym. Eng. Sci., 1983, 23, 11, 618-626.

Quayle O.R., Parachors of organic compounds. Chem. Rev. 1953, 53, 439-459.

Rayleigh J.S.W., On the instability of a thread of viscous liquid under capillary force. Phil. Mag. 1892, 34, 145-154.

Rayleigh J.S.W., Proc. London Math. Soc., 1879, 10, 4.

Roe R.-J., Bacchetta V.L., Wong P.M.G., Refinement of pendant drop method for the measurement of surface tension of viscous liquid. J. Phys. Chem., 1967, 71, 13, 4190-4193.

Rumscheidt F.D., Mason S.G., Breakup of stationary liquid threads. J. Colloid, Sci. 1962, 17, 260-269.

Rundqvist T., Cohen A., Klason C., The imbedded disk retraction method for measurement of interfacial tension between polymer melts. Rheol. Acta, 1996, 35, 458-469.

Schoolenberg G.E., During F., Coalescence and interfacial tension measurements for polymer melts: A technique using the spinning drop apparatus. Polymer 1998, 39(4), 757-763.

Schreiber H.P., Olguin A., Aspects of dispersion and flow in Thermoplastic - Elastomer blends. Polym. Eng. Sci., 1983, 23, 3, 129-134.

Schummer P., Tebel K.H., Production of monodispersed drops by forced disturbance of a free jet. Ger. Chem. Eng., 1982, 5, 209-220.

Scott C.E., Macosko C.W., Morphology development during the initial stages of polymer-polymer blending. Polymer, 1995, 36, 3, 461-470.

Scott C.E., Macosko C.W., Polym. Bull., 1991, 26, 341.

Scott C.E., Ph.D. Thesis, University of Minnesota, 1990.

Serpe G., Jarrins J., Dawans F., Morphology - processing relationships in PE-PA blends., Polym. Eng. Sci., 1990, 30, 9, 553-565.

Shih C.K., Tynan D.G., Denelsbeck D.A., Rheological properties of multicomponent polymer systems undergoing melting or softening during compounding. Polym. Eng. Sci., 1991, 31, 23, 1670-1673.

Sigillo I., di Santo L., Guido S., Grizzuti N., Comparative measurements of interfacial tension in a model polymer blend. Polym. Eng. Sci. 1997, 37(9), 1540-1549.

Small P. A., Some factors affecting the solubility of polymers, J. Appl. Chem. 1953, 3, 71-80.

Staicopolus D.N., The computation of surfacetension and of contact angle by the sessile-drop method. J. Coll. Sci., 1962, 17, 439-447.

Starke J.U., Michler G.H., Grellmann W., Seidler S., Gahleitner M., Fiebig J., Nezbedova E., Fracture toughness of polypropylene copolymers: influence of interparticle distance and temperature. Polymer, 1998, 39, 1, 75-82.

Stone H.A., Leal L.G., Relaxation and breakup of an initially extended drop in an otherwise quiescent fluid. J. Fluid Mech. 1989, 198, 399.

Stone H.A., Bentley B.J., Leal L.G., An experimental study of transient effects in the breakup of viscous drops. J. Fluid. Mech. 1986, 173, 131-158.

Sundararaj U., Dori Y., Macosko C. W., Sheet formation in immiscible polymer blends : model experiments on initial blend morphology. Polymer, 1995a, 36(10), 1957-1968.

Sundararaj U., Macosko C.W., Nakayama A., Inoue T., Milligrams to kilograms: An evaluation of mixers for reactive polymer blending. Polym. Eng. Sci., 1995b, 35(1), 100-114.

Sundararaj U., Macosko C.W., Rolando R.J., Chan H.T., Morphology development in polymer blends. Polym. Eng. Sci., 1992, 32(24), 1814-1823.

Sundararaj U., Morphology development during polymer blending. 1994, Ph.D. Thesis submitted to The University of Minnesota.

Taylor G. I., The viscosity of a fluid containing small drops of another fluid. proc. Roy. Soc. London, 1932, A138, 41-48.

Tjahjadi M., Ottino J.M., Stretching and breakup of drops in chaotic flows. J. Flu. Mech., 1991, 232, 191-219.

Tjahjadi M., Ottino J.M., Stone H.A., Estimating interfacial tension via relaxation of drop shapes and filament breakup. AIChE J. 1994, 40(3), 385-394.

Tomotika S., On the instability of a cylindrical thread of a viscous liquid surrounded by another viscous fluid. Proc. R. Soc. London 1935, A150, 322-337.

Unsworth L., Unpublished work, University of Alberta 1996.

Usami T., Gotoh Y., Takayama S., Generation mechanism of short-chain branching distribution in linear low-density polyethylene. Macromolecules 1986, 19, 2722-2726.

Utracki L.A., Comment on "Estimation of interfacial tension using shape evolution of short fibers". J. Rheology 1990, 34(4), 609.

Van Krevelin D.W., Properties of polymers, their estimation and correlation with chemical structure. 3rd Ed., Elsevier Scientific Publishing Co.,Amsterdam, 1990.

Van Oene H., Modes of dispersion of viscoelastic fluids in flow. J. Coll. Int. Sci. 1972, 40, 3, 448-467.

Vasely D., Microstructural characterization of polymer blends. Poly. Eng. Sci., 1996, 36, 12, 1586-1593.

Verhoogt H., Morphology, properties and stability of thermoplastic polymer blends. Ph.D. Thesis, Delft Technical University 1992.

Wang C. Liu C.-R., Transcrystallization of polypropylene composites: nucleating ability of fibres. Polymer, 1999, 40, 289-298.

Wang X., Wang Z., Jiang W., Liu C., Yang H., Zhang H., Jiang B., Toughened blend of polycarbonate and epoxidized ethylene propylene diene rubber. Polymer, 1997, 38, 25, 6251-53.

Watkins V.H., Hobbs S.Y., Determination of interfacial tension between BPA polycarbonate and SAN copolymers from capillary thread instability measurements. Polymer, 1993, 34, 18, 3955-3959.

Westphal S.P., Ling M.T.K., Ding S.Y., Woo L., Further studies on metallocene ULDPE/PP blends impact morphology relationships. SPE ANTEC Proc., 1997, 2631-2635.

Wild L., Temperature rising elution fractionation. Adv. Polym. Sci., Separation techniques. Thermodynamics. Liquid crystal polymers., 1991, 98, 1-47.

Wild L., Ryle T. R., Knobeloch D.C., Peat I.R. Determination of branching distributions in polyethylene and ethylene copolymers. Am. Chem. Soc., Div. Polym. Chem., Polym. Prepr., 1982, 18, 182-.

Wu J., Mai Y.-W., Yee A.F., Fracture toughness and fracture mechanisms of PBT/PC/impact modifier blends. J. Mat. Sci., 1994, 29, 4510-22.

Wu S., Formation of dispersed phase in incompatible polymer blends: Interfacial and rheological effects. Polym. Eng. Sci. 1987, 27, 5, 335-343.

Wu S., Phase structure and adhesion in polymer blends: A criterion for rubber toughening. Polymer, 1985, 26, 1855-1863.

Wu S., Calculation of interfacial tension in polymer systems. J. Polym. Sci.: Part C 1971, 34, 19-30.

Wu S., Surface and interfacial tension of polymer melts. J. Coll. Int. Sci., 1969, 31, 153-161.

Yamaguchi M., Effect of molecular structure in branched polyethylene on adhesion properties with polypropylene. J. App. Polym. Sci. 1998, 70, 3, 457-463.

Yang L.Y., Theodore G.S., Bigio D., Melt Blending of LLDPE ans PS in a Haake mixer. Part 1: Compatibilization and morphology development. & Part 2: Morphology-processing relationships. J. App. Polm. Sci., 1995, 58, 1, 117.

Yee A.F., Pearson R.A., Chapter 8. Fractography and failure mechanisms of Polymer and composites. Edited by Roulin-Moloney A.C., Elsevier App. Sci., 1988.

Yu T.C., Polymer selection for polypropylene modification. SPE ANTEC 1995, 2374-2385.

Yuan B.-L., Wool R.P., Strength development at incompatible semicrystalline polymer interfaces. Polym. Eng. Sci., 1990, 30, 22,1454-1464.

APPENDIX A : TREF Details

Contents

A-I : Program for TREF crystallization and elution equipment. 143

A-II : Program code for filtering TREF data. 144

A-III : Program code for analysing TREF data. 146

Appendix A-I : Program for TREF crystallization and elution

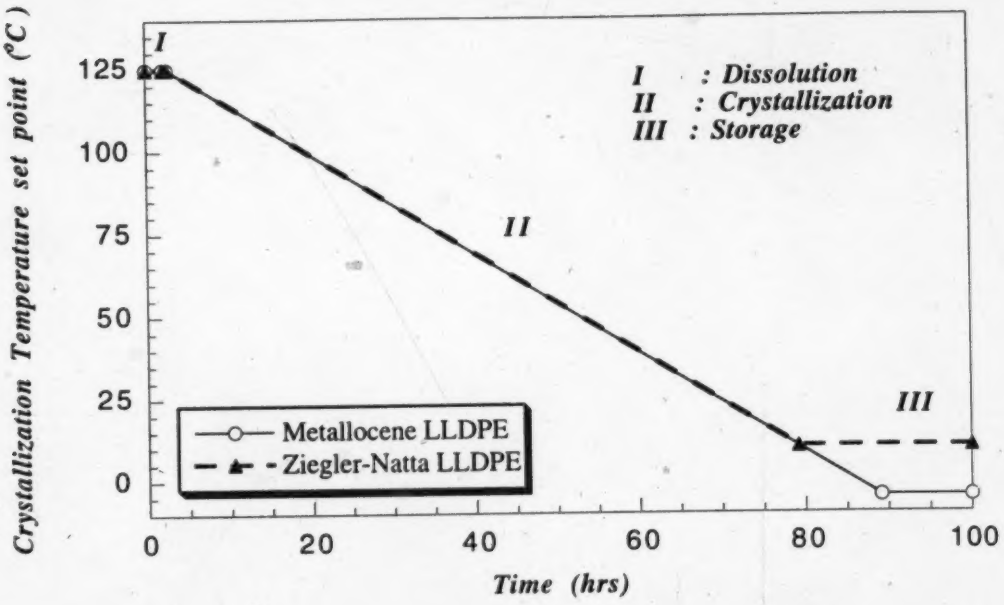

Figure A-I (a) Temperature set points used for the programmable temperature controlled bath for crystallization.

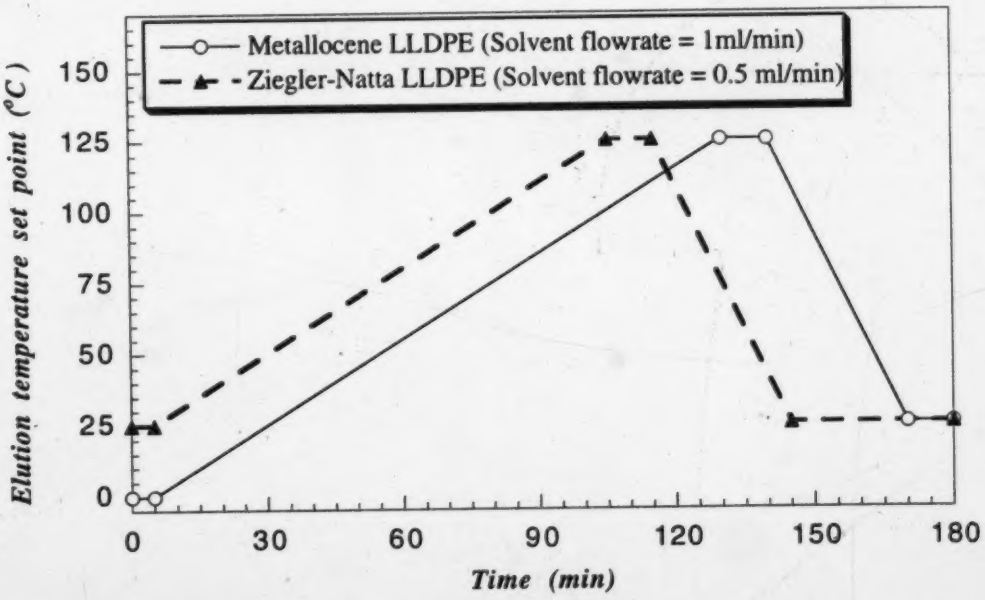

Figure A-I (b) Temperature set points used in the programmable oven for TREF elution.

Appendix A-II (a) : Program code for filtering TREF profiles.

```
Program Noise (trefin, trefout, output);

{This Pascal program removes unwanted data from tref profiles such as unusual dips in
temperature and also averages out the recurring variables representing the same
temperature. The input file should contain two columns of real number data, the first is
the Temperature and the second, the IR signal and the datafile must not exceed 700 data
points. A reduced datafile called trefout will contain the sorted data.}

var
i,j,k          :integer;
T,IR           :array[1..700] of real;
B, Bir         :array[1..4] of real;
trefin         :text;
trefout        :text;
countdown      :integer;
endofdata      :boolean;


begin{main}

reset(trefin);
rewrite(trefout);
k:=0; j:=1; countdown:=3; endofdata:=false;

for i:=1 to 3 do
If not eof(trefin) then
        readln(trefin, B[i], Bir[i]);

T[1]:=B[1]; IR[1]:=Bir[1];

while (not endofdata) and (j<701) do
  begin
      If not eof(trefin) then                          {Reading New Data}
            readln(trefin, B[4], Bir[4])
      else
        begin
            countdown:=countdown - 1;
            if countdown = 0 then
                  endofdata:=true;
        end;

      if B[2]>B[1] then
```

```
        begin
            if B[3]<B[2] then
              begin
                  if B[4]<B[2] then
                    begin
                        B[2]:=B[3]; Bir[2]:=Bir[3];
                    end;
                  B[3]:=B[4]; Bir[3]:=Bir[4];

                  If not eof(trefin) then                    {Reading New Data}
                        readln(trefin, B[4], Bir[4])
                  else
                    begin
                        countdown:=countdown - 1;
                        if countdown = 0 then
                        endofdata:=true;
                    end;
              end;
        end;

      if T[j]=B[1] then
        begin
            k:=k+1;
            IR[j]:=((k-1)*IR[j] + Bir[1])/k;
        end
      else
            if T[j]<B[1] then
              begin
                  k:=1; j:=j+1;
                  T[j]:=B[1]; IR[j]:=Bir[1];
              end;

      B[1]:=B[2]; Bir[1]:=Bir[2];
      B[2]:=B[3]; Bir[2]:=Bir[3];
      B[3]:=B[4]; Bir[3]:=Bir[4];
  end;{ of while}

writeln('Writing data to file...') ;
writeln(trefout, ' T ',' IR ');
for i:=1 to j do
writeln(trefout, T[i]:3:2,'    ', IR[i]:3:2);
writeln('Your data is stored in the file: trefout');

end.{Program}
```

Appendix A-II (b) : Program code for analysing TREF profiles.

```
Program CALCMSL (trefin, mslout, normdata, output);
{This program accepts T vs IR signal columns in a data file called trefin and returns either
a normalized signal or the methylene sequence length at each temperature in the form of T
vs Normalized IR signal (file normdata) or T vs MSL column data (file mslout). The
program uses the Trapezoidal rule to integrate the area between the baseline (user
specified) and the TREF profile in order to obtain normalized IR signal data and the Coho
ratio.}

const
maxnum=700;

type
list=array[1..maxnum] of real;

var
i,j,k                       :integer;
T,IR,MSQ,IRnorm             :list;
B, Bir                      :array[1..4] of real;
trefin                      :text;
mslout,normdata             :text;
countdown                   :integer;
endofdata,tonormalize       :boolean;
conv,response               :char;
methlen                     :integer;
IRo,M,CH3av                 :real;

Procedure find_MSL(T_el :real; var MSL :integer; var CH3_1000C :real; var c:char);

const
a = 374.1;
b = 0.006583;

var
i                           :integer;
k,MSL1,MSL2                 :real;
converged                   :boolean;

begin
        if T_el<100 then
        begin
                converged:=false; i:=0;
                MSL1:=MSL;
                T_el:=T_el + 273.15;
```

```
            k:=b/((1/T_el)-(1/a));
            while (i<10) and (not converged) do
            begin
            i:=i+1;
            MSL2:=MSL1 -( ( (MSL1-k*ln(MSL1))*(1-k/MSL1) ) / ( sqr(1-k/MSL1)
                  - ( k* (MSL1-k*ln(MSL1)) /sqr(MSL1) ) ) );
            converged:=((MSL2-MSL1)<0.6);
            MSL1:=MSL2;
            end;

            MSL:=round(MSL2);
            if converged then c:='c' else c:='n' ;

            CH3_1000C:=2000/(MSL+2);
      end {of if}
      else
            CH3_1000C:=0;

end;{of procedure find_MSL}


Procedure normalizeIR( T,IR: list; j: integer; IRo,M :real;
                        var IRnorm:list );

var
i                       :integer;
Area,dA,A_copol         :real;
Coho, Tcoho             :real;
IR_red                  :list;
response                :char;

begin
      Area:=0; dA:=0; A_copol:=0; Tcoho:=92;{degree C} response:='n';
      Writeln('Do you want the coho ratio? (y/n)');
      readln(response);
      If ((response = 'y') or (response = 'Y')) then
      begin
            write('T coho (in degree C)= ');
            readln(Tcoho);
      end;

      IR_red[1]:=IR[1]-(IRo+ M*T[1]);                    {baseline correction}
      for i:= 2 to j do
      begin
            IR_red[i]:=IR[i]-(IRo + M*T[i]);
```

```
            dA  :=(IR_red[i]+IR_red[i-1])*(T[i]-T[i-1])/2;
            Area:=Area + dA;                                    {trepezoidal rule}
            if T[i]<=Tcoho then A_copol:=Area;
        end;

        for i:= 1 to j do
        IRnorm[i]:=IR_red[i]/Area;

        Coho:=A_copol/(Area-A_copol);
        If ((response ='y') or (response ='Y')) then
            writeln('Coho ratio= ',Coho:3:2);

end;{of procedure normalizeIR}


            { ******************    MAIN    ****************** }


begin{main}

reset(trefin);
k:=0; j:=1; countdown:=3; endofdata:=false;

for i:=1 to 3 do
If not eof(trefin) then
        readln(trefin, B[i], Bir[i]);

T[1]:=B[1]; IR[1]:=Bir[1];

while (not endofdata) and (j<(maxnum+1)) do
  begin
        If not eof(trefin) then                                 {Reading New Data}
            readln(trefin, B[4], Bir[4])
        else
          begin
            countdown:=countdown - 1;
            if countdown = 0 then
                endofdata:=true;
          end;

        if B[2]>B[1] then
          begin
            if B[3]<B[2] then
              begin
```

```
                    if B[4]<B[2] then
                      begin
                          B[2]:=B[3]; Bir[2]:=Bir[3];
                      end;
                    B[3]:=B[4]; Bir[3]:=Bir[4];

                    If not eof(trefin) then                    {Reading New Data}
                          readln(trefin, B[4], Bir[4])
                    else
                      begin
                          countdown:=countdown - 1;
                          if countdown = 0 then
                          endofdata:=true;
                      end;
                end;
          end;

       if T[j]=B[1] then
          begin
              k:=k+1;
              IR[j]:=((k-1)*IR[j] + Bir[1])/k;
          end
       else
              if T[j]<B[1] then
                begin
                    k:=1; j:=j+1;
                    T[j]:=B[1]; IR[j]:=Bir[1];
                end;

       B[1]:=B[2]; Bir[1]:=Bir[2];
       B[2]:=B[3]; Bir[2]:=Bir[3];
       B[3]:=B[4]; Bir[3]:=Bir[4];
  end;{ of while}


tonormalize:=false; response:='n';
Writeln('Do you want to normalize the IR signal?(y/n)');
Readln(response);
If (response='y') or (response='Y') then
begin
        tonormalize:=true;
        writeln('Please input parameters for baseline: IR = IRo + M*T(degC)');
        write('IRo = ');
        readln(IRo);
```

```
        write('M = ');
        readln(M);
        normalizeIR(T,IR,j,IRo,M,IRnorm);
        rewrite(normdata);
end
else
        rewrite(mslout);


writeln('Writing data to file...') ;
If tonormalize then
        writeln(normdata,'  T  ','  IRnorm ')
else
        writeln(mslout, ' T ',' IR ', ' MSQ',' convergence');

if T[1] <=60 then methlen:= 79;
if (60< T[1] ) and (T[1] <=70)  then methlen:=128;
if (70< T[1] ) and (T[1] <=75)  then methlen:=169;
if (75< T[1] ) and (T[1] <=80)  then methlen:=217;                    {initial guess}
if (80< T[1] ) and (T[1] <=85)  then methlen:=292;
if (85< T[1] ) and (T[1] <=90)  then methlen:=429;
if  90< T[1]   then methlen:=807;

CH3av:=0;
for i:=1 to j do
begin
        find_MSL(T[i],methlen,MSQ[i],conv);

        If tonormalize then
        begin
                if i>1 then
                CH3av:= CH3av + (MSQ[i]+MSQ[i-1])*(IRnorm[i]+
                                                        IRnorm[i-1])*(T[i]-T[i-1])/4;
                writeln(normdata,T[i]:6:2,'  ', IRnorm[i]:8:5)
        end
        else
                writeln(mslout,T[i]:6:2,'  ', IR[i]:5:2,'  ',methlen:4,'  ', MSQ[i]:5:2,'  ',
                        conv);

end;{for}

if tonormalize then
begin
        writeln('The average number of methyl groups per 1000 carbon atoms is:',
                CH3av:3:2);
```

```
        writeln('Your data is stored in the file: normdata')
end
else
        writeln('Your data is stored in the file: mslout');

end.{Program}
```

Appendix B : LLDPE Synthesis Using Slurry Phase Polymerization

Introduction

This section deals with the synthesis of linear low density polyethylenes made with varying concentrations of 1-butene comonomer. It deals with the effect of comonomer concentration on branching and yield of copolymer formed. The slurry phase polymerization procedure has been outlined. It will be very interesting to see the effect of comonomer distribution on the interfacial tension.

Theory

Commercial synthesis of LLDPEs is carried out by low pressure polymerization processes conducted in the gas phase, slurry phase or solution phase. Although most commercial processes use either the gas phase (such as the UNIPOL technology developed by Union Carbide) or the solution phase (such as the Sclairtech process of DuPont, which is now owned by Nova Chemicals Ltd.) routes, there are great advantages in using slurry phase polymerization process for laboratory synthesis of LLDPEs. The advantages include ease of conducting the experiment, higher activity and hence yield due to the affinity of ethylene to distribute in the solvent phase and increasing its concentration in that phase, lower rate of catalyst deactivation owing to effective shielding of catalyst particles from moisture and oxygen by the solvent, and finally better heat transfer rates and better temperature control. In this study, slurry phase polymerization was carried out to obtain LLDPEs with different comonomer distributions. The intention was to increase the 1-butene concentration and thereby increase the density of side branches along the main chain of the polymer molecule thus formed, while keeping other reactant concentrations the same. If successful, the same would then be tried out for different comonomers such as 1-hexene and 1-octene.

In slurry phase polymerization, a solution of ethylene and the comonomer is fed to the reactor and the catalyst particles are suspended in a solvent typically decane or heptane. The polymer is produced around the catalyst and forms a suspension in the solution. Although the exact coordination mechanism of the reaction is not known, the reaction can be divided into three steps, namely, initiation, propagation and termination. The catalyst is a Ti based bisupported catalyst which acts in the presence of a cocatalyst, typically triethyaluminium, to coordinate with an ethylene molecule. With the transfer of the active center, the next molecule is inserted into the growing chain. Hydrogen participates in the chain termination step and is used to control the molar mass of the resulting polymer. Both the cocatalyst and 1-butene are also suspected to act as chain transfer agents and assist with the chain termination.

Experimental

The LLDPE samples were all synthesized in a 1 litre stainless steel reactor. Attempts prior to this were carried out in a glass reactor. The pressures achievable within safety limits were not high enough to obtain good product yield in the glass reactor and hence a steel reactor had to be used to conduct the runs. This equipment, otherwise used for gas-phase polymerization, has been described earlier by Huang (1995) and by Lynch and Wanke (1991). A schematic of the polymerization equipment is shown in Figure B.1.

The material needed for synthesizing polyethylene included a Ti-based Ziegler Natta catalyst (supplied by Nova Chemicals), hydrogen, nitrogen, ethylene, 1-butene and the carrier solvent heptane. The general procedure started by assembling the reactor and testing the reactor seal by applying nitrogen at a pressure of 2 MPa and checking for bubbles by immersing into the oil bath. The reactor was evacuated overnight at 90°Cto get rid of any moisture because the catalyst deactivates in the presence of moisture or oxygen. A catalyst slurry was prepared in heptane for this reason. The exact concentration of the

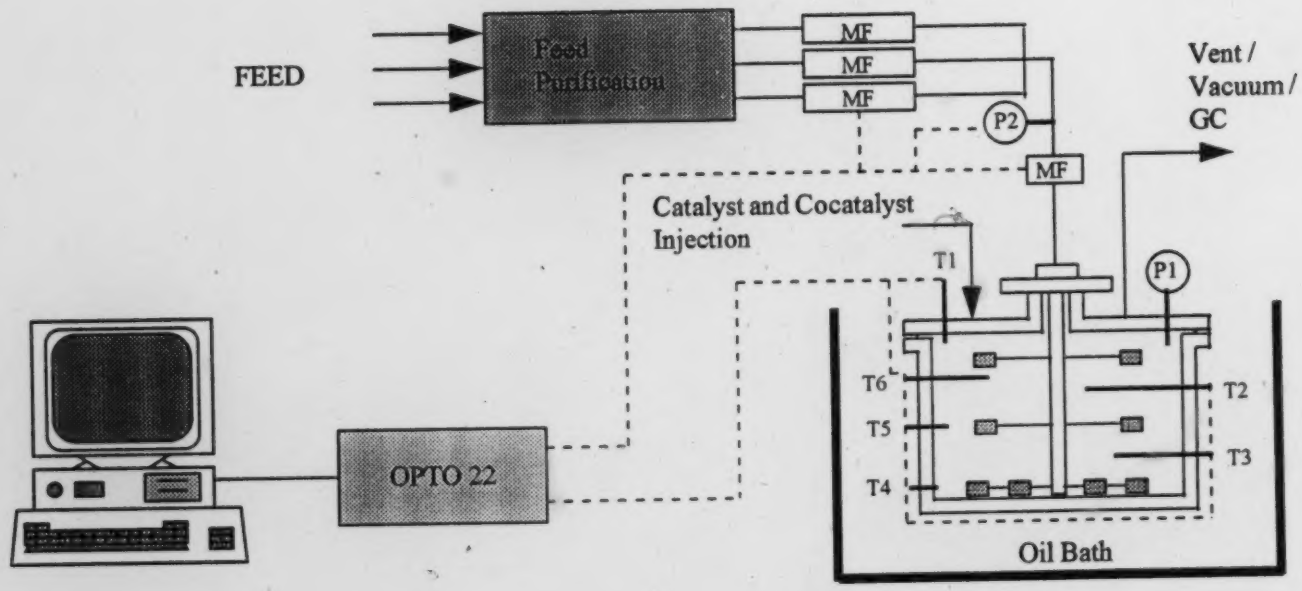

Figure B.1 Schematic of the Polymerization Equipment. (Adapted from Wanke and Lynch, 1991)

slurry was determined by weighing the vial, seal and aluminium cap prior to adding the catalyst. The catalyst suspension was prepared inside the glove box and the vial was sealed. The sealed vial was again removed from the glove box and weighed. This gives the total weight of catalyst used. A measured amount of heptane is introduced in the vial by a syringe. This is again carried out inside the glove box. Extreme care is taken to protect the catalyst from deactivating. The vial containing the catalyst slurry is capped for subsequent use.

Before the run, the bath temperature was adjusted to about 68°C, just a little lower than the run temperature considering that the reaction was exothermic. Nitrogen was allowed into the reactor upto a pressure of 14 psi. Approximately 300 ml of solvent, heptane, was introduced into the reactor using a syringe under nitrogen pressure. The vent is kept slightly open to avoid back pressure while filling heptane. Triethylaluminium cocatalyst was loaded (0.5 ml) into a syringe, again in the glove box, as it is highly reactive to moisture or oxygen. The volume of catalyst slurry corresponding to approximately 60mg of catalyst, was measured in a syringe. This step is tricky since the catalyst particles sink to the bottom of the vial preventing a uniform concentration in each load. To reduce this effect, the vial was simultaneously stirred while loading. To minimize the deactivation of the catalyst, the cocatalyst was fed before the catalyst. The cocatalyst reacts with any traces of moisture or oxygen in the reactor. The next step was introduction of the comonomer. The 1-butene was pressurized to liquefy it and the desired amount was pumped into the reactor. There could be some loss of the comonomer in the lines connecting the pump to the reactor. Without losing much time, hydrogen was fed to the reactor to create a hydrogen partial pressure of approximately 80 psi. Total pressure was around 100 psi at this point. Hydrogen supply was cut off as hydrogen consumption in the reaction is low and hydrogen partial pressure remains almost constant until the end of the run (Wanke and Lynch, 1995). Ethylene gas was introduced next at a partial pressure of 260 psi. The run was allowed to proceed for approximately three hours for a reasonable yield. Once the activity became low, the ethylene flow was stopped and the reactor was removed from the oil bath to cool it down. At a temperature of 40°C or lower, the reactor

was dissembled and heptane decanted off and polyethylene granules were scraped out in a beaker and kept overnight in a low temperature oven to remove volatile solvent. Polymer was weighed and stored in Ziplock bags for further use.

Results and Discussion

Butene copolymers were synthesized with 0, 5, 10, 20, 30, and 40 ml 1-butene with hydrogen pressure nearly the same. Table B.1 summarizes the run conditions. An ethylene pressure of 260 psi was used. The activity (amount of reactants consumed) along with the pressure and temperature for the runs are shown in Figure B.2 (a) - (g). In the initial minutes of all runs the activity shot up beyond the observable range of 1000 cc/min, as the initiation step consumes all the ethylene available. A circulation bath equipped with a cooling coil is provided to compensate for the rise in temperature which accompanies the high activity. The ethylene consumption stabilizes during the propagation step. In some cases the convective heat transfer is insufficient to handle the initial rise in temperature. When heat is not convected away, thermal runaway can result due to higher catalyst activity at higher temperature. The ethylene feed was shut off manually when this occurred until the temperature came down to the run temperature of 70°C. This occurred in runs NR6 (Fig. B.2 (d)) and NR7 (Fig. B.2 (e)). The control of the reaction temperature is critical since the catalyst deactivates at higher temperatures. Other problems such as plugging and polymer agglomeration can also occur due to the polymer dissolution and melting at high temperatures.

The polymers were characterized for dynamic viscosity using the RMS 800 Rheometrics rheometer. Frequency sweeps were performed at 200°C and 10% strain from 0.01 to 10 rad/s as described earlier in Chapter 2. Figure B.3 (a) shows the Cross model fitted to the viscosity data. The effect of 1-butene amount on the zero shear viscosity follows a gradually decreasing trend (see Fig. B.3 (b)), with the exception of NR6, which shows a sharp dip in the viscosity value. The homopolymer NR5 corresponding to 0 ml 1-

butene, shows the highest viscosity and probably the highest molar mass due to the absence of the comonomer which is believed to act as one of the chain termination agents.

Table B.1 Conditions for slurry phase Ziegler Natta polymerization of 1-butene copolymers in a 1L reactor at 70°C.

Polymer	1-butene (ml)	$P(H_2)$ (psia)	$P(C_2H_4)$ (psia)	Catalyst (mg)	Run time (min)	Yield (gm/gm cat)
NR5	0	78	260	77.42	243	840
NR3	10.06	80	260	61.14	270	1000
NR4	20.80	73	263	61.14	250	1060
NR6	29.84	80	257	77.42	190	1650
NR7	38.26	82	197	61.04	190	1230

This could also be due to the fact that higher 1-butene concentration reduces the ethylene concentration in the slurry phase. This then causes a lower molar mass homopolymer to form. The high density fraction is known to control polymer properties such as viscosity and melt index. TREF profiles of runs NR3 and NR4 show greater amounts of copolymer formed.

An unusual dip in the zero shear viscosity is observed for LLDPE NR6. Low zero shear viscosity indicates a low molar mass. The reason for this occurrence could be that during the initial period of run NR6 (Fig. B.2 (f)), the ethylene feed exceeded the critical flowrate causing a temperature to steadily rise. At a temperature of 90°C the ethylene flowrate was stopped completely and resumed only after temperature dropped back to 70 °C. As most of the polymerization takes place in the initial 10-20 minutes, the absence of ethylene feed during this period could have affected chain propagation causing a low molar mass homopolymer fraction to form. More importantly, the chain termination activation energy is much lower at higher temperature and is responsible for the lower molar mass. The other factor is that the catalyst deactivates at higher temperatures, which might also be a contributing factor for the reduction in molar mass of LLDPE-NR6.

The sharp rise in temperature in run NR6 could have been caused by a higher amount of catalyst than measured. Precise control over the amount of catalyst fed into the reactor is difficult as the catalyst is fed in the form of a slurry in heptane. While loading the slurry in a syringe, settling results in lesser amount of catalyst loaded in the first draw while a greater amount shows up in the later draws from the same vial. Run NR6 involved one of the later catalyst draws from the second batch of catalyst slurry prepared. Another related problem was the accumulation of the catalyst, during injection, at the syringe wall just before the nozzle. A skillful loading technique involving tapping the syringe simultaneously while injecting the slurry minimized this. Neat heptane was charged and injected to wash the catalyst into the reactor when such sedimentation was noticed. This increases the chances of letting in small quantities of dissolved air into the reactor.

In run NR7 the hydrogen pressure at the beginning of the run was much higher than the other runs. A small volume of vapour was vented out to bring the total pressure back to 100 psi. Although 1-butene mainly distributes in the liquid phase, a small amount might have been expelled along with the vapour. The effective hydrogen partial pressure would also be less than 80 psi due to this operation. The effect of a lower 1-butene content is a lower comonomer incorporation and a lower hydrogen concentration would result higher molar mass polymer as hydrogen is an effective chain terminating agent (Jejelowo et al., 1991). Since the zero shear viscosity does not show a sharp decrease the molar mass does not seem to be much different than that expected. A look at the normalized TREF profile of NR7 however shows a higher homopolymer peak than NR6 and lower copolymer distribution than NR6. This is possible since NR6 involved a lower ethylene pressure during the initial period and hence lesser crystalline fraction formed as a result of more 1-butene incorporation The normalized TREF curves would then show NR7 with lower copolymer content, which is what was observed.

The zero shear viscosities observed for all the LLDPEs synthesized was fairly high and regarded unsuitable for the breaking thread method. The breaking thread method, as

explained in the following chapter involves observing the deformation of thin cylindrical polymer threads, embedded in a matrix polymer, into droplets and as viscosity is a rate determining parameter for deformation, it was decided that lower viscosity LLDPEs would be required for measuring the interfacial tension using this method. Furthermore, the TREF profiles show that the difference in comonomer incorporated is not substantial, hence the errors in the interfacial measurements would likely overshadow the effect of the increase in branching density. It was therefore decided that commercial polymers would be easier to study in the time frame of this study.

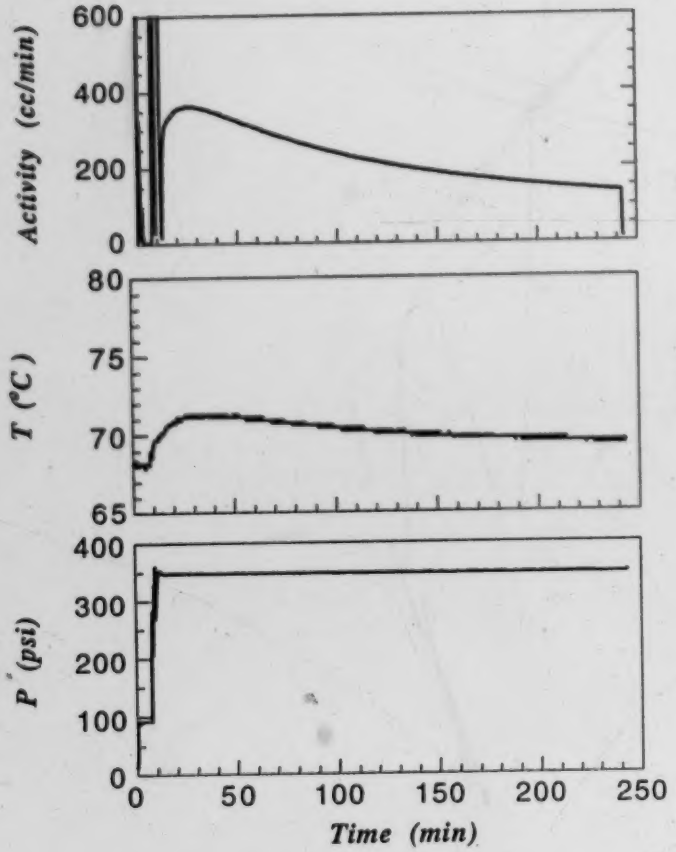

Figure B.2 (a) : Process conditions for Run NR5 in the steel reactor. (Homopolymer)

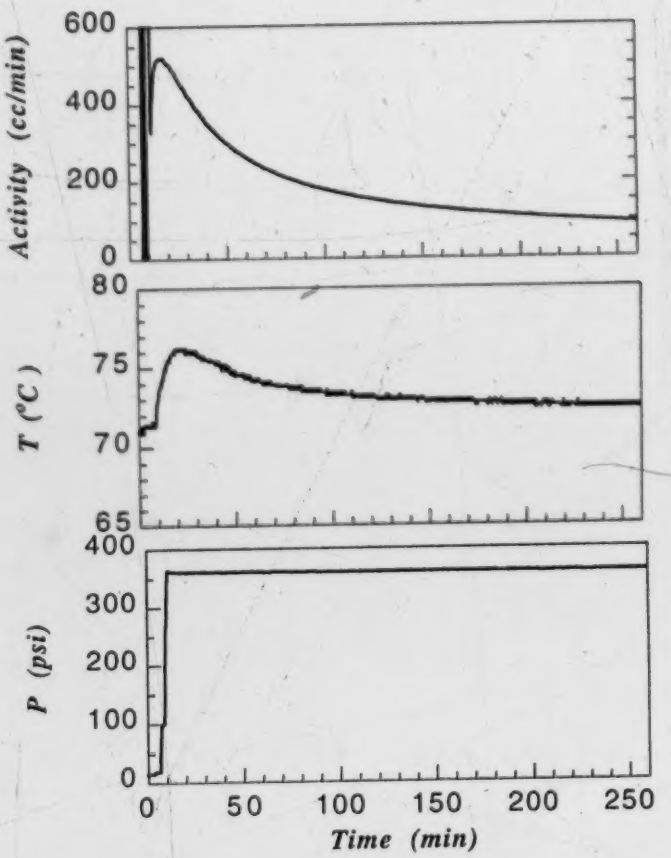

Figure B.2 (b) : Process conditions for Run NR3 in the steel reactor. (10ml 1-butene)

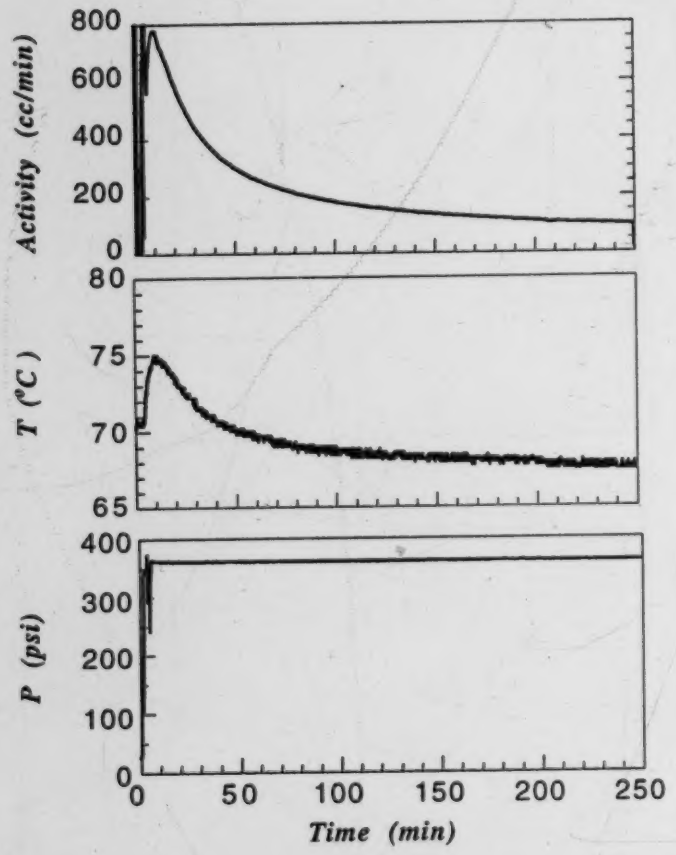

Figure B.2 (c) : Process conditions for Run NR4 in the steel reactor. (20ml 1-butene)

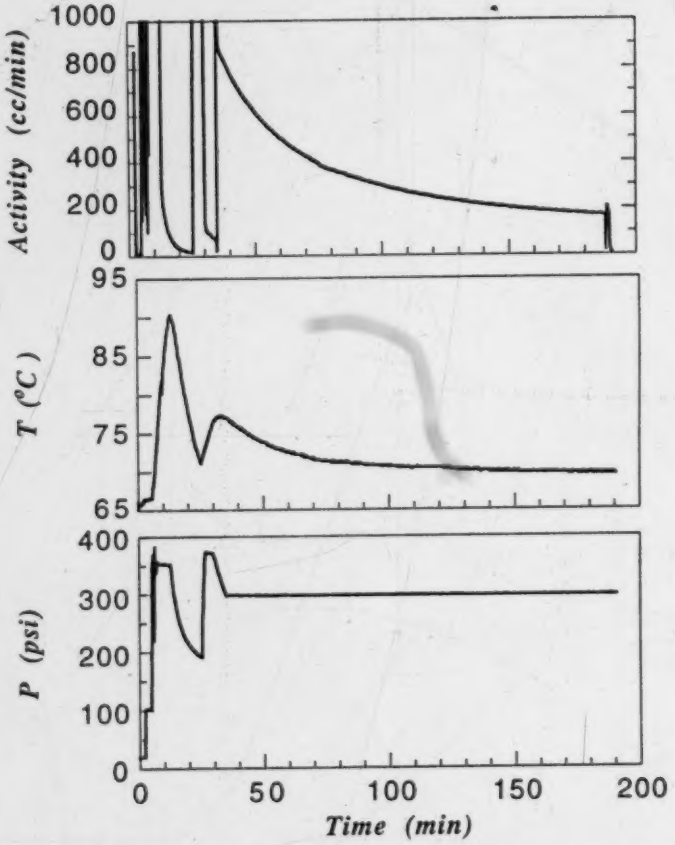

Figure B.2 (d) : Process conditions for Run NR6 in the steel reactor. (30ml 1-butene)

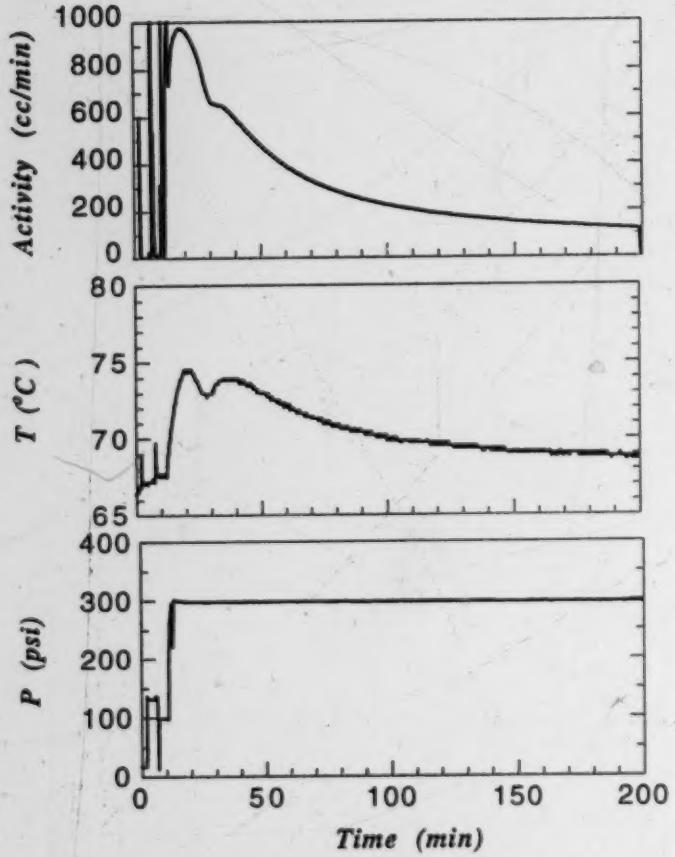

Figure B.2 (e) : Process conditions for Run NR7 in the steel reactor. (40ml 1-butene)

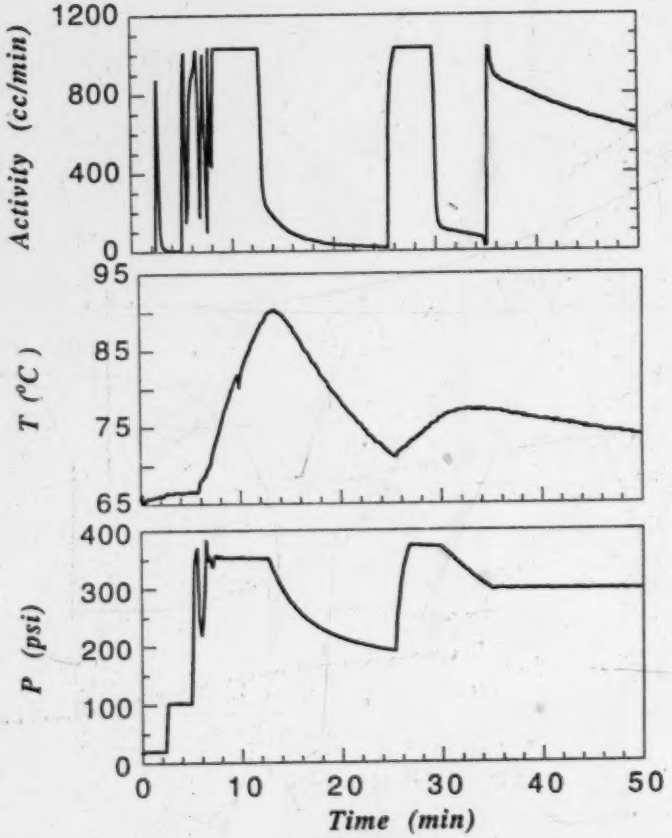

Figure B.2 (f) : Initial process conditions while charging reactants for Run NR6. (30ml 1-butene)

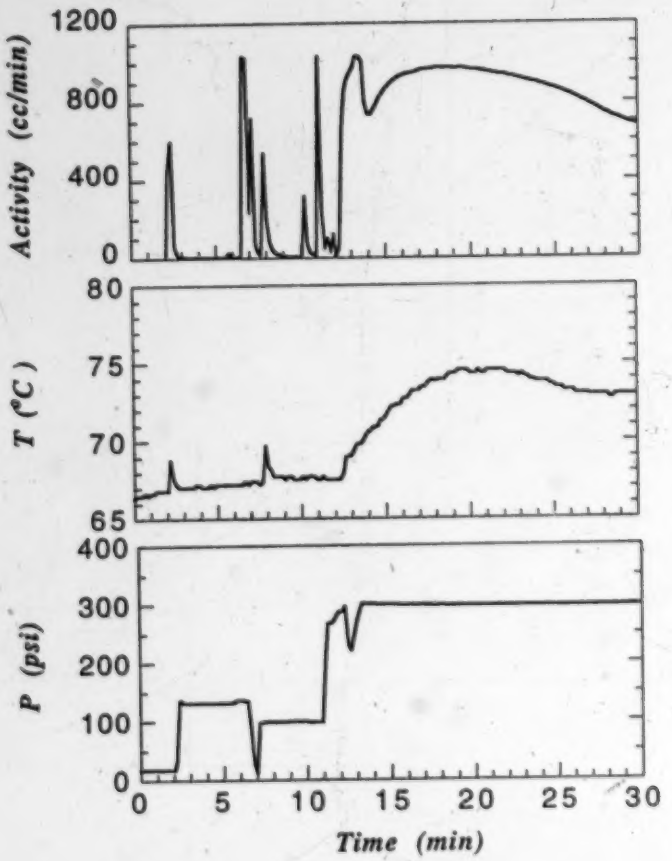

Figure B.2 (g) : Initial process conditions while charging reactants for Run NR7. (40ml 1-butene)

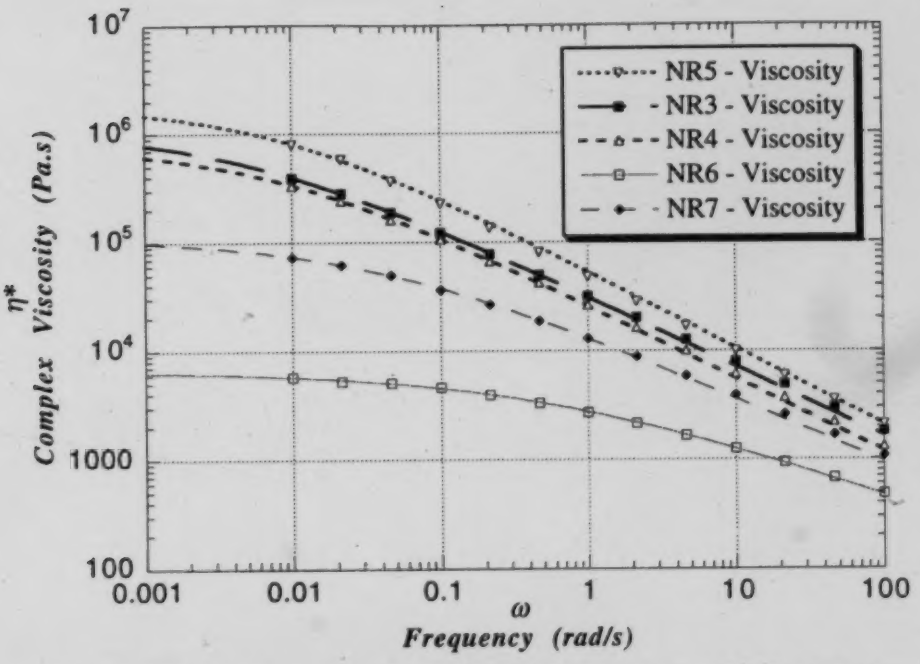

Figure B.3 (a) Complex viscosity of laboratory synthesized butene copolymers at 200°C and 10% strain.

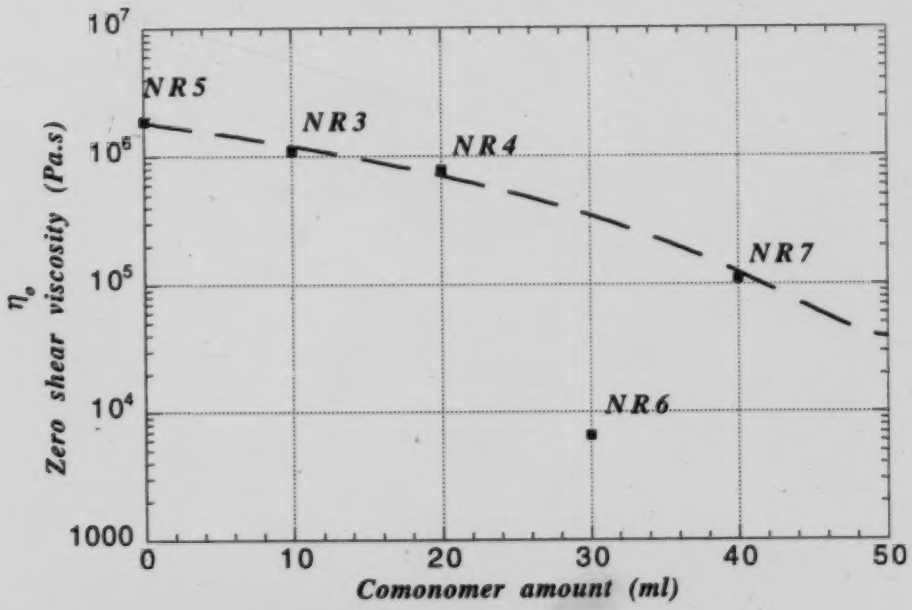

Figure B.3 (b) The effect of comonomer addition on the zero shear viscosity of butene copolymers.

Appendix C: Details of Interfacial Tension Measurements

Contents

C-I	Tomotika's distortion function charts.	166
C-II	Summary of PP/PS experiments using the breaking thread method.	
	(a) PP/PS at 200°C	167
	(b) PP/PS with different additives in PP phase at 200°C	168
C-III	Summary of PP/LLDPE experiments using the breaking thread method.	
	(a) PP/LLDPE at 200°C	169
	(b) PP/LLDPE at 220°C	170
	(c) PP/LLDPE at 260°C	172

Appendix C-I :
Tomotika's Distortion function charts.

The parameters used in the breaking thread method are as follows:

p : viscosity ratio.
D_o : thread diameter (microns).
λ : wavelength of distortion.
χ : wavenumber ($= \pi D_o / \lambda$).
χ_m : dominant wavenumber at viscosity ratio p.
Ω : Tomotika's distortion function.
Ω_m : Tomotika's distortion function for breakup occuring at dominant wavelength.
q : Exponential growth factor for distortion.
σ : Interfacial tension (mN/m).
σ_{mp} : Most probable Interfacial tension. Only σ values for which $\chi \sim \chi_m$ are chosen and averaged to get this value.

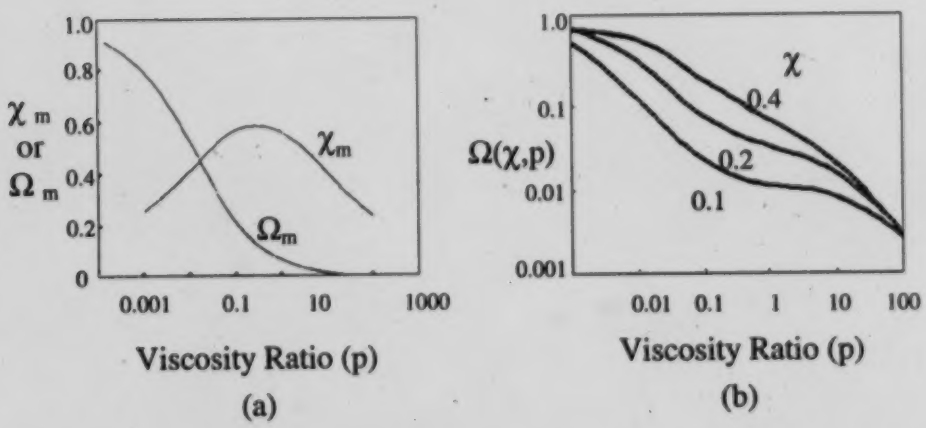

Figure C-I : Tomotika's distortion function plotted against viscosity ratio: (a) Profiles for breakup via dominant wavelength at a particular viscosity ratio. (b) Distortion function for breakup occurring at wavelengths other than dominant wavelength. *Adapted from Chappelear, 1964.*

Table C-II (a) : Breaking thread method parameters and interfacial tensions of PP/PS systems at 200°C.

Run	Pg.	Thread	p	Do	λ	χ	χ_m	Ω	Ω_m	$qx10^3$	σ	σ_{mp}
				(μm)	(μm)					(s^{-1})	(mN/m)	(mN/m)
2	12	PP1	0.052	109	632	0.54	0.54	0.29	0.29	3.04	6.5	6.5
3	13		0.52	100	450	0.7	0.54	0.25	0.29	6.11	14.2	
5	17		0.52	54	410	0.41	0.54	0.27	0.29	6.6	7.7	
6	18		0.52	118	530	0.7	0.54	0.25	0.29	3.5	9.6	
7	19		0.52	97	485	0.63	0.54	0.28	0.29	4.66	9.4	
12	25	PP2	0.114	55	248	0.69	0.57	0.19	0.21	11.08	18.5	
13	26		0.114	58	541	0.38	0.57	0.12	0.21	14.68	41.2	
14	27		0.114	38	233	0.51	0.57	0.2	0.21	21.6	23.8	
15	27		0.114	64	321	0.62	0.57	0.2	0.21	14.7	27.1	27
16	28		0.114	62	372	0.52	0.57	0.2	0.21	16.9	30.1	
21	34	PP3	0.136	128	1706	0.24	0.58	0.08	0.19	4.7	44.7	
1NR			0.136	76	570	0.42	0.58	0.18	0.19	8.42	20.6	20.6
2NR			0.136	142	574	0.78	0.58	0.16	0.19	8.22	42.3	
3NR		PP4	0.564	139	576	0.76	0.58	0.072	0.095	0.69	7.7	
1NRo			0.564	107	627	0.54	0.58	0.093	0.095	0.91	6.1	
3NRo			0.564	135	747	0.57	0.58	0.095	0.095	1.29	10.7	6.2
6NRo			0.564	110	530	0.65	0.58	0.089	0.095	0.89	6.3	
7NRo			0.564	97	577	0.61	0.58	0.093	0.095	1.5	9.1	
19	29	PP5	2.369	141	716	0.62	0.52	0.046	0.047	0.35	6.2	18
6NR			2.369	104	640	0.51	0.52	0.047	0.047	1.4	18	

Table C-II (b) : Breaking thread method parameters and interfacial tensions of PP1/PS systems with different contracst enhancing additives at 200°C.

Run	Pg.	Thread	p	Do	λ	χ	χ_m	Ω	Ω_m	$qx10^3$	σ	σ_{mp}
				(μm)	(μm)					(s^{-1})	mN/m	mN/m
2	12	PP1	0.052	109	632	0.54	0.54	0.29	0.29	3.04	6.5	6.5
3	13		0.52	100	450	0.7	0.54	0.25	0.29	6.11	14.2	
5	17		0.52	54	410	0.41	0.54	0.27	0.29	6.6	7.7	
6	18		0.52	118	530	0.7	0.54	0.25	0.29	3.5	9.6	
7	19		0.52	97	485	0.63	0.54	0.28	0.29	4.66	9.4	
4	15	$PP1_{c.b.}$	0.052	100	391	0.8	0.54	0.19	0.29	4.36	13.3	
34	42		0.052	68	412	0.52	0.54	0.28	0.29	4.47	6.3	6.3
35	43		0.052	71	590	0.38	0.54	0.25	0.29	5.87	9.9	
7NR		$PP1_{dye}$	0.052	74	474	0.05	0.05	0.29	0.29	7.2	10.7	10.7

c.b. : carbon black; dye : Phthalocyanine dye;

Table C-III (a) : Breaking thread method parameters and interfacial tensions of PP/LLDPE systems at 200°C.

Run	Pg.	Matrix	p	Do	λ	χ	χ_m	Ω	Ω_m	$qx10^3$	σ	σ_{mp}
				(μm)	(μm)					(s^{-1})	(mN/m)	(mN/m)
8NR1	31	5o	0.02	41	191	0.67	0.47	0.35	0.44	0.46	0.81	0.81
9L	22	7h	0.038	71	271	0.82	0.53	0.18	0.34	0.53	1.67	
10L	23	7h	0.038	61	241	0.9	0.53	0.11	0.34	1.21	5.3	1.26
11L	24	7h	0.038	60	269	0.81	0.53	0.19	0.34	0.34	0.86	
30L	40	8b	0.067	56	308	0.57	0.55	0.25	0.25	0.44	0.42	
32L	41	8b	0.067	49	221	0.7	0.55	0.22	0.25	1.12	0.42	0.42

Table C-III (b) : Breaking thread method parameters and interfacial tensions of PP/LLDPE systems at 220°C.

Run	Pg.	Matrix	p	Do	λ	χ	χ_m	Ω	Ω_m	$qx10^3$	σ	σ_{mp}
				(μm)	(μm)					(s^{-1})	(mN/m)	(mN/m)
17NR	22	1b	0.037	29	235	0.39	0.52	0.32	0.34	0.21	0.2	
21NR	29	1b	0.037	25	250	0.37	0.52	0.31	0.34	0.71	0.6	0.6
10NR	54	2o	0.047	54	213	0.79	0.53	0.19	0.3	1.16	2.3	
11NR	74	2o	0.047	74	272	0.85	0.53	0.14	0.3	0.52	2.7	2
12NR	62	2o	0.047	62	243	0.8	0.53	0.19	0.3	0.71	1.6	
13NR	18	3h	0.146	34	140	0.76	0.58	0.15	0.19	3.66	1.9	
14NR	19	3h	0.146	44	250	0.55	0.58	0.18	0.19	3.25	1.9	1.9
15NR	20	4p	0.691	59	265	0.7	0.58	0.08	0.09	5.37	2	
16NR	21	4p	0.691	41	184	0.7	0.58	0.08	0.09	7.97	2	2

Table C-III (b) cont. : Breaking thread method parameters and interfacial tensions of PP/LLDPE systems at 220°C.

Run	Pg.	Matrix	p	Do	λ	χ	χ_m	Ω	Ω_m	$qx10^3$	σ	σ_{mp}
				(μm)	(μm)					(s^{-1})	(mN/m)	(mN/m)
26NR	34	5o	0.03	38	250	0.48	0.51	0.35	0.36	0.67	0.83	0.83
18NR	25	6b	0.054	34	309	0.34	0.54	0.2	0.27	3.71	3.93	
19NR	27	6b	0.054	52	235	0.34	0.54	0.2	0.27	2.8	4.2	
20NR	28	6b	0.054	43	138	0.51	0.54	0.27	0.27	2.85	2.6	2.6
24NR	32	7h	0.029	29	154	0.6	0.54	0.27	0.27	2.14	1.9	
25NR	33	7h	0.029	21	147	0.44	0.54	0.26	0.27	2.84	1.3	1.9
27NR	37	8b	0.088	32	184	0.55	0.57	0.22	0.22	1.15	0.66	
28NR	38	8b	0.088	26	175	0.47	0.57	0.21	0.22	0.55	0.39	0.39

Table C-III (c) : Breaking thread method parameters and interfacial tensions of PP/LLDPE systems at 260°C.

Run	Pg.	Matrix	p	Do	λ	χ	χ_m	Ω	Ω_m	$qx10^3$	σ	σ_{mp}
				(μm)	(μm)					(s^{-1})	(mN/m)	(mN/m)
8L	20	1b	0.026	60	252	0.75	0.49	0.26	0.39	0.49	0.66	
4NR2	5	1b	0.026	82	529	0.49	0.49	0.39	0.39	0.57	0.7	0.7
8NR2	12	1b	0.026	87	735	0.37	0.49	0.35	0.39	0.63	0.91	
20L	33	5o	0.028	69	530	0.41	0.48	0.37	0.45	0.04	0.05	0.05
22L	35	7h	0.033	61	589	0.33	0.51	0.29	0.36	0.92	0.87	
23L	36	7h	0.033	126	750	0.53	0.51	0.35	0.36	0.4	0.64	0.64
31L	40	8b	0.088	51	250	0.64	0.57	0.21	0.23	1.18	0.49	
33L	42	8b	0.088	59	272	0.68	0.57	0.2	0.23	1.63	0.82	
5NR2	8	8b	0.088	81	468	0.54	0.57	0.23	0.23	0.56	0.34	0.34

Appendix D : Izod Impact Testing of PP blends.

As already mentioned in Chapter 4, the Izod specimen for the LLDPE/PP blends were prepared by transferring the blend directly from the mixer to the carver laboratory press which was maintained at 220°C, same as the blend temperature. Both ASTM D4101-95b for propylene plastic injection and extrusion materials and ASTM D4703 for compression molded thermoplastic materials were consulted and suitable modifications made to adapt to the small amounts of blend yielded by the mixer. A mold was used to form a sheet of dimensions 3" x 3.5". Six specimen were machined into izod specimen from this sheet as indicated by dotted lines in Figure D.1 (a). The five best ones, with the least burrs and trapped bubbles were used for Izod impact testing using ASTM D256-93a. The dimensions of the Izod specimen and the notch machined to initiate the crack are shown in Figure D.1(b) and the tolerances are indicated in ASTM D256. A summary of the Izod impact strengths of various LLDPE/PP blends are shown in Table D.1. Uneven fractures resulted in Izod values far from the average values. If the fractured surface of the Izod specimen showed evidence such as a bubble or secondary crack propagation, then the corresponding data was not included for calculation of the average impact strength.

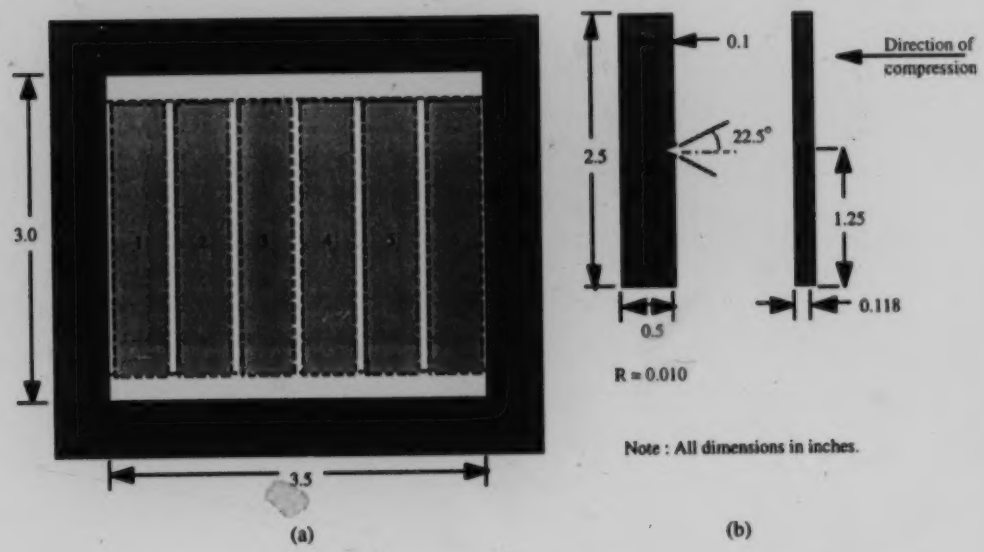

Figure D.1 (a) Mold for Izod specimen preparation. (b) Dimensions of Izod specimen.

Appendix D contd.

Table D.1 : Izod Impact Testing* of Polypropylene Blends at 23°C using ASTM D256-93a

Wt%	Disp. Phase	Sample	# 1	# 2	# 3	# 4	# 5	Average	Std. Dev.	Omitted	Comments:
0%	(PP As is)	S1	0.491	0.624	0.629	0.583	0.492	0.564	0.068		
0%	(PP 5m blend)	S2		0.682	0.614	0.685	0.635	0.654	0.035		Instrument malfunction
0%	PP 10m blend	S3	0.634	0.749	0.549	0.637		0.642	0.082		Only four specimen molded
5%	1b	S4	0.716	0.727	0.775	0.721	0.874	0.763	0.067		
10%	1b	S5	0.95	0.853	0.775	0.856	0.887	0.864	0.063		
20%	1b	S6	1.149	0.861	1.083	1.286	1.339	1.144	0.188		
5%	2o	S15	0.815	0.703	0.991	0.694		0.801	0.138	1.433	Secondary crack growth
10%	2o	S18	0.943	0.965	1.214	0.88	0.86	0.972	0.142		
20%	2o	S19	1.177	0.879	1.175	0.927	1.004	1.032	0.138		
5%	3h	S10	0.768	0.691	0.707	0.695	0.808	0.734	0.052		
10%	3h	S13	0.933	0.84	0.987	0.861	0.887	0.902	0.059		
20%	3h	S14	1.022	1.207	1.309	1.053	1.096	1.137	0.119		
5%	4p	S7	0.866	0.803	0.867	0.747	0.808	0.818	0.050		
10%	4p	S8	0.991	0.851	0.901	0.807	1.003	0.911	0.086		
20%	4p	S9	1.076	0.881	0.825	0.698	0.749	0.846	0.147		
5%	5o	S29	0.927	0.681	0.797	0.58	0.755	0.748	0.130		
10%	5o	S30	0.723	0.798	0.93	0.815	0.734	0.800	0.083		
20%	5o	S31	1.053	0.915	0.914	0.904	1.063	0.970	0.081		
5%	6b	S20	0.716	0.721	0.582	0.749	0.839	0.721	0.092		
10%	6b	S21	0.798	0.701	0.771	0.845	0.871	0.797	0.066		
20%	6b	S22	0.767	0.89	0.899	0.83	0.977	0.873	0.079		
5%	7h	S26	0.814	0.797	0.827	0.85	0.833	0.824	0.020		
10%	7h	S27	0.905	0.724	0.987	0.918	0.858	0.878	0.098		
20%	7h	S28	0.858		0.908	0.802	1.264	0.958	0.209		Instrument malfunction
5%	8b	S23	0.778	0.756	0.852	0.799	0.891	0.815	0.055		
10%	8b	S24	0.836	1.003	0.895	0.825	0.782	0.868	0.085		
20%	8b	S25	1.036		0.836	0.94	0.897	0.927	0.084	1.364	Secondary crack growth

* Impact strength units: ft.lb/in.

Appendix E : Dropsize measurement using SEM.

Procedure

The procedure used here to analyze dropsizes was the same as that used earlier by Ghodgaonkar (1995). An SEM picture of the fracture surface was first obtained at a convenient magnification (see Fig E.1 (a)).The droplets and holes were then carefully traced with a sharp tipped permanent marker onto a transparent plastic sheet along with the scale bar. The number of droplets analyzed was at least 200-300 in order to obtain a meaningful average. Both droplets and voids were traced. When droplets shrunk inside the voids, the inner periphery was traced as the matrix could have stretched out due to plastic deformation. The sheet is scanned and converted to a bitmap format and thresholded to get a sharp contrast in the scanned image of the drops and voids (see Fig. E.1 (b)). The size of the file was manipulated to around 300K so that it could be analyzed using a program called 'NIH Image 1.58b33 f' developed by National Institute of Health. The areas of the encircled shapes, obtained from NIH Image was then transferred to an appropriate numerical software to obtain the radii of the droplets. The number average diameter was obtained in this study.

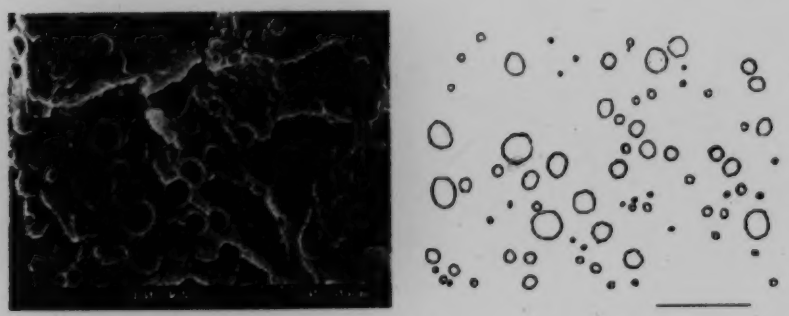

(a) (b)

Figure E.1 Reducing an SEM pictograph to a bitmap file for dropsize analysis. (a) SEM pictograph. (b) traced and scanned bitmap file of droplets and voids in a blend.

Comments

Some error in tracing the droplets is inevitable due to human error, but the variation in dropsizes is likely to overshadow this error. Higher resolution images can reduce this error and so can automatic droplet identification. Dharmarajan and Yu (1996) have used phase contrast option in NIH Image to automatically distinguish the dispersed phase from the matrix using the SEM pictures directly. In this study, dark lines appeared in place of ridges formed by the crack and cavitation caused due to shrinkage of the dispersed phase when phase contrast was used. Thus subjective judgment on dropsizes cannot be handled easily by automated programs and is certainly an advantage with the current method.